On longevity and the aging process

a magnetic resonance imaging study of the brain

Irmhild Altmann-Schneider

This thesis was printed by drukkerij Mostert, Leiden, The Netherlands.

ISBN/EAN 978-94-90858-36-0

On longevity and the aging process

a magnetic resonance imaging study of the brain

Proefschrift

ter verkrijging van

de graad van Doctor aan de Universiteit Leiden,

op gezag van Rector Magnificus prof.mr. C.J.J.M. Stolker,

volgens het besluit van het College voor Promoties

te verdedigen op dinsdag 26 mei 2015

klokke 15:00

door

Irmhild Altmann-Schneider

geboren te Stuttgart, Duitsland

in 1982

Promotiecommissie:

Promotores:

Prof. dr. M.A. van Buchem

Prof. dr. R.G.J. Westendorp

Copromotores:

Dr. J. van der Grond

Dr. A.J.M. de Craen

Overige leden:

Prof. dr. P.E. Slagboom

Prof. dr. S.A. Rombouts

Dr. M.W. Vernooij (Erasmus Medisch Centrum, afdeling Radiologie)

Dr. B. Sabayan

Financial support by Sectra Benelux, ChipSoft and the Netherlands Consortium for Healthy Ageing is gratefully acknowledged.

Für meine Familie

Table of contents

1

General introduction and outline of the thesis

General introduction

Since the middle of the 19th century life expectancy is continuously increasing in Western countries [2], resulting in an increasing number of years humans spend exposed to the effects of the aging process on their physical and psychological well-being. Unfortunately, not all years gained through increasing life expectancy are spent in a satisfying health condition. However, there are "successfully" or "healthy" aging individuals [3], who seem somehow unchallenged by the aging process resulting in healthy longevity. There is evidence that aging is not programmed and hence not inevitable [4, 5] and it is supposed to be both under environmental as well as genetic control [4]. Consequentially, disclosing the secret of healthy longevity is of huge importance to learn more about the aging process itself and to be able to translate this knowledge into appropriate health interventions to increase the healthy life span of "normally" aging individuals.

The Leiden Longevity Study (LLS) was designed to investigate factors associated with human familial longevity [6]. Dutch Caucasian families were eligible for the study if at least two siblings were long-living. The siblings had to fulfil the following inclusion criteria: (1) men had to be aged 89 years or older, women had to be aged 91 years or older; (2) there had to be at least two living siblings per family, who fulfilled the age criterion; (3) the long-living siblings had to have the same parents. Middle-aged to elderly offspring of the nonagenarian siblings, who are supposed to have a higher susceptibility to become long-lived as well, were included along with their spouses as an environmentally and age-matched control group. The propensity to become long-lived in the middle-aged to elderly offspring as compared to their spouses is marked by beneficial serum levels of lipid and thyroid parameters and preservation of insulin sensitivity [7-9].

To investigate whether human familial longevity is also reflected by a lower susceptibility to age-related structural brain damage, and more specifically to its magnetic resonance imaging (MRI) correlates, was the main purpose of this thesis. It should be kept in mind though that to date it is still not known where to draw the line between "normal" age-related structural brain changes - if they exist at all - and pathologic changes or even disease. Examples for imaging correlates of structural brain changes, which often occur "silent" and are thus not inevitably linked to an obvious loss of brain function or disease, are brain atrophy, white matter hyperintensities, lacunar brain infarcts, microbleeds and enlarged perivascular spaces [10]. New imaging technologies, such as diffusion tensor imaging (DTI) and magnetization transfer imaging (MTI) offer the possibility to assess brain tissue integrity non-invasively on the microstructural and macromolecular level and thus to study subtle brain damage even before it becomes overt on conventional imaging techniques.

Aging of the human brain though cannot be studied without bearing in mind that there might be factors with a modifying effect on age-related brain changes, in a "negative" or "positive" way, i.e. accelerating or decelerating the "normal" course of age-related deterioration of the brain [11]. Probably the most well-known example is arterial hypertension, which is both genetically and environmentally determined and known to be associated with "age-related" brain changes such as white matter hyperintensities, lacunar brain infarcts and microbleeds [12-14]. Prevalence of coronary artery calcification, which is widely accepted as a marker of atherosclerosis [15, 16], increases with chronological age and is higher in individuals with a history of coronary artery disease as compared to individuals without coronary artery disease [17]. Although coronary artery calcification has been shown to be predictive of future cardiovascular events [18, 19], the underlying clinical correlates of arteriosclerotic brain damage are still less obvious. Within

the Leiden Longevity Study, we aimed to systematically assess the association of coronary artery calcification with vascular brain damage as a potential modifying factor of age-related brain pathology in a large study cohort of elderly individuals on the macrostructural as well as microstructural level, also taking the spatial distribution of brain damage into account.

Hypothesizing that a lower prevalence of age-related brain pathology might be a marker of human longevity somehow implies that a higher prevalence of age-related brain pathology might be a marker of an increased risk of mortality in the elderly. Brain atrophy and WML for example have been shown to increase the risk of mortality in the general elderly population [20]. Cerebral microbleeds (CMB) - another imaging correlate of cerebral small vessel disease - are commonly seen in healthy elderly individuals [21] and their presence has been shown to be the strongest predictor of overall mortality among a range of MRI markers of vascular damage in a memory clinic population [22]. CMB can be caused by various types of small vessel damage of which the two most common types are hypertensive vasculopathy and cerebral amyloid angiopathy (CAA), which are associated with a different distribution and location of CMB within the brain [23-29]. With regard to the relatively high prevalence of CMB in elderly individuals (≈20% in subjects aged 60 to 69 years and ≈40% in subjects aged 80 years and older) [28], we aimed to assess the prognostic value of CMB in elderly individuals also regarding the different histopathological subtypes. As CMB are particularly prevalent in elderly individuals with other vascular risk factors or known history of cerebrovascular disease, this study was performed as part of the nested MRI substudy of the Prospective Study of Pravastatin in the Elderly at Risk (PROSPER), which consists of elderly participants at high risk of or with known vascular disease [30].

Study framework

The Leiden Longevity Study was performed within the scope of the Netherlands Consortium for Healthy Ageing (NCHA). The NCHA is an alliance between the Leiden University Medical Centre, the Erasmus Medical Centre (Rotterdam), the Wageningen University and Research Centre, the University Medical Centre Groningen and VU University Medical Centre (Amsterdam) as well as the business partners Unilever, Philips, Galápagos, McRoberts, Pfizer and DSM. The NCHA was built up to promote the understanding of the aging process and age-related diseases. It was supported by the Netherlands Genomics Initiative.

The Leiden Longevity Study was funded by the Innovation Oriented Research Program on Genomics (SenterNovem; IGE01014 and IGE5007), Unilever PLC, the EU-funded Network of Excellence Lifespan (FP6 036894), the EU funded project Switchbox (FP7, Health-F2-2010-259772), and the Netherlands Consortium for Healthy Ageing (Netherlands Genomics Initiative/Netherlands Organization for scientific research NGI/NWO; 05040202 and 050-060-810). The PROSPER study was an investigator initiated study funded by Bristol-Myers Squibb.

Outline of the thesis

The first part of the thesis "Phenotyping the brain in human familial longevity using MRI" aims to describe the structural phenotype of the brain in familial longevity. By investigating age-related changes of the brain in middle-aged to elderly offspring with the propensity to become-long-lived as compared to an environmentally and age-matched control group, we aimed to learn more about the relevance of common age-related brain changes and gave possible starting points for future interventional studies to develop strategies for how to translate this knowledge into appropriate health interventions to increase the healthy life

span of "normally" aging individuals. From the aging point of view, we defined the brain structural phenotype in human longevity as brain structure associated with "biological aging", also referred to as senescence. In order to be able to differentiate properly between structural brain changes related to "chronological aging" and the brain structural phenotype in human longevity, all analyses were performed in the whole study population (covering a wide age range) to assess the association of brain structure with chronological aging and subsequently in offspring of nonagenarian siblings as compared to control subjects to assess the association with biological aging. In chapter 2 to 5 age-related brain changes were assessed beginning at the macrostructural level (chapter 2 and 3) and ending up on the microstructural (chapter 4 and 5). In total, 502 subjects (251 couples) participated in this study of which 370 subjects (194 offspring and 176 control subjects) underwent an MRI scan of the brain. In **chapter 2** automated analysis of brain tissue volumes was applied, i.e. whole brain, grey and white matter volume as well as the volumes of seven subcortical twin structures (amygdala, nucleus accumbens, hippocampus, pallidum, putamen and thalamus) were calculated and compared between offspring and control subjects. Secondly, imaging correlates of cerebral small vessel disease, such as white matter hyperintensities, lacunar brain infarcts and microbleeds, were assessed semi-quantitatively. Results are described in **chapter 3**. **Chapter 4** deals with microstructural brain tissue integrity as measured by diffusion tensor imaging (DTI). For image analysis, two relatively new analysis techniques were used: Voxel-based morphometry (VBM) and tract based spatial statistics (TBSS). Finally, **chapter 5** explores differences in macromolecular brain tissue integrity as assessed using magnetization transfer imaging (MTI) between offspring and control subjects.

The second part of the thesis “Age-related changes of the human brain - modifying factors and risk of mortality” gives one example of a potential modifying factor on age-related changes of the human brain in general and deals with the risk of mortality associated with cerebral microbleeds as a neuroimaging correlate of cerebral small vessel disease. In **chapter 6** we assessed whether coronary artery calcification is associated with age-related vascular brain pathology within the Leiden Longevity Study. **Chapter 7** describes whether cerebral microbleeds are associated with mortality within the PROSPER MRI substudy, which consists of elderly individuals at high risk of or with known vascular disease.

I

Phenotyping the brain in human familial longevity using MRI

2

Brain tissue volumes in familial longevity: the Leiden Longevity Study

Aging Cell, 2012;11:933-9

I. Altmann-Schneider
A.J.M. de Craen
P.E. Slagboom
R.G.J. Westendorp
M.A. van Buchem
A.B. Maier
J. van der Grond

Abstract

Background and purpose:

Atrophy is one of the major age-related changes in the brain. The absence of brain atrophy in elderly individuals reflects deceleration in the process of biological aging. Moreover, results from human twin studies suggest a large genetic influence on the variance of human brain tissue volumes. To investigate the association of brain volumes with exceptional longevity, we tested whether middle-aged to elderly offspring of nonagenarian siblings have larger brain volumes than their spouses.

Methods:

All subjects were from the Leiden Longevity Study. In this study, middle-aged to elderly offspring of nonagenarian siblings, who are predisposed to become long-lived as well, were contrasted to their spouses. Brain tissue volumes were assessed using 3-T MRI.

Results:

No differences in whole brain, grey matter and white matter volume were found. These brain volumes were associated with chronological age in offspring and control subjects (all $P < 0.001$). Left amygdalar volume of the offspring was larger ($P = 0.03$) compared with control subjects (mean volume offspring (cm^3) (95% confidence interval, CI) = 1.39 (1.36–1.42), mean volume control subjects (cm^3) (95% CI) = 1.32 (1.29–1.35)). Association of left amygdalar volume with familial longevity was particularly pronounced when offspring with the oldest long-lived parent were compared with control subjects ($P = 0.01$). Amygdalar volumes were not associated with chronological age in both groups.

Conclusions:

Our findings suggest that the observed association of a larger left amygdalar volume with familial longevity is not caused by a relative preservation of the left amygdala during the course of aging but most likely a result of early development caused by a genetic familial trait.

Introduction

Many neurodegenerative changes occur in the brain with increasing chronological age. One of the major changes is cerebral atrophy [31, 32]. In the last two decades, it has become clear that global and local atrophy are associated with many neurodegenerative diseases and that progression of atrophy is associated with disease progression [33, 34]. The absence of brain atrophy is generally assumed to be associated with a deceleration in the process of biological aging in elderly human individuals [35, 36].

Results from human twin and family studies suggest a large genetic influence on the variance of human brain tissue volumes [37]. Moreover, about 20–30% of the variation in human lifespan is attributable to a heritable component [38, 39]. However, data on the phenotype of human longevity are scarce and, to our knowledge, brain tissue volumes have never been assessed so far in exceptional familial longevity.

The Leiden Longevity Study was designed to investigate factors associated with human longevity. Offspring of long-lived nonagenarian siblings, who are predisposed to become long-lived as well, are contrasted with their spouses [6]. The propensity to become long-lived in the middle-aged to elderly offspring as compared to their spouses is marked by a low incidence of morbidity, beneficial serum levels of lipid and thyroid parameters and preservation of insulin sensitivity [7-9].

To investigate the association of brain tissue volumes with familial longevity, we tested whether individuals enriched for factors of familial longevity have larger

brain tissue volumes compared with their partners by means of magnetic resonance imaging (MRI).

Results

Characteristics of the study population are shown in Table 2.1. In total, 370 subjects participated in the study, 194 offspring of long-lived siblings and 176 control subjects. The mean age was 66 years for the offspring and 65 years for the control subjects. Female fraction was lower among the offspring (43%) compared with the control subjects (61%) (P = 0.001). No differences in handedness and comorbidities were found between the two groups – except for the history of diabetes mellitus, which was significantly higher among the control subjects.

Table 2.1 Characteristics of the study population

	Controls (n = 176)	Offspring (n = 194)
Demographics		
Age (years)	65 (7.4)	66 (6.1)
Women*	108 (61)	84 (43)
Right-handedness	156 (89)	170 (88)
Comorbidities		
Myocardial infarction	5 (3)	3 (2)
Stroke	4 (2)	5 (3)
Hypertension	43 (24)	40 (21)
Diabetes mellitus*	13 (7)	4 (2)
Malignancies	17 (10)	13 (7)

Values are numbers (percentage) for dichotomous variables or means (SD; standard deviation) for continuous variables.

* $P < 0.05$.

Whole brain, grey matter and white matter volumes, unnormalized as well as normalized for skull size, for offspring and control subjects are shown in Table 2.2. No differences in volumes were found between offspring and control subjects.

Table 2.2 Whole brain, grey matter and white matter volumes of offspring and control subjects

Volumes (cm^3)	Controls (n = 176)	Offspring (n = 194)	P
Unnormalized			
Males	(n = 68)	(n = 110)	
Whole brain	1123 (1103-1143)	1149 (1131-1167)	0.23
Grey matter	548 (540-557)	564 (556-572)	0.07
White matter	575 (562-588)	587 (575-598)	0.45
Females	(n = 108)	(n = 84)	
Whole brain	1042 (1029-1056)	1040 (1023-1057)	0.86
Grey matter	530 (523-536)	529 (521-537)	0.67
White matter	513 (504-521)	511 (501-521)	0.98
Normalized*			
Whole brain	1407 (1398-1417)	1406 (1397-1415)	0.67
Grey matter	705 (699-712)	702 (696-708)	0.34
White matter	702 (697-708)	704 (699-710)	0.91

Values are means (95% CI; 95% confidence interval). P-values are adjusted for age and corrected for family relationships among the offspring. * Values are means (95% CI; 95% confidence interval) normalized for skull size. P-values are additionally adjusted for sex.

To assess regional focal differences in cortical thickness in contrast to overall volumetric changes, voxel-based morphometry (VBM) analysis was performed.

VBM results did not reveal any significant focal cortical differences between the two groups. Whole brain, grey matter and white matter volume were associated with chronological age in both offspring and control subjects (Fig. 2.1, all P < 0.001). These volumes were similar in both groups across all chronological age strata.

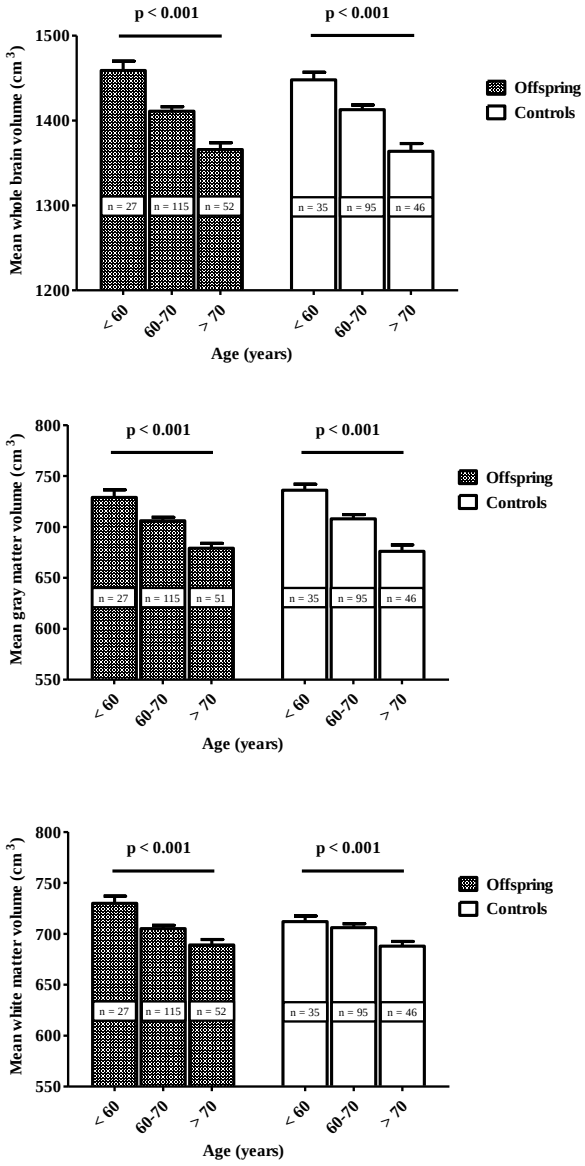

Figure 2.1 shows mean normalized whole brain, grey matter and white matter volumes and their association with chronological age separately for offspring and control subjects. P-values are adjusted for sex. Associations of brain tissue volumes with chronological age were not statistically significant different between both groups, as expressed in the P-value for interaction (P_{int}) (whole brain volume: P_{int} = 0.32, gray matter volume: P_{int} = 0.92, white matter volume: P_{int} = 0.15).

Of all subcortical structures left amygdalar volume of the offspring was larger (P = 0.03) compared with the control subjects (mean volume offspring (cm^3) (95% confidence interval, CI) = 1.39 (1.36–1.42), mean volume control subjects (cm^3) (95% CI) = 1.32 (1.29–1.35)). Figure 2.2 illustrates the output of the automated segmentation method for the right and left amygdala exemplary for one study participant.

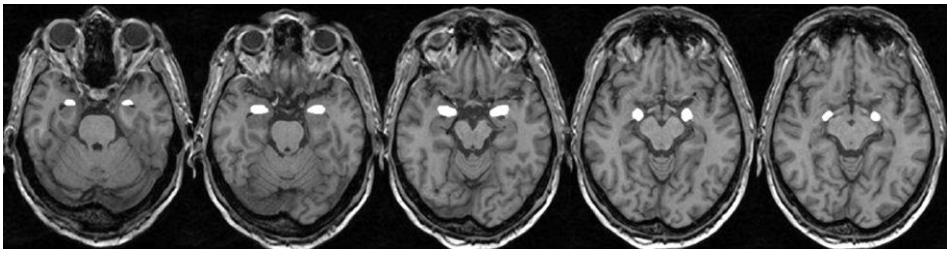

Figure 2.2 The output of the automated segmentation of the right and left amygdala is shown on transverse MRI slices exemplary for one study participant. Right and left amygdala are shown in white colour.

The association of the left and right amygdalar volume with chronological age is shown in Figure 2.3 separately for offspring and control subjects. Both left and right amygdalar volume was not associated with chronological age in both groups.

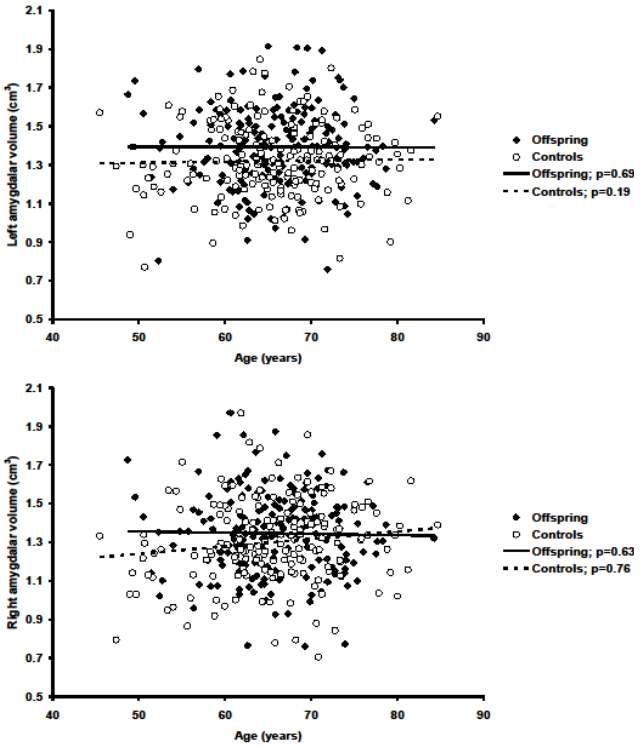

Figure 2.3 The association of left and right amygdalar volume with chronological age is shown separately for offspring (continuous line) and control subjects (broken line).

P-values are adjusted for sex. Associations of amygdalar volumes with chronological age were not statistically significant different between groups, as expressed in the P-value for interaction (P_{int}) (left amygdalar volume: P_{int} = 0.51, right amygdalar volume: P_{int} = 0.46).

To rule out coincidental volumetric findings, a shape analysis of both left and right amygdala was performed for both groups. Figure 2.4 shows the results adjusted for multiple comparisons. All vectors on the left amygdala are pointing outwards, indicating that offspring have an overall larger left amygdala than control subjects. The two blue patches on the left amygdala indicate two highly significant areas of local volume difference between the two groups. All vectors on the right amygdala are pointing outwards as well. The red colour of the right amygdala indicates that, after correction for multiple comparisons, the volume difference between the two groups was not statistically significant. With regard to the two highly significant areas of local volume difference on the mean surface of the left amygdala, a two-dimensional reconstruction of the amygdala using the atlas of the human brain from Mai et al. (2008) [40] showed that the observed areas

of local volume difference belong to the ventral part of the nucleus lateralis and the lateral part of the nucleus centralis of the left amygdala.

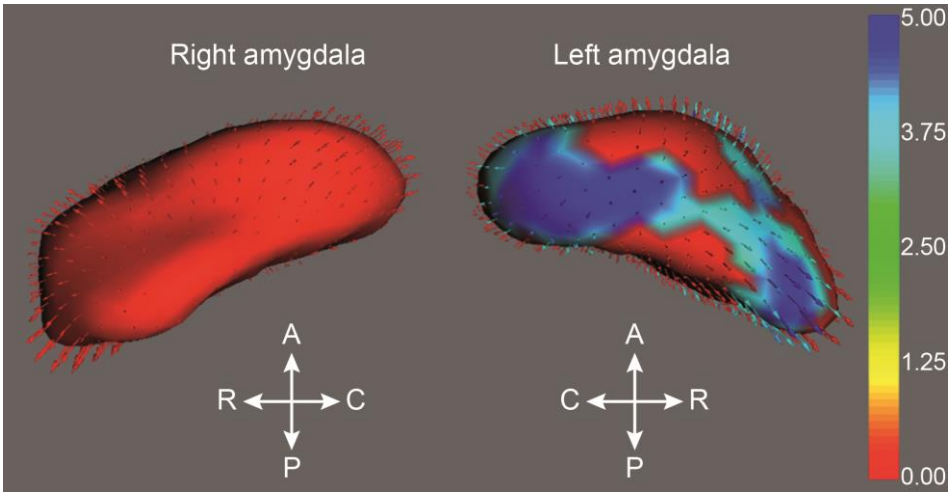

Figure 2.4 shows the results of the shape analysis of right and left amygdala of offspring and control subjects. The 3D reconstructions represent the mean surface of left and right amygdala of the control group. Both amygdalae are shown from lateral. The vectors show the direction of volume change, which would be necessary to transform the mean amygdalar surface of the control group into the mean amygdalar surface of the group of offspring. The colour bar indicates the statistic values. A change of colour from red to blue indicates an increasing statistical significance of the difference between both groups. A, anterior; P, posterior; C, caudal; R, rostral.

To further investigate the association of a larger left amygdalar volume with exceptional familial longevity, offspring were dichotomized based on the mean age (96.8 years) of their long-lived parent and compared with the control subjects separately. Offspring, whose long-lived parent was aged > 96.8 years, had a significantly larger ($P = 0.01$) left amygdalar volume compared with the control subjects (Table 2.3). By contrast, no difference of left amygdalar volume was found between offspring, whose long-lived parent was aged ≤ 96.8 years and control subjects.

Table 2.3 Amygdalar volumes of offspring and control subjects

Amygdalar volumes (cm^3)	Controls (n = 176)	Offspring (n = 194)			
		Group 1 (n = 89)	P	Group 2 (n = 105)	P
Left	1.32 (1.29-1.35)	1.37 (1.33-1.41)	0.32	1.41 (1.37-1.45)	**0.01**
Right	1.30 (1.27-1.33)	1.33 (1.28-1.37)	0.95	1.36 (1.32-1.40)	0.17

Values represent unnormalized means (95% CI; 95% confidence interval). P-values, indicating the statistical significance of the difference in mean amygdalar volumes between offspring group 1 and control subjects and offspring group 2 and control subjects respectively, are adjusted for age and sex and corrected for family relationships among the offspring. Bold indicates significance value.
Group 1: offspring whose long-lived parent was aged ≤ 96.8 years.
Group 2: offspring whose long-lived parent was aged > 96.8 years.

Discussion

Our study shows that middle-aged to elderly individuals, who are enriched for familial factors of longevity, have larger left amygdalar volumes compared with control subjects, whereas no association of the left amygdalar volume with chronological age was found in both groups within an age range of 46–85 years. Familial longevity was not associated with larger whole brain, grey and white matter volumes in middle-aged to elderly individuals.

In contrast to the association of amygdalar volume with the propensity of familial longevity, no difference in association with chronological age was found in both groups. These findings may suggest that the observed increased left amygdalar volume is not caused by a relative preservation of the left amygdala during the course of aging but most likely a result of early development caused by a genetic

familial trait. This hypothesis is further supported by the fact that the association of left amygdalar volume with familial longevity was particularly pronounced when offspring with the oldest long-lived parent were compared with the control subjects. Studies on the genetic influence on the variance of amygdalar volumes in middle-aged to elderly individuals are scarce. In a human twin study, a high heritability of 0.80 for the left and 0.50 for the right amygdalar volume has been described [41]. This supports our hypothesis that offspring of long-lived siblings display larger left amygdalar volumes owing to a genetic predisposition. Structural and functional changes within the human amygdalae have been shown to be associated with several neurodegenerative and neuropsychiatric diseases, such as Alzheimer's disease [42], post-traumatic stress disorder, schizophrenia, major depression disorder [43, 44], bipolar disorder [45], social anxiety disorder [46], or Parkinson's disease [47]. A recent study showed that patients with Alzheimer's disease and elderly schizophrenia patients have significantly lower left amygdalar volumes compared with healthy elderly controls [48]. Moreover, symptoms in schizophrenia patients correlated with a relatively lower left amygdala compared with the right amygdala [48]. Further research is needed to disentangle the consequences of a larger left amygdalar volume in human familial longevity.

Our data do not show any association of amygdalar volume with chronological age in any of the groups. During the last two decades, age-related changes of the amygdalar volume have been assessed in several studies of the aging brain, but results remain controversial. Whereas some studies found an age-related decline of the amygdalar volume [49-52], others found a relative preservation of the amygdalae compared with other brain structures [53-55]. Data about side differences in amygdalar volume measurements are sparse. The mentioned studies either did not differentiate between right and left amygdalar volumes [49] or did not find any side difference [50, 52] with one exception: showing smaller right amygdalar volumes in healthy right-handed elderly individuals compared with young study

participants [51]. However, most of the mentioned studies have assessed the association of amygdalar volume with age cross-sectionally with a wide age range of study subjects, rather small numbers of study participants and using different analysis techniques. All these facts complicate a proper comparison of study results.

Our study showed a strong inverse association of whole brain, grey matter and white matter volume with chronological age. These findings are in line with findings from other studies of the aging brain [31, 32, 55]. There are only a few studies, which have found an age-related volume loss of total white matter volume [32, 56, 57]. However, a regional age-related white matter volume loss has consistently been described in literature [31, 54]. No differences in whole brain, grey matter and white matter volume were found between offspring and control subjects. Human twin and family studies on the influence of genetic factors on the variation of human brain tissue volumes have indicated a high heritability for total brain, grey matter and white matter volume [37]. However, to our knowledge, there have been no studies so far exploring a possible association of these brain volumes with human familial longevity. Our findings suggest that the phenotype of familial human longevity is not reflected by larger volumes of whole brain, grey matter or white matter. As our study participants were relatively young concerning age-related volume loss of brain tissues, further studies are needed to investigate whether differences possibly emerge at a higher mean age.

One of the strengths of our study is the unique study design of comparing middle-aged to elderly individuals, who are enriched for familial factors of longevity, to their spouses. This allowed us to gain more insight into the relevance of age-related changes of the human brain, which can be frequently detected on MRI scans in the general aging population. Second, by including couples if possible,

the influence of the socioeconomic and geographical background was relatively low, which makes the two groups highly comparable in terms of environmental factors. Third, our inclusion algorithm resulted in a large study sample, which allows us to assess even small differences between the two groups. The fact that the study subjects were relatively young concerning age-related changes of the human brain is a limitation of this study. As differences between the two groups are likely to be rather small, a higher mean age of the study groups would probably facilitate the detection of possible differences. Second, our analyses were adjusted for the most common confounding parameters of brain tissue volume analysis: age and sex. It cannot be excluded that cardiovascular risk factors, such as diastolic blood pressure, diabetes or smoking, small vessel disease or physical activity, may (partly) have an additional effect [58, 59]. Also, amygdalar activity and therefore amygdalar volumes might have been affected by differences in emotional aspects and personality factors between groups [60-63]. Finally, as an automated segmentation method was used to segment subcortical structures, deviations may be found when compared to manual segmentation as the golden standard.

In conclusion, this is the first study to our knowledge comparing age-related changes of brain tissue volumes between middle-aged to elderly individuals with a familial predisposition to become long-lived and their spouses. Our findings indicate that, at a mean age of about 66 years, the left amygdalar volume is larger in offspring of nonagenarians compared with their spouses. The lack of an association of amygdalar volume with chronological age and the fact that the association of left amygdalar volume with familial longevity was particularly pronounced when offspring with the oldest long-lived parent were selected, suggest that the observed volume difference is determined by genetic predisposition. The association of a lower amygdalar volume with several

neurodegenerative and neuropsychiatric diseases suggests that middle-aged to elderly individuals, who are enriched for factors of familial longevity, may be less prone to disorders such as Alzheimer's disease.

Methods

Study participants

Participants were included from the LLS, which has been described in more detail elsewhere [6]. The LLS was set up to investigate parameters and pathways associated with and contributing to the longevity phenotype. In short, 421 Dutch Caucasian families were enrolled in the study between 2002 and 2006 based on the following inclusion criteria: (i) there were at least two living siblings per family, who fulfilled the age criteria and were willing to participate; (ii) men had to be aged ≥ 89 years and women had to be aged ≥ 91 years; and (iii) the sib pairs had to have the same parents. Additionally, offspring of these long-lived siblings were included. A survival benefit of approximately 30% has been shown in three generations of LLS families. Hence, the longevity phenotype is inherited in the LLS families. Partners of the offspring of the long-lived siblings were included as a control group as they are likely to have the same age, socioeconomic and geographical background. The current study focused on the investigation of brain imaging markers of the longevity phenotype.

For the current study, participants were recruited from the offspring of the long-lived siblings and their spouses. In total, 502 subjects participated in the study of which 370 subjects (194 offspring and 176 controls) underwent an MRI scan of the brain. Subjects were included as couples, however, some offspring (n = 57) and controls (n = 75) were excluded because of contraindications for MRI. Ninety-three of 194 offspring were related to at least one other offspring, who participated in the current study.

MRI acquisition

All imaging was performed on a whole body MR system operating at a field strength of 3T (Philips Medical Systems, Best, The Netherlands). Three-dimensional T1-weighted images were acquired from all study participants with the following imaging parameters:

TR = 9.7 ms, TE = 4.6 ms, FA = 8°, FOV = 224 x 177 x 168 mm, resulting in a nominal voxel size of 1.17 x·1.17 x·1.4 mm, covering the entire brain with no gap between slices, acquisition time was approximately 5 min.

MRI analysis

All MRI scans were analysed using different tools of FMRIB Software Library (FSL; [64, 65]).

Whole brain volume, grey matter and white matter volumes were calculated using the FSL-tool Structural Image Evaluation, using Normalization, of Atrophy (SIENAX; [66, 67]). SIENAX starts by extracting brain and skull images from the single whole-head input data [68]. The brain image is then affine-registered to MNI152 space [69, 70], using the skull image to determine the registration scaling. This is primarily performed to obtain the volumetric scaling factor, to be used as a normalization for head size. Next, tissue-type segmentation with partial volume estimation is performed [71] to calculate total volume of brain tissue, including separate estimates of volumes of grey matter and white matter.

To assess regional focal differences in cortical thickness in contrast to overall volumetric changes, FSL-VBM, a voxel-based morphometry style analysis [54, 72], was performed. First, structural images were brain-extracted using Brain Extraction Tool [68]. Next, tissue-type segmentation was carried out using FMRIB's Automated Segmentation Tool (FAST4; [71]). The resulting gray matter partial volume images were aligned to MNI152 standard space using the affine registration tool FMRIB's Linear Image Registration Tool [69, 70], followed by

nonlinear registration using FMRIB's Nonlinear Image Registration Tool [73, 74]. The resulting images were averaged to create a study-specific template, to which the native grey matter images were then nonlinearly reregistered. To correct for local expansion or contraction, the registered partial volume images were modulated by dividing by the Jacobian of the warp field. The modulated segmented images were smoothed with an isotropic Gaussian kernel with a sigma of 3 mm. Finally, voxel wise general linear model (GLM) was applied using permutation-based nonparametric testing, correcting for multiple comparisons across space.

FMRIB's Integrated Registration and Segmentation Tool (FIRST) was used to determine the volume of the brain stem and the volumes of the subcortical twin structures nucleus accumbens, amygdala, caudate nucleus, hippocampus, pallidum, putamen and thalamus. FIRST starts by registering all images to MNI152 templates. Second it fits models for all different structures (meshes) to the images and finally applies boundary correction for the volumetric output [75]. The shape/appearance models used in FIRST are constructed from manually segmented images provided by the Center for Morphometric Analysis, MGH, Boston. Most (if not all) manual volumetric methods for amygdala segmentation used coronal plane to delineate amygdala boundary. All amygdalar volumes measures below -3 or above 3 standard deviations were excluded from statistical analysis.

By means of FIRST vertex analysis, local changes of vertex locations of subcortical structures were investigated. This type of analysis does not require boundary correction to be performed, as it works directly with the vertex coordinates (in continuous space) of the underlying meshes. Vertex analysis is performed by carrying out a multivariate test on the three-dimensional coordinates of corresponding vertices. Each vertex is analysed independently, with appropriate multiple-comparison correction methods, for example false

discovery rate or surface- based cluster corrections. The changes in position (global rotation and translation) between different subjects were removed by rigid alignment of the individual meshes. Subsequently, a multivariate F-test was performed for each vertex separately using the multivariate GLM [75].

Statistical analysis

If not otherwise stated, data are presented as mean with standard deviation (SD) (characteristics of the study population) or mean with 95% CI to assess differences between groups. Differences in sex, handedness and comorbidities between offspring and control subjects were calculated using Chi-square tests. Differences in age were tested using independent samples t-tests. Brain tissue volumes were normally distributed. Analyses of differences between offspring and control subjects were assessed using a logistic regression model. Robust standard errors were calculated to correct for family relationships among the offspring. All analyses of differences between offspring and control subjects were adjusted for age and sex. A linear regression model was used to assess the association of the various brain tissue volume measurements with chronological age separately for offspring and control subjects. To test whether there was a significant difference in the association of a certain brain tissue volume with age between offspring and control subjects univariate general linear modelling was used. The P-value for interaction (Pint) estimates the statistical significance of the difference of the association of the brain tissue volumes with chronological age between the two groups. For statistical analyses, SPSS software for windows (version 17.0.1; SPSS, Chicago, IL, USA) was used. Robust standard errors were calculated with STATA software for windows (version 10; STATA, College Station, TX, USA).

3

Lower susceptibility to cerebral small vessel disease in human familial longevity: the Leiden Longevity Study

Stroke, 2013;44:9-14

I. Altmann-Schneider
J. van der Grond
P.E. Slagboom
R.G.J. Westendorp
A.B. Maier
M.A van Buchem
A.J.M. de Craen

Abstract

Background and purpose:

On MRI, cerebral white matter lesions, lacunar infarcts, and cerebral microbleeds are common imaging correlates of cerebral small vessel damage in apparently healthy elderly individuals. We investigated whether middle-aged to elderly offspring of nonagenarian siblings, who are predisposed to become long-lived as well, have a lower prevalence of white matter lesions, lacunar infarcts, and cerebral microbleeds than control subjects.

Methods:

All subjects were from the Leiden Longevity Study. In this study, middle-aged to elderly offspring of nonagenarian siblings, who are predisposed to become long-lived as well, were contrasted to their spouses. Cerebral small vessel disease was assessed using 3-T MRI.

Results:

Offspring were less likely to have severe periventricular frontal caps (odds ratio (OR), 0.3; 95% confidence interval (CI), 0.1–1.1; P trend = 0.01) and severe periventricular bands (OR, 0.4; 95% CI, 0.2–0.8; P trend = 0.02). Moreover, offspring were less likely to have frontal (OR, 0.4; 95% CI, 0.2–0.9; P trend = 0.05), parietal (OR, 0.4; 95% CI, 0.1–0.9; P trend = 0.001), temporal (OR, 0.3; 95% CI, 0.1–0.8; P trend = 0.004), and occipital subcortical white matter lesions (OR, 0.3; 95% CI, 0.1–0.6; P trend = 0.001). Prevalence of lacunar infarcts also was lower in offspring (OR, 0.3; 95% CI, 0.1–1.1; P = 0.07). Prevalence of microbleeds was not significantly different in offspring and control subjects.

Conclusions:

Exceptional familial longevity is associated with a lower susceptibility to white matter lesions and lacunar infarcts, but not cerebral microbleeds.

Introduction

Cerebral small vessel disease is common in old age [76]. On MRI, cerebral white matter lesions (WML), lacunar infarcts, and cerebral microbleeds (CMB) frequently can be detected in apparently healthy elderly individuals as imaging correlates of cerebral small vessel damage [13, 77, 78]. Presence of WML, lacunar infarcts, and CMB in the elderly has been shown to be associated with cerebrovascular disease, such as ischemic stroke or cerebral haemorrhage [79-81], progression of these diseases [82], and increased mortality risk [20, 79, 83]. For WML, a high degree of heritability has been reported [84, 85]. The relative absence of WML, lacunar infarcts, and CMB thus may reflect a decelerated process of biological aging and serve as a marker for the phenotype of human longevity.

The Leiden Longevity Study was designed to investigate factors associated with human longevity. Offspring of long-lived nonagenarian siblings, who are predisposed to become long-lived as well, were contrasted to their spouses [6]. The propensity to become long-lived in the middle-aged to elderly offspring as compared with their spouses is marked by a low incidence of morbidity, beneficial serum levels of lipid and thyroid parameters, preservation of insulin sensitivity, and a lower prevalence of myocardial infarction, hypertension, diabetes mellitus, and use of cardiovascular medication [7-9, 86].

To study whether the phenotype of human familial longevity also is reflected by a lower susceptibility to cerebral small vessel disease, we investigated whether middle-aged to elderly individuals, who are enriched for familial factors of longevity, have a lower WML load and a lower amount of lacunar infarcts and CMB compared with their spouses using MRI.

Methods

Study participants

Subjects were included from the Leiden Longevity Study, which has been described in more detail elsewhere [6]. In short, 421 Dutch white families were enrolled in the study between 2002 and 2006 based on the following inclusion criteria: (1) there were at least 2 living siblings per family who fulfilled the age criteria and were willing to participate; (2) men had to be aged ≥ 89 years and women had to be aged ≥ 91 years; and (3) the sib pairs had to have the same parents. Additionally, offspring of these long-lived siblings were included because they have a 35% lower mortality rate compared with the general population. Their partners, who share the same socioeconomic and geographic background, were enrolled as the age-matched control group [6].

For the current study, subjects were recruited from the offspring of the long-lived siblings and their spouses. In total, 502 subjects (251 couples) participated in the current study, of which 370 subjects (194 offspring and 176 control subjects) underwent an MRI scan of the brain. Some offspring (n=57) and control subjects (n=75) were excluded because of contraindications for MRI. Of 194 offspring, 93 were related to at least one other offspring who participated in the current study. The Medical Ethical Committee of the Leiden University Medical Centre approved the study, and written informed consent was obtained from all subjects. The study was performed in accordance with institutional guidelines.

MRI acquisition

All imaging was performed on a whole-body magnetic resonance system operating at a field strength of 3-T (Philips Medical Systems). Three-dimensional (3-D) T1-weighted, T2-weighted, fluid attenuated inversion recovery (FLAIR), and T2*-weighted images were acquired with the following imaging parameters.

3-D T1-Weighted Images

Repetition time was 9.7 ms, time to echo was 4.6 ms, flip angle was 8°, and field of view was 224×177×168 mm, resulting in a nominal voxel size of 1.17×1.17×1.4 mm, covering the entire brain and with no gap between slices. Acquisition time was ≈5 minutes.

T2-Weighted Images

Repetition time was 4200 ms, time to echo was 80 ms, flip angle was 90°, field of view was 224×180×144 mm, matrix size was 448×320, and 40 transverse slices covered the entire brain, with a slice thickness of 3.6 mm with no gap between slices.

FLAIR

Repetition time was 11 000 ms, time to echo was 125 ms, flip angle was 90°, field of view was 220×176×137 mm, matrix size was 320×240, and 25 transverse slices covered the entire brains, with a slice thickness of 5 mm with no gap between slices.

T2-Weighted Images*

Repetition time was 45 ms, time to echo was 31 ms, flip angle was 13°, and field of view was 250×175×112 mm.

Because of technical problems, T2-weighted and FLAIR images were available for 368 subjects (194 offspring and 174 control subjects) and T2*-weighted images were available for 285 subjects (149 offspring and 136 control subjects).

MRI analysis

Cerebral white matter lesions and lacunar infarcts

MRI scans were visualized using the freely available software Medical Image Processing, Analysis, and Visualization (MIPAV). WML and lacunar infarcts were analysed blinded to subject identity, age, sex, and affiliation to the study group. WML were defined as areas within the cerebral white matter with

increased signal intensity on both FLAIR and T2-weighted images and without mass effect. WML were rated according to a slightly modified version of the semi-quantitative rating scale of Scheltens et al. [1]. Periventricular and subcortical WML were rated separately, and semi-quantitative regional scores were obtained by taking the size, amount, and anatomical distribution of the high signal abnormalities into account (Figure 3.1). For each of these two categories, more detailed scores for further anatomical subdivisions are provided.

Periventricular white matter lesions			
Caps	occipital	0/1/2	0 = absent
	frontal	0/1/2	1 = ≤ 5 mm
Bands lateral ventricles		0/1/2	2 = > 5 mm and < 10 mm
Subcortical white matter lesions			
Frontal		0/1/2/3/4/5/6	0 = no abnormalities
Parietal		0/1/2/3/4/5/6	1 = < 4 mm, n ≤ 5
Occipital		0/1/2/3/4/5/6	2 = < 4 mm, n > 5
Temporal		0/1/2/3/4/5/6	3 = 4-10 mm, n ≤ 5
			4 = 4-10 mm, n > 5
			5 = ≥ 10 mm, n ≥ 1
			6 = confluent

Figure 3.1 Slightly modified version of the semi-quantitative rating scale of Scheltens et al.[1]

Presence and number of lacunar infarcts were assessed on FLAIR, T2-weighted, and 3-D T1-weighted images. Lacunar infarcts were defined as parenchymal defects within the cerebral white matter not extending into the cortical grey matter, with a signal intensity centrally corresponding to that of cerebrospinal fluid on all three imaging sequences, surrounded by a rim of increased signal intensity on FLAIR. Diameter of lacunar infarcts was defined to be > 2 mm. To distinguish lacunar infarcts from normal dilated perivascular spaces (Virchow-Robin-Spaces), lesions within the lower one-third of the corpus striatum of the basal ganglia and a diameter of < 2 mm were excluded [87].

Cerebral microbleeds

MRI scans were visualized using the freely available software MIPAV. CMB were analysed blinded to subject identity, age, sex, and affiliation to the study group. CMB were defined as focal areas of signal void on T2-weighted images,

which increased in size on T2*-weighted images (blooming effect). In this way, CMB were distinguished from vascular flow voids. Symmetric hypointensities in the basal ganglia, likely to represent calcifications or nonhaemorrhagic iron deposits, were disregarded [25]. For each subject, the number and localization (corticosubcortical junction, deep white matter, and basal ganglia) were recorded.

Statistical analysis

If not otherwise stated, data are presented as mean with SD (characteristics of the study population) or odds ratios (ORs) with 95% CI to assess differences among groups. Differences in sex, history of hypertension, diabetes mellitus, smoking, myocardial infarction, and stroke between offspring and control subjects were calculated using χ^2 tests. Differences in age, body mass index, and levels of cholesterol were tested using independent samples t tests. To assess differences in WML load, presence of lacunar infarcts, and CMB between offspring and control subjects, a logistic regression model was applied. Study participants with no lesions were set as a reference group and ORs were calculated for all other groups relative to the reference group. The P value for trend indicates whether the OR increases with increasing degree of severity of a certain type of lesion. All analyses of differences between offspring and control subjects were adjusted for age and sex (Model 1) and additionally for cardiovascular risk factors (history of hypertension, diabetes mellitus, myocardial infarction, stroke and smoking, body mass index, and cholesterol; Model 2). Robust standard errors were calculated to correct for family relationships among the offspring. Significance thresholds were set at $P < 0.05$. For statistical analysis, SPSS software for windows (version 17.0.1; SPSS) was used. Robust standard errors were calculated with Stata statistical software for windows (version 10; Stata).

Results

Characteristics of the study population are shown in Table 3.1. In total, 368 subjects participated in the study (194 offspring of long-lived siblings and 174 control subjects). The mean age was 66 years for offspring and 65 years for control subjects, with a significantly lower female percentage of 43% among offspring compared with 61% among control subjects (P = 0.001). All analyses of differences between offspring and control subjects were, therefore, adjusted for sex. Moreover, significantly more control subjects had a history of diabetes mellitus compared with the offspring. No differences were found concerning other cardiovascular risk factors. Five offspring (3%) and four control subjects (3%) had a history of clinical stroke.

Table 3.1 Characteristics of the study population

	Offspring (n = 194)	Controls (n = 174)
Demographics		
Age (years)	66 (6)	65 (7)
Women*	84 (43)	106 (61)
Cardiovascular risk factors		
Hypertension	40 (23)	43 (28)
Diabetes mellitus*	4 (2)	13 (8)
Myocardial infarction	3 (2)	5 (3)
Stroke	5 (3)	4 (3)
Total cholesterol (mmol/L)	5.65 (1.26)	5.71 (1.17)
Smoking	20 (10)	24 (14)
Body mass index (kg/m^2)	25.2 (3.3)	25.5 (3.4)

Values are numbers (percentage) for dichotomous variables or means (standard deviation) for continuous variables. * $P < 0.05$.

Different degrees of severity of periventricular and subcortical WML are shown in Figure 3.2. Prevalence of periventricular WML in offspring and control subjects is shown in Table 3.2. Offspring of long-lived siblings were less likely to have severe frontal caps compared with control subjects (OR, 0.3; 95% CI, 0.1–1.1; P trend = 0.01), which remained after additional adjustment for cardiovascular risk factors (P trend=0.03). Moreover, offspring of long-lived siblings were less likely to have severe periventricular bands (OR, 0.4; 95% CI, 0.2–0.8; P trend = 0.02). After additional adjustment for cardiovascular risk factors, effect estimates remained similar, whereas significance attenuated (P trend = 0.06). Prevalence of occipital caps was not significantly different between the 2 groups.

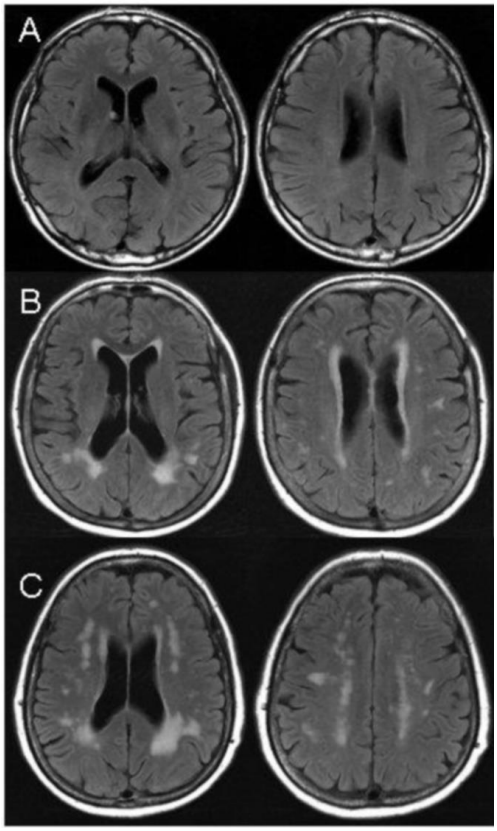

Figure 3.2 Different degrees of periventricular and subcortical white matter lesions (WML) on magnetic resonance imaging (MRI): (A) subject without WML, (B) subject with a severe degree of frontal and occipital caps and periventricular bands (score 2/2/2), and (C) subject with a severe degree of subcortical WML (score 6/6/6/6).

Table 3.2 Periventricular white matter lesion load in offspring and control subjects

	Offspring (n = 194)	Controls (n = 174)	OR (95% CI) Model 1	P	OR (95% CI) Model 2	P
Frontal caps						
0	10 (5)	5 (3)	1.0 (ref)		1.0 (ref)	
1	140 (72)	109 (63)	0.6 (0.2-1.8)	0.35	0.6 (0.2-1.8)	0.37
2	44 (23)	60 (35)	0.3 (0.1-1.1)	0.07	0.3 (0.1-1.1)	0.09
P trend				0.01		0.03
Bands						
0	40 (21)	24 (14)	1.0 (ref)		1.0 (ref)	
1	134 (69)	122 (70)	0.6 (0.4-1.1)	0.14	0.6 (0.3-1.1)	0.14
2	20 (10)	28 (16)	0.4 (0.2-0.8)	0.02	0.4 (0.2-1.0)	0.06
P trend				0.02		0.06
Occipital caps						
0	78 (40)	59 (34)	1.0 (ref)		1.0 (ref)	
1	93 (48)	86 (49)	0.8 (0.5-1.3)	0.40	0.7 (0.4-1.2)	0.25
2	23 (12)	29 (17)	0.6 (0.3-1.1)	0.10	0.5 (0.2-1.1)	0.11
P trend				0.11		0.09
Total score						
0	6 (3)	2 (1)	1.0 (ref)		1.0 (ref)	
1 (1-3)	145 (75)	113 (65)	0.4 (0.1-2.0)	0.22	0.4 (0.1-2.0)	0.21
2 (4-6)	43 (22)	59 (34)	0.2 (0.04-1.1)	0.05	0.2 (0.04-1.1)	0.05
P trend				0.01		0.01

Values are numbers (percentage) or OR (odds ratios) (95% CI, confidence interval). P values are adjusted for age and sex and corrected for family relationships among the offspring (Model 1), and are additionally adjusted for cardiovascular risk factors (Model 2).

Prevalence of subcortical WML for offspring and control subjects is shown in Table 3.3. Offspring of long-lived siblings were less likely to have frontal (OR,

0.4; 95% CI, 0.2–0.9; P trend = 0.05), parietal (OR, 0.4; 95% CI, 0.1–0.9; P trend = 0.001), temporal (OR, 0.3; 95% CI, 0.1–0.8; P trend = 0.004), and occipital subcortical WML (OR, 0.3; 95% CI, 0.1–0.6; P trend = 0.001). All associations remained similar after additional adjustment for cardiovascular risk factors.

Prevalence of lacunar infarcts was low, with a nonsignificant difference between offspring (2%) and control subjects (5%) (OR, 0.3; 95% CI, 0.1–1.1; Table 3.4). Prevalence of CMB was similar in offspring (14%) and control subjects (13%) (OR, 1.0; 95% CI, 0.5–2.1). Additional adjustment for cardiovascular risk factors did not alter the results.

Table 3.3 Subcortical white matter lesion load of offspring and control subjects

	Offspring (n = 194)	Controls (n = 174)	OR (95% CI) Model 1	P	OR (95% CI) Model 2	P
Frontal						
0	37 (19)	25 (14)	1.0 (ref)		1.0 (ref)	
1 (1-3)	132 (68)	111 (64)	0.8 (0.5-1.5)	0.60	0.9 (0.5-1.7)	0.76
2 (4-6)	25 (13)	38 (22)	0.4 (0.2-0.9)	0.05	0.5 (0.2-1.1)	0.13
P trend				0.05		0.13
Parietal						
0	95 (49)	52 (30)	1.0 (ref)		1.0 (ref)	
1 (1-3)	87 (45)	106 (61)	0.4 (0.3-0.7)	< 0.001	0.4 (0.3-0.7)	0.001
2 (4-6)	12 (6)	16 (9)	0.4 (0.1-0.9)	0.03	0.4 (0.2-1.1)	0.07
P trend				0.001		0.004
Temporal						
0	100 (52)	67 (39)	1.0 (ref)		1.0 (ref)	
1 (1-3)	85 (44)	92 (53)	0.5 (0.4-0.9)	0.01	0.5 (0.3-0.9)	0.01
2 (4-6)	9 (5)	15 (9)	0.3 (0.1-0.8)	0.02	0.4 (0.1-1.1)	0.08
P trend				0.004		0.01
Occipital						
0	128 (66)	96 (55)	1.0 (ref)		1.0 (ref)	
1 (1-3)	52 (27)	48 (28)	0.7 (0.4-1.1)	0.16	0.9 (0.5-1.5)	0.70
2 (4-6)	14 (7)	30 (17)	0.3 (0.1-0.6)	0.001	0.3 (0.1-0.7)	0.01
P trend				0.001		0.02
Total score						
0	31 (16)	18 (10)				
1 (1-6)	109 (56)	83 (48)	0.8 (0.4-1.5)	0.48	0.9 (0.4-1.8)	0.74
2 (7-12)	35 (18)	41 (24)	0.5 (0.2-1.0)	0.06	0.5 (0.2-1.1)	0.09
3 (13-24)	19 (10)	32 (18)	0.3 (0.1-0.7)	0.01	0.4 (0.1-1.0)	0.07
P trend				0.001		0.01

CI indicates confidence interval; OR, odds ratio. P values are adjusted for age and sex and corrected for family relationships among the offspring (Model 1), and are additionally adjusted for cardiovascular risk factors (Model 2). Values are numbers (percentage) or OR (95% CI).

Table 3.4 Lacunar infarcts and cerebral microbleeds of offspring and control subjects

	Offspring (n = 194)	Controls (n = 174)	OR (95% CI) Model 1	P	OR (95% CI) Model 2	P
Lacunar infarcts						
Absent	190 (97.9)	166 (95.4)	1.0 (ref)		1.0 (ref)	
Present	4 (2.1)	8 (4.6)	0.3 (0.1-1.1)	0.07	0.5 (0.1-1.8)	0.27
CMB						
Absent	128 (86)	118 (87)	1.0 (ref)		1.0 (ref)	
Present	21 (14)	18 (13)	1.0 (0.5-2.1)	0.92	1.2 (0.5-2.6)	0.73

CI indicates confidence interval; OR, odds ratio. Values are numbers (percentage) or OR (95% CI) adjusted for age and sex and corrected for family relationships among the offspring (Model 1), and are additionally adjusted for cardiovascular risk factors (Model 2).

Discussion

This study shows that middle-aged to elderly individuals who have a familial higher susceptibility to become long-lived have a lower periventricular as well as subcortical WML load and a lower prevalence of lacunar infarcts compared with control subjects independent of their cardiovascular risk profile. In contrast, prevalence of CMB was similar in both groups.

Our findings suggest that exceptional familial longevity is associated with a lower susceptibility to WML as well as lacunar infarcts. Studies on the genetic determinants of cerebral WML have reported a high degree of heritability in younger study subjects with a low prevalence of cerebral WML, suggesting WML to be an excellent genetic marker of brain aging [84, 85]. The *Notch3* gene, apolipoprotein E (*APO E*) gene, and the angiotensin-converting enzyme (*ACE*) gene are examples of genes that have been identified to be associated with the formation of WML [88-90]. However, it is not known, so far, whether the genetic

difference in the susceptibility to the formation of WML is because of genetic differences in the aging process itself or because of a genetically determined different susceptibility to cardiovascular damage or both [84]. In our study, additional adjustment for cardiovascular risk factors did not change the association of exceptional familial longevity with a lower prevalence of periventricular as well as subcortical WML, suggesting a genetically determined lower susceptibility of the offspring to the formation of cerebral WML in the course of aging, regardless of their cardiovascular risk profile. Several genes have been identified to be associated with the presence of lacunar infarcts [90-93]. In this study, a lower prevalence of lacunar infarcts was associated with familial longevity, barely reaching statistical significance. Reported prevalence of lacunar infarcts in the general elderly population ranges from 5% to ≈30% [94-96]. Thus, overall prevalence in our study population (3%) was relatively low. Because the prevalence of lacunar infarcts increases with age, with a low prevalence at an age of ≈60 years, our study subjects were, with a mean age of 66 years, relatively young for the detection of lacunar infarcts [97]. A higher mean age of the study population could have increased the detected difference in prevalence of lacunar infarcts between both groups. Additional adjustment for cardiovascular risk factors did not alter the results, suggesting that offspring of long-lived siblings have a lower susceptibility to the formation of lacunar infarcts during the aging process compared with control subjects, regardless of their cardiovascular risk profile. However, the low prevalence of lacunar infarcts hampers a proper interpretation of the data.

In the Leiden Longevity Study, the propensity to become long-lived in the middle-aged to elderly offspring as compared with control subjects is marked by a low incidence of morbidity, beneficial serum levels of lipid and thyroid parameters, preservation of insulin sensitivity, and a lower prevalence of myocardial infarction, hypertension, diabetes mellitus, and use of cardiovascular

medication [7-9, 86]. In the current substudy, offspring also showed a lower prevalence of hypertension, diabetes mellitus, and myocardial infarction, with the difference only reaching statistical significance for history of diabetes mellitus. This is most likely because of the lower number of study participants as compared with the original cohort.

Exceptional familial longevity was not associated with a lower prevalence of CMB. The age-specific prevalence of CMB has been reported to increase from ≈7% in individuals aged 45 to 50 years to ≈36% in individuals aged ≥ 80 years in the population-based Rotterdam Scan Study [98]. The *APOE ε4* gene was associated with the presence of strictly lobar CMB [98, 99]. Overall, prevalence of CMB in our study confirms the age-stratified prevalence of CMB reported in the Rotterdam Scan Study (mean age of our study population, 66 years; age range, 46–85 years) [98]. Prevalence of CMB was similar in offspring and control subjects, suggesting that the propensity of familial longevity is not associated with a lower susceptibility to CMB.

One of the strengths of our study is the unique study design of comparing middle-aged to elderly individuals, who have a genetically determined higher susceptibility to become long-lived, with control subjects. This will allow us to gain more insight in the relevance of age-related changes of the human brain, which can be frequently detected on MRI scans in the general aging population. Second, by including the partners of the offspring of the long-lived siblings as the control group, the two groups were highly comparable concerning their socioeconomic and geographic background. Finally, our inclusion algorithm resulted in a large study sample, which allows us to investigate even small differences between the two groups.

The fact that the study subjects were relatively young concerning age-related changes of the human brain belongs to the limitations of this study. Because differences between the two groups are likely to be small, a higher mean age of

the study groups would probably facilitate the detection of possible differences. Second, some individual categories did not reach statistical significance or did not remain significant after full adjustment for cardiovascular risk factors. The described phenomenon mostly appeared in categories with a low number of study participants, which have relatively low statistical power and were usually the most severe categories. However, a clear dose–response could be observed for almost all abnormalities in both models, which was expressed in decreasing ORs with increasing severity of the lesions. This also was indicated by the P value for trend.

To the best of our knowledge, this is the first study to compare imaging markers of cerebral small vessel disease between elderly individuals with a familial predisposition to become long-lived and their partners. Our findings indicate that at a mean age of 66 years, exceptional familial longevity is associated with a lower susceptibility to WML and lacunar infarcts but not CMB. Because this association did not change after additional adjustment for cardiovascular risk factors, it is likely that differences in the susceptibility to WML and lacunar infarcts between offspring of long-lived siblings and control subjects are because of genetic differences in the process of aging and are not driven by a genetically determined different susceptibility to cardiovascular damage.

4

Preserved white matter integrity is a marker of familial longevity

Ann Neurol, 2013;74:883-92

I. Altmann-Schneider
A.J.M. de Craen
I.M. Veer
A.A. van den Berg-Huysmans
P.E. Slagboom
R.G.J. Westendorp
M.A. van Buchem
J. van der Grond

Abstract

Background and purpose:

Brain tissue integrity is highly heritable, and its decline is a common phenomenon of aging. This study aimed to determine whether the phenotype of familial longevity is marked by a relative preservation of brain tissue microstructure.

Methods:

Participants were enrolled in the Leiden Longevity Study. In total, 185 middle-aged to elderly offspring of nonagenarian siblings, who were enriched for familial factors of longevity, were contrasted with 171 environment- and age-matched controls. All subjects underwent 3T whole brain magnetic resonance diffusion tensor imaging.

Results:

Voxel-wise analysis revealed widespread age-related decrease of white matter fractional anisotropy and increases of axial, radial, and mean diffusivity (all $P < 0.003$). Offspring showed higher mean white matter fractional anisotropy (mean (standard error): offspring, 0.3232 (0.0009); controls, 0.3212 (0.0009); $P = 0.04$) compared to control subjects independent of cardiovascular risk factors. When differences in white matter diffusion parameters between offspring and control subjects were assessed voxel-wise, offspring showed higher white matter fractional anisotropy and lower white matter radial diffusivity predominantly in the callosal genu and body (both $P < 0.003$). With the effect of chronological age on white matter microstructure taken into account, offspring can be considered 4.5 years "biologically younger" compared to control subjects with regard to white matter integrity.

Conclusions:

Both middle-aged to elderly offspring of nonagenarian siblings and control subjects show common age-related decline of white matter integrity, but it is less marked in the callosal genu and body in the offspring. This corresponds to a biological age benefit of 4.5 years of the offspring as compared to the control subjects.

Introduction

Loss of brain tissue integrity is common in old age and can be assessed noninvasively by using magnetic resonance diffusion tensor imaging (DTI) [100, 101]. DTI contrast is based on diffusion of water protons, which is characterized by random (isotropic) motion in regions with no constraints. Diffusion within tissues is usually not random; it is instead restricted (anisotropic) by physiological boundaries such as fibre components, which results in different diffusion rates dependent on the diffusion direction [102]. Commonly, the rate of diffusion, or diffusivity, is described in three perpendicular directions per voxel. For white matter, diffusivity along the axons is assumed to be the largest and is characterized by the eigenvalue L1 (axial diffusivity, AxD). The rate of diffusion perpendicular to the axial diffusivity is called radial diffusivity (RD) and is described by the mean of the eigenvalues L2 and L3 [103]. Fractional anisotropy (FA) is a summary measure comprising the three-dimensional (3D) diffusion information and reflecting the orientational coherence of the underlying tissue. In contrast, mean diffusivity (MD) is a measure of diffusion magnitude within a certain voxel without orientational information, representing the mean of the three eigenvalues L1, L2, and L3 [104]. Due to its microstructural organization, white matter is by far the most frequently assessed brain tissue in DTI studies of the aging brain, particularly because DTI allows the detection of even subtle white matter damage that is not visible using conventional magnetic resonance imaging (MRI) and therefore yields additional insight into age-related neurodegenerative brain changes.

Studies on age-related changes of white matter integrity consistently report a decline of white matter FA [100, 105]. For axial, radial, and mean diffusivity, different patterns of age-related changes have been reported for different brain regions [106,

[107]. Moreover, an anterior–posterior gradient of age-related loss of white matter integrity has been described [101, 108, 109], which is also reflected by the age-related deterioration of predominantly frontally located functional networks [108]. This anterior–posterior gradient is assumed to be based on late-myelinating regions, such as the white matter of the frontal lobes or the genu of the corpus callosum, being composed of thinner axons with a higher vulnerability to age-related myelin breakdown as compared with early myelinating brain regions [110-112]. According to human twin studies, white matter integrity, even in old age, is under significant genetic control [113, 114]. Thus, a relative preservation of brain tissue integrity against age-related neurodegeneration might reflect a decelerated process of biological aging that is at least partly genetically determined.

The Leiden Longevity Study was designed to investigate factors associated with human longevity. Offspring of long-lived nonagenarian siblings, who are predisposed to become long-lived as well, were contrasted with their spouses [6]. In middle-aged to elderly offspring, the propensity to become long-lived is marked by beneficial serum levels of lipid and thyroid parameters; preserved insulin sensitivity; lower prevalence of myocardial infarction, hypertension, diabetes mellitus, and use of cardiovascular medication; and lower prevalence of cerebral white matter lesions (WML) as well as lacunar infarcts [7-9, 86, 115].

The primary aim of the current study was to study whether the phenotype of familial longevity is reflected by a relative preservation of brain tissue microstructural integrity. Additionally, changes of brain tissue integrity with chronological age were assessed in the whole study population to enable proper differentiation between biological and chronological aging.

Methods

Study participants

Subjects were participants in the Leiden Longevity Study, which has been described in more detail elsewhere [6]. In short, 421 Dutch Caucasian families were enrolled in the study between 2002 and 2006 based on the following inclusion criteria: (1) there were at least two living siblings per family, who fulfilled the age criteria and were willing to participate, (2) men had to be aged ≥ 89 years and women had to be aged ≥ 91 years, and (3) the sib pairs had to have the same parents. Additionally, offspring of these long-lived siblings were included because they have a 35% lower mortality rate compared with the general population. Their partners, who shared the same socioeconomic and geographical background, were enrolled as an environment and age-matched control group [6, 86]. All couples in which the partner met the inclusion criteria for the offspring group were excluded from the study.

The current study focused on the offspring of the long-lived siblings and their spouses. In total, 502 subjects (251 couples) participated in the study, 370 of whom underwent an MRI scan of the brain (194 offspring, 176 control subjects). Some offspring (n = 57) and control subjects (n = 75) were excluded due to contraindications for MRI. Contraindications were determined according to the standardized MRI patient questionnaire of the Leiden University Medical Centre. Excluded subjects were comparable to included subjects with regard to age, sex, and comorbidities. Ninety-three of 194 offspring were related to at least one other offspring in the study. The Medical Ethical Committee of the Leiden University Medical Centre approved the study, and written informed consent was obtained from all subjects.

MRI acquisition

Imaging was performed on a whole body magnetic resonance system operating at a field strength of 3T (Philips Medical Systems, Best, The Netherlands). 3D T1-weighted images were acquired with the following imaging parameters: repetition time (TR) = 9.7 milliseconds, echo time (TE) = 4.6 milliseconds, FA = 8°, field of view (FOV) = 224 x 177 x 168 mm, resulting in a nominal voxel size of 1.17 x 1.17 x 1.4 mm, covering the entire brain with no gap between slices; acquisition time was approximately 5 minutes. The imaging parameters for DTI images were as follows: TR = 9,592 milliseconds, TE = 56 milliseconds, FA = 90°, FOV = 220 x 220 x 128 mm, matrix size 112 x 110, 64 transverse slices to cover the entire brain with a slice thickness of 2 mm with no gap between slices, 32 measurement directions, and b-value = 1,000.

Due to technical problems, DTI images were only available for 360 subjects (189 offspring, 171 control subjects). Four subjects (four offspring) were excluded from data analyses because of severe scan artefacts.

MRI analysis

All MRI analyses were performed with blinding to the subject status (offspring vs control subjects). For analysis of DTI scans, different tools of the Functional MRI of the Brain (FMRIB) Software Library (FSL) software package were used [64, 65].

Pre-processing

The individual raw diffusion tensor images were pre-processed to create individual FA, L1, L2, L3, and MD images using FDT (FMRIB's Diffusion Toolbox) tools [116-118]. The original images were corrected for effects of head movement and eddy currents in the gradient coils, which induce stretches and shears in the DTI images, using affine registration to a non–diffusion-weighted

reference volume. A diffusion tensor model was fitted to the eddy current-corrected images to create individual FA, L1, L2, L3, and MD images.

Global quantification of brain tissue FA, AxD, RD, and MD

3D T1-weighted images were skull stripped using BET (Brain Extraction Tool) [68] and subsequently segmented using FAST (FMRIB's automated segmentation tool)[71] and FIRST (FMRIB's integrated registration and segmentation tool) [75], resulting in individual brain masks for white matter, grey matter, and the following subcortical grey matter structures: amygdala, caudate nucleus, hippocampus, nucleus accumbens, pallidum, putamen, and thalamus. All segmented brain structures were aligned into common space using the linear registration tool FLIRT (FMRIB's linear image registration tool) [69, 70]. Mean FA, AxD, RD, and MD values were calculated for the regions of interest.

Voxel-based analysis of white matter FA, AxD, RD, and MD

Voxel-wise statistical analysis of white matter FA data was performed using Tract-Based Spatial Statistics (TBSS) [119]. All subjects' FA data were aligned into common space using the nonlinear registration tool FNIRT (FMRIB's nonlinear image registration tool) [73, 74]. A mean FA image was created and thinned to create a mean FA skeleton representing the centres of all tracts common to the group. Each subject's aligned FA data were projected onto this skeleton. Likewise, individual AxD, RD, and MD images were prepared for voxel-wise statistics.

Statistical analysis

If not otherwise stated, data are presented as mean with standard deviation or mean with standard error (SE) to assess differences between groups. Differences in sex, handedness, and comorbidities between offspring and control subjects were calculated using chi-square tests. Differences in age were tested using

independent samples t tests. A linear regression model was used to assess the association of diffusion parameters with chronological age in the whole study population adjusted for sex and affiliation with the offspring or control group. For all analyses concerning the association between diffusion parameters and chronological age, Bonferroni post hoc test was used to correct for multiple comparisons. Allowing for n = 36 comparisons, the significance threshold was set at $p < 0.0014$. Differences in diffusion parameters between offspring and control subjects were assessed using a linear regression model, adjusted for age and sex. To take the potential effect of cardiovascular comorbidities and risk factors on brain tissue DTI parameters into account, the following models were additionally used in the regression analysis. First, all study subjects with a history of stroke or myocardial infarction were excluded from analysis, which was adjusted for age and sex. Second, the analysis was additionally adjusted for history of diabetes mellitus, and third it was additionally adjusted for history of hypertension. Robust standard errors were calculated to correct for family relationships among the offspring. Statistical tests concerning the association between diffusion parameters and biological age were not Bonferroni corrected. For statistical analyses, Statistical Package for the Social Sciences (SPSS) software for Windows (version 20.0.1; IBM, Armonk, NY) was used. Robust standard errors were calculated with Stata software for Windows (version 12; StataCorp, College Station, TX).

For voxel-wise statistics, the FSL randomize tool was used to perform permutation-based nonparametric testing (n = 5,000 permutations). Threshold-free cluster enhancement (TFCE) was applied to correct for multiple comparisons across space, which is generally more robust and avoids the need for the arbitrary initial cluster-forming threshold. Significance was set at a TFCE-corrected $P < 0.05$. Differences between offspring and control subjects were assessed and adjusted for age and sex. To assess the association of chronological age with

diffusion parameters, the same model was used, although with contrasts of interest made for the age regressor instead of the two regressors describing group membership.

Results

Characteristics of the study population are shown in Table 4.1. In total, 356 subjects participated in the study, 185 offspring and 171 control subjects. The mean age of each group was 66 years, with a lower female percentage among offspring (44%) compared with control subjects (61%). More control subjects had a history of diabetes mellitus (9% vs 2%, P = 0.02). No differences were found concerning other comorbidities.

Table 4.1 Characteristics of the study population

	Offspring (n = 185)	Controls (n = 171)	P
Demographics			
Age (years)	66 (6)	66 (7)	0.77
Women	82 (44)	104 (61)	0.002*
Right-handedness	165 (90)	151 (89)	0.92
Comorbidities			
Myocardial infarction	3 (2)	5 (3)	0.39
Stroke	4 (2)	4 (3)	0.88
Hypertension	35 (21)	42 (28)	0.15
Diabetes mellitus	4 (2)	13 (9)	0.02*
Malignancies	13 (8)	17 (11)	0.27

Values are numbers (percentage) for dichotomous variables or means (standard deviation) for continuous variables. * $P < 0.05$.

Brain tissue diffusion parameters and chronological age

FA, AxD, RD, and MD of grey matter, white matter, and subcortical grey matter structures were quantified globally in the whole study population to assess their association with chronological age (Tables 4.2 and 4.3). FA of all structures decreased with increasing chronological age, except for cortical grey matter, amygdala, caudate nucleus, nucleus accumbens, and putamen. AxD rose with increasing chronological age in all structures, except for the pallidum. Likewise, RD and MD also rose with increasing chronological age in all structures, except for the nucleus accumbens. No sex differences in the association of chronological age with brain tissue diffusion parameters were found.

Figure 4.1 shows the spatial distribution of age-related changes of white matter FA (see Fig. 4.1A) and white matter AxD, RD, and MD (see Fig. 4.1B) within the white matter skeleton. FA of the main white matter tracts was negatively associated with chronological age ($P < 0.003$) except for the callosal splenium and partly the corona radiata. RD was positively associated with chronological age ($P < 0.003$) in predominantly the same regions of the main white matter tracts, whereas the positive association of AxD and MD with chronological age ($P < 0.003$) was more widespread, including the splenium of the corpus callosum and the corona radiata.

Table 4.2 FA, AxD, RD, and MD of cortical grey matter and white matter and their association with chronological age

Outcome measures, Mean (SE)	Total group (n = 356)	Age range; Mean age (years) 45-61; 58 (n = 96)	62-65; 64 (n = 90)	66-69; 68 (n = 76)	70-84; 74 (n = 94)	P
Grey matter						
FA	0.197 (0.0004)	0.198 (0.001)	0.198 (0.001)	0.197 (0.001)	0.196 (0.001)	0.11
AxD (x 10^{-3}) (mm^2/s)	1.372 (0.004)	1.331 (0.006)	1.361 (0.006)	1.383 (0.007)	1.422 (0.007)	<0.001*
RD (x 10^{-3}) (mm^2/s)	1.014 (0.003)	0.979 (0.005)	1.004 (0.005)	1.025 (0.005)	1.056 (0.006)	<0.001*
MD (x 10^{-3}) (mm^2/s)	1.128 (0.003)	1.092 (0.005)	1.118 (0.005)	1.139 (0.006)	1.173 (0.006)	<0.001*
White matter						
FA	0.322 (0.001)	0.326 (0.001)	0.325 (0.001)	0.320 (0.001)	0.316 (0.001)	<0.001*
AxD (x 10^{-3}) (mm^2/s)	1.221 (0.002)	1.198 (0.003)	1.211 (0.004)	1.226 (0.004)	1.253 (0.005)	<0.001*
RD (x 10^{-3}) (mm^2/s)	0.761 (0.002)	0.738 (0.003)	0.751 (0.003)	0.768 (0.004)	0.791 (0.004)	<0.001*
MD (x 10^{-3}) (mm^2/s)	0.913 (0.002)	0.891 (0.003)	0.903 (0.003)	0.921 (0.004)	0.944 (0.005)	<0.001*

Probability values are adjusted for sex and for affiliation with the offspring or control group. Probability values are corrected for multiple comparisons using Bonferroni post hoc test.

* Probability values that remain significant after Bonferroni correction.

AxD = axial diffusivity; FA = fractional anisotropy; MD = mean diffusivity; RD = radial diffusivity; SE = standard error.

Table 4.3 FA, AxD, RD, and MD of subcortical grey matter structures and their association with chronological age

		Age range; mean age (years)				
Outcome measures, Mean (SE)	Total group (n = 356)	45-61; 58 (n = 96)	62-65; 64 (n = 90)	66-69; 68 (n = 76)	70-84; 74 (n = 94)	P
Amygdala						
FA	0.222 (0.001)	0.223 (0.002)	0.225 (0.002)	0.224 (0.002)	0.217 (0.002)	0.01
AxD (x 10^{-3}) (mm^2/s)	1.049 (0.004)	1.024 (0.007)	1.044 (0.008)	1.051 (0.008)	1.082 (0.009)	<0.001*
RD (x 10^{-3}) (mm^2/s)	0.760 (0.003)	0.737 (0.005)	0.753 (0.007)	0.764 (0.007)	0.791 (0.008)	<0.001*
MD (x 10^{-3}) (mm^2/s)	0.850 (0.003)	0.831 (0.005)	0.843 (0.006)	0.855 (0.006)	0.877 (0.008)	<0.001*
Caudate nucleus						
FA	0.268 (0.002)	0.269 (0.003)	0.270 (0.003)	0.270 (0.003)	0.264 (0.003)	0.04
AxD (x 10^{-3}) (mm^2/s)	1.270 (0.012)	1.184 (0.019)	1.242 (0.021)	1.273 (0.026)	1.389 (0.026)	<0.001*
RD (x 10^{-3}) (mm^2/s)	0.884 (0.011)	0.817 (0.017)	0.857 (0.018)	0.882 (0.022)	0.983 (0.024)	<0.001*
MD (x 10^{-3}) (mm^2/s)	0.993 (0.010)	0.933 (0.016)	0.982 (0.019)	1.004(0.022)	1.069 (0.023)	<0.001*
Hippocampus						
FA	0.216 (0.001)	0.219 (0.001)	0.218 (0.001)	0.217 (0.001)	0.210 (0.002)	<0.001*
AxD (x 10^{-3}) (mm^2/s)	1.204 (0.004)	1.178 (0.006)	1.189 (0.007)	1.207 (0.007)	1.245 (0.007)	<0.001*
RD (x 10^{-3}) (mm^2/s)	0.880 (0.003)	0.852 (0.005)	0.865 (0.005)	0.881 (0.006)	0.922 (0.006)	<0.001*
MD (x 10^{-3}) (mm^2/s)	0.983 (0.003)	0.960 (0.005)	0.973 (0.006)	0.989 (0.006)	1.019 (0.006)	<0.001*
Nucleus accumbens						
FA	0.242 (0.001)	0.237 (0.002)	0.243 (0.002)	0.243 (0.002)	0.244 (0.002)	0.02
AxD (x 10^{-3}) (mm^2/s)	0.924 (0.002)	0.915 (0.004)	0.922 (0.004)	0.922 (0.005)	0.936 (0.006)	0.001*
RD (x 10^{-3}) (mm^2/s)	0.655 (0.002)	0.654 (0.003)	0.652 (0.003)	0.654 (0.004)	0.661 (0.004)	0.10
MD (x 10^{-3}) (mm^2/s)	0.742 (0.002)	0.738 (0.003)	0.741 (0.003)	0.743 (0.004)	0.748 (0.004)	0.04
Pallidum						
FA	0.378 (0.001)	0.383 (0.003)	0.386 (0.003)	0.374 (0.003)	0.368 (0.003)	<0.001*
AxD (x 10^{-3}) (mm^2/s)	1.020 (0.003)	1.013 (0.004)	1.020 (0.005)	1.017 (0.006)	1.031 (0.006)	0.003
RD (x 10^{-3}) (mm^2/s)	0.568 (0.002)	0.558 (0.003)	0.560 (0.003)	0.571 (0.004)	0.585 (0.004)	<0.001*
MD (x 10^{-3}) (mm^2/s)	0.716 (0.002)	0.709 (0.003)	0.713 (0.003)	0.720 (0.004)	0.726 (0.003)	<0.001*
Putamen						
FA	0.269 (0.001)	0.269 (0.001)	0.272 (0.002)	0.268 (0.002)	0.269 (0.002)	0.28
AxD (x 10^{-3}) (mm^2/s)	0.924 (0.002)	0.913 (0.003)	0.917 (0.003)	0.922 (0.005)	0.944 (0.005)	<0.001*
RD (x 10^{-3}) (mm^2/s)	0.615 (0.002)	0.604 (0.002)	0.608 (0.003)	0.617 (0.004)	0.631 (0.004)	<0.001*
MD (x 10^{-3}) (mm^2/s)	0.712 (0.001)	0.707 (0.002)	0.708 (0.002)	0.711 (0.003)	0.725 (0.003)	<0.001*
Thalamus						
FA	0.336 (0.001)	0.339 (0.001)	0.337 (0.002)	0.335 (0.001)	0.332 (0.002)	<0.001*
AxD (x 10^{-3}) (mm^2/s)	1.253 (0.008)	1.210 (0.012)	1.227 (0.015)	1.266 (0.016)	1.312 (0.017)	<0.001*
RD (x 10^{-3}) (mm^2/s)	0.793 (0.006)	0.752 (0.008)	0.774 (0.012)	0.807 (0.012)	0.842 (0.014)	<0.001*
MD (x 10^{-3}) (mm^2/s)	0.936 (0.006)	0.903 (0.009)	0.910 (0.011)	0.951 (0.012)	0.990 (0.015)	<0.001*

Probability values are adjusted for sex and for affiliation with the offspring or control group. Probability values are corrected for multiple comparisons using Bonferroni post hoc test.

* Probability values that remain significant after Bonferroni correction.

AxD = axial diffusivity; FA = fractional anisotropy; MD = mean diffusivity; RD = radial diffusivity; SE = standard error.

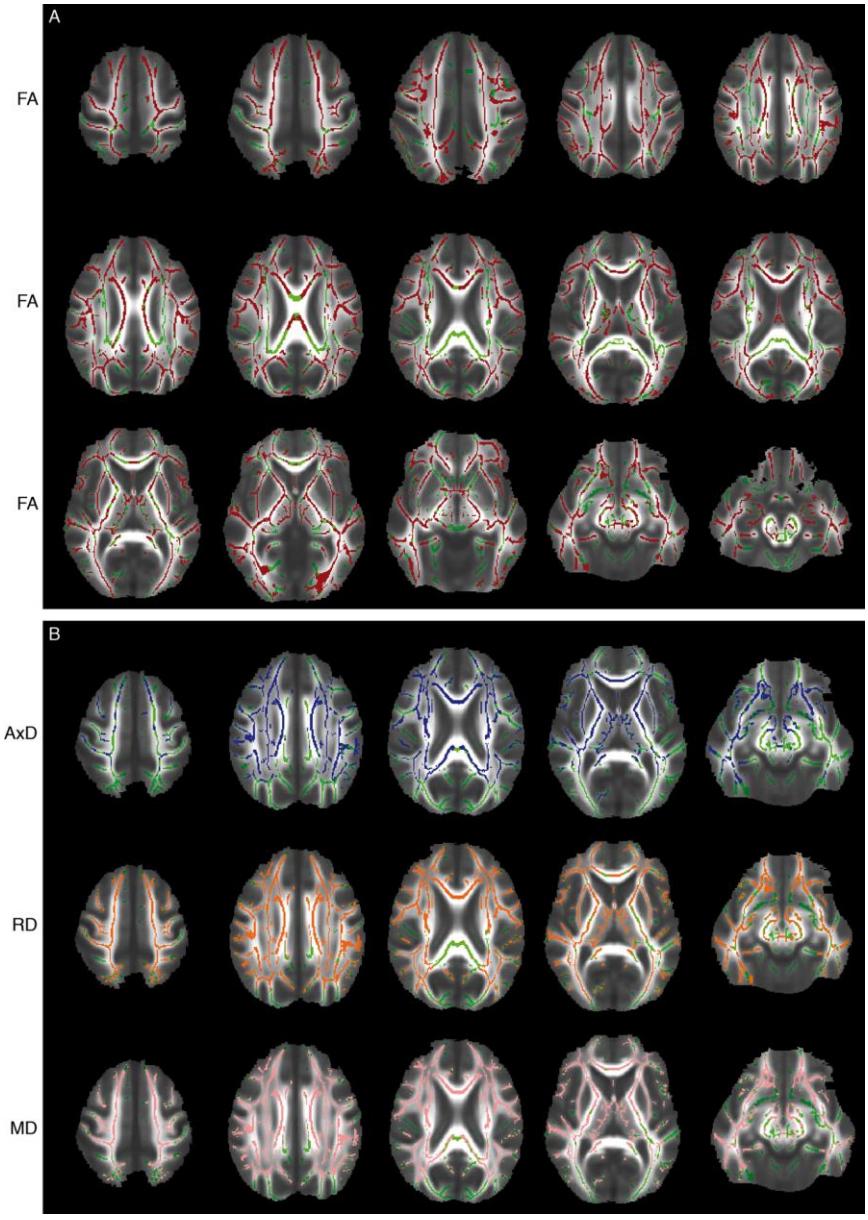

Figure 4.1 Age-related changes of white matter fractional anisotropy (FA), axial diffusivity (AxD), radial diffusivity (RD), and mean diffusivity (MD) in the whole study population. (A) Red colour indicates white matter regions showing age-related decrease of FA. (B) Regions of age-related increase in AxD (blue), RD (orange), and MD (pink; all $P < 0.003$). Results and mean white matter skeleton (green) are projected on the mean FA image of all study participants.

Brain tissue diffusion parameters and biological age

To assess the association of biological age with brain tissue diffusion parameters, offspring were contrasted with control subjects. Mean whole brain white matter FA was higher in offspring (mean FA (SE) = 0.3232 (0.0009)) compared to control subjects (mean FA (SE) = 0.3212 (0.0009)) adjusted for age and sex ($P = 0.04$). After additional correction for family relationships among the offspring, the P value for the difference in white matter FA between offspring and control subjects changed from 0.04 to 0.06. Exclusion of study participants with a history of stroke or myocardial infarction as well as additional adjustment for history of diabetes mellitus and hypertension did not alter the results. The differences in whole brain white matter FA between offspring and control subjects were similar at all ages and for both sexes. No differences in mean whole brain white matter AxD, RD, or MD between offspring and control subjects were found.

When differences in white matter diffusion parameters between offspring and control subjects were assessed voxel-wise, regions of higher white matter FA as well as lower white matter RD were found in offspring as compared to control subjects. The spatial distribution of the observed differences in white matter FA and RD between both groups is shown in Figure 4.2. Offspring showed preserved white matter integrity in the callosal genu and body as expressed in higher FA (see Fig. 4.2A) and lower RD values (see Fig. 4.2B) in these regions (both $P < 0.003$). Taking the annual rate of change for FA (-0.000578; adjusted for sex and affiliation with the offspring or control group) and the age- and sex-adjusted β of the difference between offspring and control subjects in FA (-0.00261) into account, offspring can be considered 4.5 years "biologically younger" compared to control subjects.

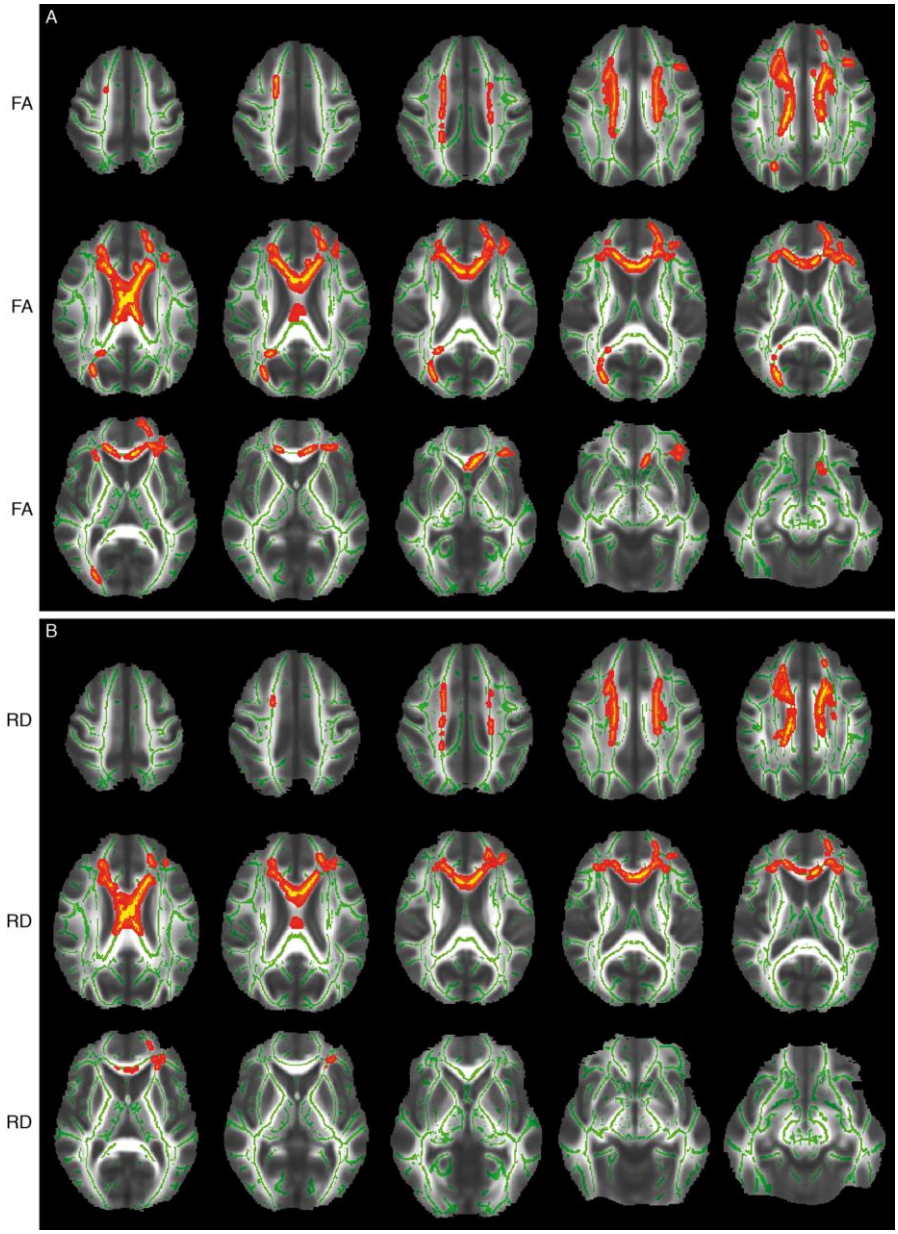

Figure 4.2 Differences in white matter fractional anisotropy (FA) and radial diffusivity (RD) between offspring and control subjects. (A) Regions of higher white matter FA and (B) lower white matter RD in offspring as compared to control subjects are displayed in red and yellow (both $P < 0.003$). Results and mean white matter skeleton (green) are projected on the mean FA image of the whole study population.

There were few differences in diffusion parameters of cortical and subcortical grey matter between offspring and control subjects, and none would have survived Bonferroni correction. The significant uncorrected differences are listed here for completeness: mean FA of the nucleus accumbens was higher (P = 0.04) and mean AxD of the putamen was lower (P = 0.03) in offspring as compared to control subjects.

Discussion

The most important finding of this study is that offspring of nonagenarian siblings show preserved white matter integrity predominantly in the callosal genu and body as compared to environment- and age-matched control subjects, independent of cardiovascular comorbidities or risk factors. Moreover, this study demonstrates that grey matter, white matter, and subcortical grey matter structures show specific patterns of age-related changes of tissue integrity.

Our findings suggest that preserved white matter integrity marks the phenotype of familial longevity and metabolic health in middle age. The genu and body of the corpus callosum were the most representative parts of the brain, showing more highly preserved white matter microstructural integrity in offspring of nonagenarian siblings as compared to control subjects. It is likely that these features are driven by the genetic component involved in familial longevity. A study on the heritability of the callosal microstructure in monozygotic and dizygotic elderly male twins has shown that both the callosal genu and splenium are under significant genetic control. Genetic relative to environmental influence on white matter FA was higher in the callosal splenium (67% genetic, 33% environmental) than in the genu (49% genetic, 51% environmental) [113]. Chiang et al [120] have demonstrated high heritability of white matter integrity in bilateral frontal and parietal lobes and left occipital lobes in young adult monozygotic and

dizygotic twins, which has been shown to be additionally influenced by socioeconomic status and intelligence quotient [114]. AxD is assumed to reflect axonal size and extra-axonal space, whereas RD is sensitive to (age-related) differences in myelination. By contrast, FA, as a summary measure reflecting the extent to which AxD exceeds RD, seems less specific concerning underlying microstructural changes [103]. In our study, the age-related decrease of white matter FA was accompanied by age-related increases in AxD as well as RD and MD in the whole study population, showing an anterior to posterior gradient, which was more pronounced for FA and RD as compared to AxD and MD. This is in line with results from previous studies [101, 103, 106, 107, 109]. The observed anterior to posterior gradient lends support to a "last in first out theory," [121] assuming that the predominantly frontally located late-myelinating regions, which consist of thinner myelinated axons, are more prone to age-related myelin breakdown [122]. Against the backdrop of these findings, our results suggest that both offspring and control subjects show common age-related loss of white matter microstructural integrity, which is particularly less marked in the callosal genu and body of the offspring, structures that have been reported to be most affected by chronological aging and to be at the same time under significant genetic control. In terms of white matter integrity, offspring with the propensity to become long-lived can be considered 4.5 years "biologically younger" than environment- and age-matched control subjects. Moreover, recent studies have shown that age-related WML in otherwise healthy elderly subjects were accompanied by a decrease in callosal FA and an increase in callosal RD [123, 124]. Offspring also showed lower periventricular as well as subcortical WML load compared to control subjects [115]. Hence, preserved white matter integrity of the callosal genu and body among the offspring might be a reflection of a lower amount of spatially remote white matter damage.

One of the strengths of our study is its unique design of comparing middle-aged individuals who have a genetically determined higher propensity to become long-lived compared to their spouses as environment- and age-matched controls. This will allow us to gain more insight into the relevance of age-related changes of the brain, which are frequently detected on MRI scans of elderly individuals. With the inclusion of the partners of the offspring as the control group, the two groups were highly comparable with regard to their socioeconomic and geographical background. Finally, our inclusion algorithm resulted in a large study sample, which allowed us to investigate even small differences between the two groups.

Study subjects were relatively young for age-related changes of the brain, which is a limitation of this study. Because differences between the two groups were likely to be small, a higher mean age of the study groups would probably have facilitated the detection of differences. Moreover, not all offspring would have inherited the beneficial longevity-predisposing effects, which are consequently diluted with respect to the genetic longevity component. There are limitations inherent to the chosen DTI analysis approach. A whole brain analysis approach is particularly prone to distortions at tissue interfaces caused by different magnetic susceptibility of brain tissues, image stretch or compression caused by eddy currents, or partial volume between different brain tissues. Moreover, the use of TBSS to assess the spatial distribution of changes in FA, AxD, RD, and MD does not accommodate the potentially confounding effect of WML on the proper calculation of the white matter skeleton [125]. Finally, it cannot be totally precluded that the presented differences between offspring and control subjects might be false-positive results due to chance alone; therefore, the findings should be considered as hypothesis generating rather than conclusive.

In conclusion, this is the first study to compare brain tissue diffusion parameters between middle-aged and elderly offspring of nonagenarian siblings and control subjects. Our findings suggest that, at a mean age of 66 years, both offspring and

control subjects show common age-related loss of white matter microstructural integrity, which is less marked in the callosal genu and body among the offspring, independent of cardiovascular comorbidities or risk factors. In terms of white matter microstructure, offspring of nonagenarian siblings can be considered 4.5 years "biologically younger" compared to environment- and age-matched control subjects.

5

An in vivo study on brain microstructure in biological and chronological aging

PLoS One, 2015;10

I. Altmann-Schneider
A.J.M. de Craen
A.A. van den Berg-Huysmans
P.E. Slagboom
R.G.J. Westendorp
M.A. van Buchem
J. van der Grond

Abstract

Background and purpose:

This study aimed to investigate whether magnetization transfer imaging (MTI) parameters of cortical grey and white matter and subcortical grey matter structures differ between subjects enriched for human familial longevity and control subjects to provide a thorough description of the brain phenotype of familial longevity. Moreover, we aimed to describe cerebral aging effects on MTI parameters in an elderly cohort.

Methods:

All subjects were included from the Leiden Longevity Study and underwent 3 Tesla MTI of the brain. In total, 183 offspring of nonagenarian siblings, who are enriched for familial factors of longevity, were contrasted with 163 environmentally and age-matched controls.

Results:

No differences in cortical and subcortical grey matter and white matter MTI parameters were found between offspring and control subjects using histogram-based and voxel-wise analyses. Cortical grey matter and white matter MTI parameters decreased with increasing chronological age (all $p < 0.001$). Decrease of white matter magnetization transfer ratio (MTR) was homogeneous throughout the whole mean white matter skeleton except for parts of the callosal splenium and partly the posterior limb of the internal capsule and superior region of the corona radiata ($p < 0.05$). Mean MTR of subcortical grey matter structures decreased with increasing age (p amygdala, caudate nucleus and putamen < 0.001; p pallidum = 0.001, p thalamus = 0.002).

Conclusions:

The brain phenotype of human familial longevity is - at a mean age of 66 years - not characterized by preserved macromolecular brain tissue integrity.

Introduction

The human brain undergoes notable structural changes during the normal aging process. The human lifespan is known to be influenced by genes as well as environmental factors [126] and it has been reported that extreme longevity is at least partly clustered in families [127]. Studying the brain phenotype in familial longevity is a valuable tool to learn more about the relevance of common age-related brain changes.

The Leiden Longevity Study was designed to investigate which factors in middle-aged humans associate with familial longevity. Offspring of long-lived nonagenarian siblings, who as a group are predisposed to become long-lived, are contrasted with their partners who represent the general population and serve as control subjects [6]. Compared to the control subjects, aging in the offspring is marked by beneficial serum levels of lipid and thyroid parameters, preservation of insulin sensitivity, lower prevalence of myocardial infarction, hypertension, diabetes mellitus and use of cardiovascular medication and lower prevalence of cerebral white matter lesions (WML) and lacunar infarcts and preserved white matter microstructural integrity as measured using diffusion tensor imaging (DTI) [7-9, 86, 115, 128]. Despite having the same chronological age, body mass index (BMI) and lifestyle [86] as the control subjects, the offspring generally display a younger biological age and for many other parameters appear healthier, such as for example better renal function [129] and a lower susceptibility to rheumatoid arthritis [130].

Recently, magnetization transfer imaging (MTI) has been put forward as a highly sensitive tool to study changes in the myelin content of the brain. MTI contrast is based on magnetization transfer between protons, which are bound to macromolecules and therefore restricted in motion, and protons in water, which

can move freely [131]. Within the brain, myelin water contributes disproportionately to the magnetization transfer ratio (MTR), which therefore has been suggested to be a relatively specific measure of myelin integrity [132-134]. In recent studies it has been shown that MTR shows a steep decline in cortical and subcortical structures during lifespan (subjects aged 11 years-85 years) [135-143], indicating a decrease in myelin integrity. Still, in elderly subjects, 65 years of age and older, little MTI data are available [139-141]. Thus, the aim of this paper is twofold: To describe and partly reproduce cerebral aging effects in MTI in an elderly cohort. Second to investigate whether the preserved white matter microstructural organization in human familial longevity is accompanied by preserved white matter tissue composition in the sense of preserved myelin integrity [144] to provide a thorough description of the brain phenotype of familial longevity.

Methods

Study participants

All subjects were included from the Leiden Longevity Study and underwent 3T MRI of the brain. The Leiden Longevity Study has been described more detailed elsewhere [6]. In short, 421 Dutch Caucasian families were enrolled in the study between 2002 and 2006 based on the following inclusion criteria: (1) there were at least two living siblings per family, who fulfilled the age criteria and were willing to participate, (2) men had to be aged ≥ 89 years and women had to be aged ≥ 91 years and (3) the sib pairs had to have the same parents. Additionally, offspring of these long-lived siblings were included as they have a 35% lower mortality rate compared to the general population. Their partners, who share the same socio-economic and geographical background, were enrolled as age-matched control group [6]. In the current study, 183 offspring of nonagenarian

siblings, who are enriched for familial factors of longevity, were contrasted with 163 environmentally and age-matched controls.

The work described in this article has been carried out in accordance with the Code of Ethics of the World Medical Association (Declaration of Helsinki) and the study has been approved by the Medical Ethical Committee of the Leiden University Medical Centre (Leiden, The Netherlands). Written informed consent was obtained from all subjects.

MRI acquisition

All imaging was performed on a whole body MR system with a field strength of 3T (Philips Medical Systems, Best, The Netherlands). The following images were acquired:

3DT1-weighted: TR = 9.7 ms, TE = 4.6 ms, FA = 8°, FOV = 224 x 177 x 168 mm, resulting in a nominal voxel size of 1.17 x 1.17 x 1.4 mm, covering the entire brain with no gap between slices.

T2-weighted: TR = 4200 ms, TE = 80 ms, FA = 90°, FOV = 224 x 180 x 144 mm, matrix size 448 x 320, 40 transverse slices to cover the entire brain with a slice thickness of 3.6 mm with no gap between slices.

FLAIR (fluid-attenuated inversion recovery): TR = 11000 ms, TE 125 ms, FA = 90°, FOV = 220 x 176 x 137 mm, matrix size 320 x 240, 25 transverse slices to cover the entire brain with a slice thickness of 5 mm with no gap between slices.

DTI (diffusion tensor imaging): TR = 9592 ms, TE = 56 ms, FA = 90°, FOV = 220 x 220 x 128 mm, matrix size 112 x 110, 64 transverse slices to cover the entire brain with a slice thickness of 2 mm with no gap between slices, 32 measurement directions, b-value = 1000.

MTI (magnetization transfer imaging): TR = 100 ms, TE = 11 ms, FA = 9°, FOV = 224 x 180 x 144 mm, matrix size 224 x 169, 20 transverse slices to cover the entire brain with a slice thickness of 7.2 mm with no gap between slices.

MRI analysis

For analyses of MRI scans, different tools of the FSL (Functional MRI of the Brain Software Library) software package were used [64, 65].

Image pre-processing

Raw magnetization transfer scans were split in the M0-sequence (acquired without saturation pulse) and the M1-sequence (acquired after application of a saturation pulse).

Quantification of cortical grey matter, white matter and subcortical grey matter MTI parameters using histogram analysis

3D T1-weighted images were skull-stripped using BET (brain extraction tool) [68] and segmented using FAST (FMRIB's automated segmentation tool) [71] and FIRST (FMRIB's integrated registration and segmentation tool) [75], resulting in individual brain masks for white matter, cortical grey matter, amygdala, caudate nucleus, hippocampus, pallidum, putamen and thalamus. Individual 3D T1-weighted images were registered to the individual non-saturated M0 images using FMRIB's linear image registration tool (FLIRT) [69, 70]. Registration matrices from the previous step were used to coregister the non-saturated M0 images and the individual brain masks for all above mentioned brain structures so that the MTR maps could be masked with these brain masks. To correct for possible partial volume effects, an eroded mask of these segmentations was created by removing one voxel in-plane for all mentioned volumes-of interest (VOIs) [145]. Individual MTR maps were calculated voxel by voxel following the equation MTR = (M0-M1)/M0 and MTR histograms were generated for the above mentioned VOIs. Mean MTR, MTR peak height, normalized for the size of the VOI, and MTR peak location were calculated from each MTR histogram [146]. Mean MTR reflects the average MTR value per structure. MTR peak location reflects the most

common MTR value. The peak height of the MTR histogram indicates the number of voxels showing the most common MTR value, and is a measure of uniformity of the underlying voxels in terms of MTR values. As the size of the VOI influences the number of voxels having the most common MTR value, MTR peak height was normalized by dividing the number of voxels with the most common MTR value by the number of voxels within the VOI. All MTI measures below -3 or above 3 standard deviations were excluded from statistical analysis.

Automated segmentation of white matter lesions and quantification of MTR within these lesions

For the automated measurement of white matter lesion (WML) volume, 3DT1-weighted images were skull stripped [68] and the FLAIR and 3DT1 image were co-registered [69, 70]. The brain extracted FLAIR image was affine-registered to MNI152 standard space using FLIRT. A conservative MNI152 standard space white matter mask was used to extract the white matter from the FLAIR image. Subsequently, a threshold was set to identify which white matter voxels were hyperintense, followed by manually checking and editing for quality control. A mean MTR for all WML per subject was determined by masking the MTR maps with the registered WML masks.

Voxel-based analysis of white matter MTR maps

Voxel-wise statistical analysis of white matter MTR data was performed using TBSS (Tract-Based Spatial Statistics) [119, 147], which was based on the creation of a mean white matter skeleton from fractional anisotropy (FA) images, derived from a DTI sequence. FA images were created by fitting a tensor model to the raw diffusion data using FDT (FMRIB's diffusion tool box) and then brain-extracted using BET [68]. All subjects' FA images were aligned into MNI152 standard space using non-linear registration (FNIRT) [73, 74]. Next, the mean FA

image (from the whole study population) was created and thinned to generate a mean FA skeleton which represents the centres of all tracts common to the group. The threshold for the mean FA skeleton was set to 0.2. All subjects' non-saturated M0 images and saturated M1 images were linearly registered to the DTI B0 image, which is based on a raw T2 signal without diffusion weighting. MTR maps were calculated in "B0-space" in the same manner as described above. The resulting individual MTR maps were non-linearly registered into MNI152 standard space using FNIRT [73, 74] and projected onto the mean FA skeleton.

Statistical analysis

If not otherwise stated, data are presented as mean with standard deviation (SD) or mean with standard error (SE). Differences in sex, handedness, and history of hypertension, diabetes mellitus, myocardial infarction, stroke and malignancies between offspring and control subjects were calculated using Chi-square tests. Differences in age were tested using independent samples t-tests. MTI measures of all brain tissues were normally distributed. A linear regression model was used to assess the association of brain tissue MTI parameters with chronological age, adjusted for sex and affiliation to the offspring or control group. Analyses of differences in MTI parameters between offspring and control subjects were adjusted for age and sex and robust standard errors were calculated to correct for family relationships among the offspring. For statistical analyses, Statistical Package for the Social Sciences (SPSS) software for windows (version 20.0) was used. Robust standard errors were calculated with STATA software for windows (version 12; STATA).

For voxel-wise statistical analyses, the FSL randomize tool was used to perform permutation-based non-parametric testing (n = 5000 permutations) on the data. Threshold-Free Cluster Enhancement (TFCE) was applied to correct for spatial neighbourhood information, which is generally more robust and avoids the need

for the arbitrary initial cluster-forming threshold. To correct for multiple comparisons, permutation based Family Wise Error (FWE) correction was used as a thresholding method. Significance was set at a TFCE FWE-corrected $p < 0.05$. Differences between offspring and control subjects were assessed, adjusted for age and sex. For the association between chronological age and MTI parameters, the same model was used though with contrasts of interest made for the age regressor instead of the two regressors describing group membership.

Results

Characteristics of the study population are shown in Table 5.1. Imaging parameters were available for a total of 346 study participants, 183 offspring of long-lived siblings and 163 control subjects. The mean age of both groups was 66 years with a lower female percentage of 44% among offspring compared to 61% among control subjects (P = 0.002). More control subjects had a history of diabetes mellitus compared to offspring (7% versus 2%, P = 0.02). No differences were found concerning other morbidities.

Brain tissue MTI parameters and biological age

Cortical and subcortical grey matter and white matter MTI parameters were quantified globally using histogram analysis. No differences were found between offspring and control subjects (Table 5.2). Also within white matter lesions MTI parameters were similar in offspring and control subjects: Mean MTR (SE): 35.26 (0.16) and 35.48 (0.17) respectively, P = 0.34; Mean normalized peak height (SE): 14.73 (5.39) and 14.82 (7.17) respectively, P = 0.85; Mean peak location: 37.33 (2.73) and 37.77 (1.99) respectively, P = 0.28. Moreover, the association of chronological age with brain tissue MTI parameters was not different between

offspring and control subjects. Voxel-wise analysis of white matter MTR confirmed these results.

Table 5.1 Characteristics of the study population

	Offspring (n = 183)	Controls (n = 163)	P
Demographics			
Age (years)	66 (6.0)	66 (7.5)	0.82
Women	99 (61)	81 (44)	0.002*
Right-handedness	162 (89)	146 (90)	0.76
Comorbidities			
Hypertension	37 (20)	41 (25)	0.30
Diabetes mellitus	4 (2)	12 (7)	0.02*
Myocardial infarction	3 (2)	4 (2)	0.60
Stroke	4 (2)	3 (2)	0.85
Malignancies	13 (7)	16 (10)	0.30

Values are numbers (percentage) for dichotomous variables or means (standard deviation) for continuous variables. * $P < 0.05$.

Table 5.2 MTI parameters of cortical and subcortical grey and white matter in offspring and control subjects

	Mean (SE)		
	Offspring (n = 183)	Controls (n = 163)	P
Grey matter			
MTR (%)	33.51 (0.07)	33.50 (0.08)	0.61
norm. PH (%)	7.61 (0.09)	7.58 (0.08)	0.15
PL	36.23 (0.09)	36.40 (0.08)	0.14
White matter			
MTR (%)	39.41 (0.07)	39.43 (0.05)	0.97
norm. PH (%)	11.75 (0.17)	11.76 (0.17)	0.35
PL	40.62 (0.07)	40.73 (0.08)	0.23
Amygdala			
MTR (%)	36.72 (0.13)	36.98 (0.14)	0.92
norm. PH (%)	13.36 (0.21)	13.53 (0.22)	0.69
PL	38.15 (0.15)	38.48 (0.15)	0.22
Caudate nucleus			
MTR (%)	36.33 (0.14)	36.42 (0.17)	0.77
norm. PH (%)	8.96 (0.12)	8.91 (0.12)	0.32
PL	41.81 (0.14)	42.17 (0.20)	0.13
Hippocampus			
MTR (%)	38.36 (0.12)	38.45 (0.10)	0.73
norm. PH (%)	10.80 (0.16)	11.13 (0.17)	0.54
PL	40.72 (0.16)	40.96 (0.12)	0.20
Pallidum			
MTR (%)	38.37 (0.12)	38.36 (0.11)	0.61
norm. PH (%)	14.44 (0.23)	14.63 (0.23)	0.86
PL	38.72 (0.13)	38.75 (0.12)	0.46
Putamen			
MTR (%)	35.40 (0.12)	35.31 (0.12)	0.34
norm. PH (%)	12.82 (0.22)	12.99 (0.24)	0.81
PL	38.21 (0.11)	38.22 (0.11)	0.52
Thalamus			
MTR (%)	37.99 (0.14)	38.18 (0.18)	0.64
norm. PH (%)	10.93 (0.16)	11.06 (0.16)	0.87
PL	42.32 (0.13)	42.57 (0.18)	0.22

Values represent means (standard error, SE). P-values (P) are adjusted for age and sex and corrected for family relationships among the offspring. MTR, magnetization transfer ratio; norm. PH, normalized peak height; PL, peak location.

Brain tissue MTI parameters and chronological age

MTI parameters were calculated globally for cortical grey matter, white matter, and subcortical grey matter structures using histogram analysis and their association with chronological age was assessed cross-sectionally. All cortical grey and white matter MTI parameters decreased with increasing age ($P < 0.001$) (Table 5.3). Mean MTR of all measured subcortical grey matter structures decreased with increasing age (P amygdala, caudate nucleus, pallidum and putamen < 0.001; P hippocampus = 0.02, P thalamus = 0.002). Mean normalized peak height decreased with increasing age in the amygdala, pallidum and putamen ($P < 0.001$). Mean peak location decreased in the pallidum and putamen ($P = 0.03$ and $P = 0.001$ respectively). Results are shown in Table 5.4. No differences in the association of chronological age with brain tissue MTI parameters were found between males and females except for mean MTR of the putamen, which showed a faster age-related decrease in men compared to women.

Table 5.3 Association of MTI parameters of cortical grey and white matter with chronological age

	Standardized Beta	P
Grey matter		
MTR (%)	-0.37	< 0.001
norm. PH (%)	-0.24	< 0.001
PL	-0.20	< 0.001
White matter		
MTR (%)	-0.33	< 0.001
norm. PH (%)	-0.23	< 0.001
PL	-0.25	< 0.001

Values represent standardized Betas. P-values (p) are adjusted for sex and affiliation to the offspring or control group. MTR, magnetization transfer ratio; norm. PH, normalized peak height; PL, peak location.

Table 5.4 Association of MTI parameters of subcortical grey matter structures with chronological age

	Standardized Beta	P
Amygdala		
MTR (%)	-0.23	< 0.001
norm. PH (%)	-0.18	<0.001
PL	-0.06	0.25
Caudate nucleus		
MTR (%)	-0.23	< 0.001
norm. PH (%)	-0.10	0.06
PL	-0.002	0.97
Hippocampus		
MTR (%)	-0.13	0.02
norm. PH (%)	-0.09	0.10
PL	-0.04	0.46
Pallidum		
MTR (%)	-0.19	0.001
norm. PH (%)	-0.21	<0.001
PL	-0.12	0.03
Putamen		
MTR (%)	-0.31	< 0.001
norm. PH (%)	-0.28	< 0.001
PL	-0.20	< 0.001
Thalamus		
MTR (%)	-0.17	0.002
norm. PH (%)	-0.06	0.27
PL	-0.04	0.51

Values represent standardized Betas. P-values (p) are adjusted for sex and affiliation to the offspring or control group.

MTR, magnetization transfer ratio; norm. PH, normalized peak height; PL, peak location.

FSL-TBSS was performed to assess the spatial distribution of age-related changes of white matter MTR (Figure 5.1). White matter MTR decreased throughout the whole mean white matter skeleton except for partly the callosal splenium and posterior limb of the internal capsule and superior region of the corona radiata ($P < 0.05$).

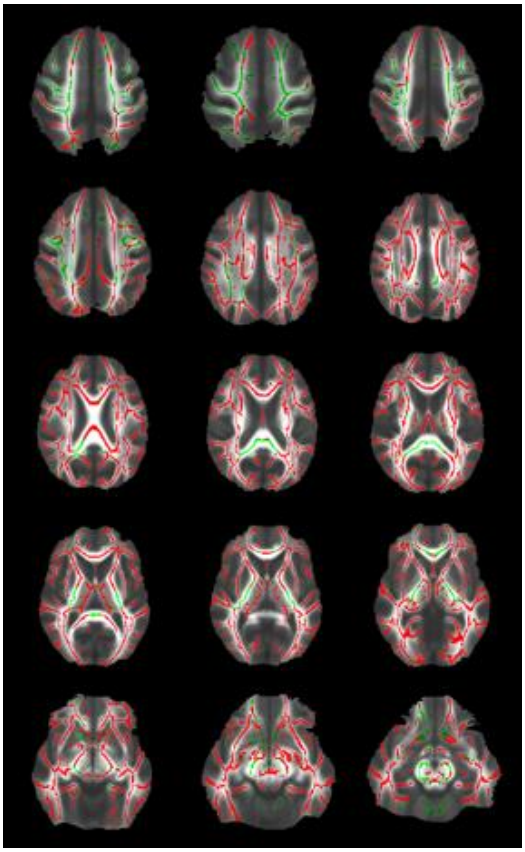

Figure 5.1 shows results from the voxel-based assessment of age-related changes of white matter magnetization transfer ratio (MTR) in the whole study population using FSL-TBSS. Results are projected on the mean fractional anisotropy (FA) image of the whole study population which is derived from a diffusion tensor imaging (DTI) scan sequence. The mean white matter skeleton of the whole study population is shown in green colour. Red colour shows areas of statistically significant decrease of white matter MTR with increasing chronological age ($P < 0.05$).

Discussion

The finding that no differences in any of the MTI parameters were found in any of the cortical and subcortical grey and white matter regions between partner and offspring is at least remarkable. Our findings indicate that preserved white matter integrity in familial longevity cannot be attributed to a lower susceptibility to white matter demyelination during the aging process. Using DTI, we have shown recently that familial longevity is associated with preserved white matter integrity in the corpus callosum, as expressed in higher FA and lower radial diffusivity (RD) values in these regions [128]. This corresponds to a biological age benefit of 4.5 years [128]. The interpretation of the data of the current study is impossible without incorporating these previous findings.

During the past decade, brain aging has been studied extensively using DT and MT imaging techniques and several attempts have been made to correlate in vivo MRI findings with knowledge from histopathological studies. FA, which reflects the extent of directionality of diffusion of water protons, is predominantly found to decrease with aging and thought to be mainly influenced by axonal packing density as anisotropic diffusion also occurs in the absence of myelin [148]. With FA being relatively unspecific concerning underlying microstructural changes (e.g. axonal loss, axonal damage or demyelination) [103], several studies have included other DTI measures, such as RD and (axial diffusivity) AxD, to characterize the underlying processes. Studies in mice have suggested that RD might be a specific measure of myelin status [134, 149]. However, studies in humans have proven that increases in RD might not only be driven by loss of myelin but rather by a decrease in axon packing density through an increasing amount of extracellular water, which can be induced by different pathological processes [106]. Likewise, MTR has been proposed to be a relatively specific measure of white matter

myelin status in humans [132], but has been shown to be additionally influenced by pathological conditions such as inflammation [150, 151], oedema [151, 152] and axon loss [153]. With both RD and MTR solely being not specific to white matter myelin loss, the combination of increased RD and reduced MTR can be considered highly suggestive of reduced myelin content. In humans, different region-specific patterns of age-related changes in white matter DTI parameters have been described [106, 107]. In the corpus callosum which belongs to the predominantly frontally located late-myelinating regions consisting of thinner myelinated axons which are more prone to age-related myelin breakdown [122], an age-related decrease in FA was accompanied by increase in RD only or increase in RD as well as AxD [107, 121, 154]. This raises the possibility that both patterns reflect different degrees of severity of the same underlying structural changes [106]. MTR of the corpus callosum has been shown to decrease with increasing age [155]. Our previous data indicated that FA was decreased and RD increased in the callosal genu in offspring of nonagenarian siblings compared to control subjects, whereas AxD and MTR of the callosal genu were not different between groups. These findings might suggest that familial longevity is not associated with a lower susceptibility to white matter demyelination in the callosal genu and that the described difference between groups is caused by different susceptibility to underlying pathology other than demyelination. Against the background of the findings of Bennett et al. [106] however, another possible explanation could be that underlying changes are still too subtle to be depicted by MTR at this mean age [156].

Our findings, in which we specifically study aging affects in an elderly cohort, add to the existing data in relatively younger subjects showing a steep decline in myelin integrity in cortical and subcortical structures during lifespan indicated by a steep MTR decrease with age [132, 138, 144].

One of the strengths of our study is the large study sample of middle-aged to elderly subjects. Secondly, the study design of comparing elderly individuals with a familial propensity to become long-lived to their partners is unique and allows us to gain more insight into which of the multiple age-related changes of the brain, frequently detected on MRI-scans in the general aging population, are likely to be a relevant reflection of health. Thirdly, it should be noted that the partners of the offspring represent a control group matched for socio-economic and geographical background and lifestyle (as measured by FFQ).

The fact that study subjects were relatively young concerning age-related changes of the brain belongs to the limitations of this study. As differences between offspring and control subjects are likely to be small, a higher mean age of the study groups would probably facilitate the detection of possible differences.

In conclusion, this is the first study to compare macromolecular brain tissue integrity between elderly offspring of nonagenarian siblings and control subjects using MTI. Our findings suggest that, preserved white matter integrity of the callosal genu in familial longevity is not driven by a lower susceptibility to white matter demyelination during aging. Moreover, at a mean age of 66 years, both offspring and control subjects show similar age-related decline of macromolecular brain tissue integrity throughout the whole brain suggesting that the phenotype of familial longevity at that age is not characterized by preserved macromolecular brain tissue integrity.

II

Age-related changes of the human brain – modifying factors and risk of mortality

6

Systematic assessment of coronary artery calcification associated brain pathology and its spatial distribution in the elderly

Submitted

I. Altmann-Schneider
A.J.M. de Craen
A.A. van den Berg-Huysmans
P.E. Slagboom
R.G.J. Westendorp
L.J.M. Kroft
A. de Roos
M.A. van Buchem
J. van der Grond

Abstract

Background and purpose:

To investigate the association of coronary artery calcification (CAC) with cerebral small vessel disease in elderly individuals on the macrostructural and microstructural level, taking the spatial distribution of brain damage into account.

Methods:

We included 328 subjects who were participants from the Leiden Longevity Study. All participants underwent 3T MRI of the brain and CT of the coronary arteries. Ordinal/binary logistic and linear regression analysis was used to assess the association of CAC with various types of vascular brain damage.

Results:

Grey and white matter volumes were not associated with CAC. Increasing CAC was associated with a 1.3-fold higher probability to have more periventricular bands, periventricular white matter lesions (WML) in general and cerebral microbleeds (OR (95% CI) 1.34 (1.10-1.63), P = 0.004; OR (95% CI) 1.32 (1.08-1.62), P = 0.006; OR (95% CI) 1.36 (1.01-1.81), P = 0.04 respectively). The probability to have lacunar infarcts was more than twofold (OR (95% CI) 2.15 (1.10-4.20), P = 0.002). Neither subcortical WML nor total volume of WML was associated with CAC. Using diffusion tensor and magnetization transfer imaging, we found that CAC was associated with decreased microstructural grey matter and white matter integrity mainly in frontal/frontoparietal regions.

Conclusions:

Beyond focal ischemic brain lesions, CAC was associated with widespread microstructural brain pathology with a spatial distribution predominantly paralleling the detrimental effects of the aging process.

Introduction

Arteriosclerosis is a common cause of morbidity and mortality in the elderly. In the entire cascade of atherosclerotic changes coronary artery calcification (CAC) occurs early in the formation of the atherosclerotic plaques. Therefore, CAC is widely accepted as marker of atherosclerosis [15]. The widespread implementation of ultrafast computed tomography (CT) in clinical practice allows for the automated detection and quantification of CAC with high specificity and sensitivity [17]. Prevalence of CAC increases with age and is higher in individuals with history of coronary artery disease compared to individuals without [17].

Although CAC has been shown to be predictive of future cardiovascular events [18], the clinical correlates of arteriosclerotic brain damage are still less obvious. Some studies have shown an association of increased CAC with brain atrophy [157-159], where other studies indicated an association with macroscopic manifestations of cerebral small vessel disease, expressed in a higher prevalence of white matter lesions (WML), silent brain infarcts and cerebral microbleeds (CMB) [158-161]. Recently, it has been shown that, in addition to these established macrostructural hallmarks of cerebral small vessel disease (brain atrophy, WML, lacunar infarcts, CMB [162]), early signs of vascular brain damage may be picked up with diffusion tensor imaging (DTI) and magnetization transfer imaging (MTI) [163], even before macrostructural damage becomes overt [164]. Beyond the potential higher sensitivity of DTI and MTI in detecting subtle changes, they allow for the visualization of the spatial distribution of potential cerebral changes.

Since previous studies investigating the association between CAC and brain pathology have focused on macrostructural damage, the aim of the current study was to systematically assess the association of CAC with cerebral small vessel

disease in a large study cohort of elderly individuals on the macrostructural and microstructural level, taking the spatial distribution of brain damage into account.

Methods

Study participants

Subjects were included from the Leiden Longevity Study, which has been described more detailed elsewhere [6]. In short, 421 Dutch Caucasian families were enrolled between 2002 and 2006 based on the following inclusion criteria: (1) there were at least two living siblings per family, who fulfilled the age criteria and were willing to participate, (2) men had to be aged ≥ 89 years and women had to be aged ≥ 91 years and (3) the sib pairs had to have the same parents. Additionally, offspring of these long-lived siblings were included as they have a 35% lower mortality rate compared to the general population. Their partners participated as environmentally and age-matched controls [6]. For this study, subjects were recruited from the offspring and their spouses. Subjects were pooled for analyses. Study protocols meet the criteria of the Declaration of Helsinki. The study has been approved by the Medical Ethical Committee of the Leiden University Medical Centre (Leiden, The Netherlands). All subjects gave written informed consent.

MRI acquisition

All imaging was performed on a whole body MR system with a field strength of 3T (Philips Medical Systems, Best, The Netherlands). 3D T1-weighted, T2-weighted, FLAIR (fluid attenuated inversion recovery), DTI, MTI and T2*-weighted images were acquired.

Imaging parameters:
3DT1-weighted: TR = 9.7 ms, TE = 4.6 ms, FA = 8°, FOV = 224 x 177 x 168 mm, nominal voxel size: 1.17 x 1.17 x 1.4 mm, no gap.
T2-weighted: TR = 4200 ms, TE = 80 ms, FA = 90°, FOV = 224 x 180 x 144 mm, matrix size 448 x 320 x 40, no gap.
FLAIR: TR = 11000 ms, TE 125 ms, FA = 90°, FOV = 220 x 176 x 137 mm, matrix size 320 x 240 x 25, no gap.
DTI: TR = 9592 ms, TE = 56 ms, FA = 90°, FOV = 220 x 220 x 128 mm, matrix size 112 x 110 x 64, no gap, 32 measurement directions, b-value = 1000.
MTI: TR = 100 ms, TE = 11 ms, FA = 9°, FOV = 224 x 180 x 144 mm, matrix size 224 x 169 x 20, no gap.
T2-weighted:* TR = 45 ms, TE = 31 ms, FA = 13°, FOV = 250 x 175 x 112 mm.

CT acquisition

CAC was evaluated by measurement of the Agatston total coronary artery calcium score using a 320-multidetector row CT scanner (Aquilion ONE, Toshiba, Otawara, Japan). Scan range was planned between the carina and cardiac apex. An unenhanced volumetric CT was acquired with prospective ECG-triggering technique within a single heart beat during breath-hold at inspiration (0.35 s rotation time). Tube voltage was 120 kV and tube current 200-400 mA, dependent on patient size and shape. Slice thickness was 0.5 mm.

Assessment of CAC

Non-overlapping 3.0 mm datasets were reconstructed and images were transferred to a workstation for analysis (Vitrea FX, version 1.0, Vital Images). Dedicated CT calcium score analysis software (VScore, Vital Images) was used. Pixels exceeding the threshold value of 130 HU were automatically recognized by the postprocessing tool and manually encircled in the courses of the coronary

arteries. The amount of CAC was automatically calculated according to Agatston et al. [17] and expressed as Agatston total score: 0 (Agatston score = 0), 1 (Agatston score = 1-10), 2 (Agatston score = 11-100), 3 (Agatston score = 101-400) and 4 (Agatston score > 400).

Parameters of brain structure and pathology

Grey and white matter volumes

Grey and white matter volumes were calculated using the FSL-tool SIENAX (Structural Image Evaluation, using Normalization, of Atrophy) [66, 67]. SIENAX starts by extracting brain and skull images from the single whole-head input data [68]. The brain image is then affine-registered to MNI152 space [69, 70], using the skull image to determine the registration scaling. This is primarily done in order to obtain the volumetric scaling factor, to be used as a normalisation for head size. Next, tissue-type segmentation with partial volume estimation is performed [71] to calculate total volume of brain tissue, including separate estimates of volumes of grey and white matter.

Assessment of WML, lacunar infarcts and CMB

MRI scans were visualized using the freely available software MIPAV (Medical Image Processing, Analysis and Visualization). WML, lacunar infarcts and CMB were analysed blinded to subject identity, age, sex and descent.

WML were defined as areas within the white matter with increased signal intensity on both FLAIR and T2-weighted images without mass-effect. WML were rated according to a slightly modified version of the semi-quantitative rating scale of Scheltens et al. [1]. Periventricular and subcortical WML were rated separately and semi-quantitative regional scores were obtained by taking the size, amount and anatomical distribution of the lesions into account [115]. For the automated measurement of WML volume 3D T1-weighted images were skull

stripped [67] and the FLAIR and 3DT1 image were co-registered in order to create a brain extracted FLAIR image [69, 70]. This brain extracted FLAIR image was subsequently affine-registered to MNI152 standard space using the FMRIB's Linear Image Registration Tool [69, 70]. A conservative MNI152 standard space white matter mask was used to extract the white matter from the FLAIR image. Finally, a threshold was set to identify which white matter voxels were hyperintense, followed by manually checking and editing for quality control. The cerebellum and brainstem were excluded from this analysis.

Presence and number of lacunar infarcts were assessed on FLAIR, T2-weighted and 3D T1-weighted images. They were defined as parenchymal defects within the white matter not extending into the cortical grey matter, with centrally a signal intensity corresponding to that of cerebrospinal fluid on all three imaging sequences, surrounded by a rim of increased signal intensity on FLAIR. Diameter of lacunar infarcts was defined to be > 2 mm. To distinguish lacunar infarcts from dilated perivascular spaces (Virchow-Robin-Spaces), lesions within the lower third of the corpus striatum and a diameter < 2 mm were excluded [87, 115].
CMB were defined as focal areas of signal void on T2-weighted images, which increased in size on T2*-weighted images ("blooming effect"). In this way, CMB were distinguished from vascular flow voids. Symmetric hypointensities in the basal ganglia, likely to represent calcifications or nonhaemorrhagic iron deposits were disregarded [25]. Number and localization (corticosubcortical junction, deep white matter and basal ganglia) were recorded [115].

Assessment of grey and white matter microstructural integrity using DTI [128]
The individual raw diffusion tensor images were pre-processed to create individual FA, L1, L2, L3 and MD images using FDT (FMRIB's Diffusion Toolbox) tools [116-118]. The original images were corrected for effects of head

movement and eddy currents in the gradient coils, which induce stretches and shears in the DTI images, using affine registration to a non-diffusion-weighted reference volume. A diffusion tensor model was fitted to the eddy current corrected images to create individual FA, L1, L2, L3 and MD images.

3D T1-weighted images were skull-stripped using BET (brain extraction tool) [68] and subsequently segmented using FAST (FMRIB's automated segmentation tool) [71] resulting in individual brain masks for grey matter and white matter. The segmented brain structures were aligned into common space using the linear registration tool FLIRT (FMRIB's linear image registration tool) [69, 70]. Mean fractional anisotropy (FA), axial diffusivity (AxD), radial diffusivity (RD) and mean diffusivity (MD) values were calculated for grey and white matter. All DTI measures below -3 or above 3 standard deviations were excluded from statistical analysis.

Voxel-wise statistical analysis of white matter FA data was performed using TBSS (Tract-Based Spatial Statistics) [119]. All subjects' FA data were aligned into common space using the nonlinear registration tool FNIRT (FMRIB's nonlinear image registration tool) [73, 74]. A mean FA image was created and thinned to create a mean FA skeleton representing the centres of all tracts common to the group. Each subject's aligned FA data was projected onto this skeleton. Likewise, individual AxD, RD and MD images were prepared for voxel-wise statistics.

Assessment of grey and white matter microstructural integrity using MTI

Raw magnetization transfer scans were split in the M0-sequence (acquired without saturation pulse) and the M1-sequence (acquired after application of a saturation pulse).

First, cortical grey matter and white matter MTI parameters were quantified using histogram analysis. 3D T1-weighted images were skull-stripped using BET (brain extraction tool) [68] and segmented using FAST (FMRIB's automated segmentation

tool) [71] resulting in individual brain masks for cortical grey matter and white matter. All individual 3D T1-weighted images were registered to the individual non-saturated M0 images using FMRIB's linear image registration tool (FLIRT) [69, 70]. Registration matrices from the previous step were used to coregister the non-saturated M0 images and the individual brain masks for the above mentioned brain structures so that the magnetization transfer ratio (MTR) maps could be masked with these brain masks. To correct for possible partial volume effects, an eroded mask of these segmentations was created by removing one voxel in-plane for all mentioned volumes-of interest (VOIs) [145]. Individual MTR maps were calculated voxel by voxel following the equation MTR = (M0-M1)/M0 and MTR histograms were generated for grey matter and white matter. Mean MTR, MTR peak height, normalized for the size of the VOI, and MTR peak location were calculated from each MTR histogram [146]. Mean MTR reflects the average MTR value per structure. MTR peak location reflects the most common MTR value. The peak height of the MTR histogram indicates the number of voxels showing the most common MTR value, and is a measure of uniformity of the underlying voxels in terms of MTR values. As the size of the VOI influences the number of voxels having the most common MTR value, MTR peak height was normalized by dividing the number of voxels with the most common MTR value by the number of voxels within the VOI. All MTI measures below -3 or above 3 standard deviations were excluded from statistical analysis.

Subsequently, voxel-based analysis of cortical grey matter MTR maps was performed. MTR maps, which were coregistered to the individual 3D T1-weighted images, were processed according to the optimized voxel-based morphometry protocol of Good et al. [54, 72], carried out with FSL tools [64]. Tissue-type segmentation was performed on the brain-extracted MTR images using FAST4 [71]. The resulting grey matter partial volume MTR maps were aligned to MNI (Montreal Neurological Institute) 152 standard space using the non-linear

registration tool FNIRT (FMRIB's non-linear registration tool) [73, 74]. To improve the quality of segmentation and normalization, a study-specific MTR template was created by averaging the obtained registered MTR maps of all study participants. The native individual MTR maps were non-linearly re-registered to this template. The segmented images were smoothed with an isotropic Gaussian kernel with a sigma of 3 mm.

Next, voxel-wise statistical analysis of white matter MTR data was performed using TBSS (Tract-Based Spatial Statistics) [119]. This analysis was based on the creation of a mean white matter skeleton from fractional anisotropy (FA) images as described above. All subjects' non-saturated M0 images and saturated M1 images were linearly registered to the DTI B0 image, which is based on a raw T2 signal without diffusion weighting. MTR maps were calculated in "B0-space" in the same manner as described above. The resulting individual MTR maps were non-linearly registered into MNI152 standard space using FNIRT [73, 74] and projected onto the mean FA skeleton.

Statistical analysis

For statistical analyses, Statistical Package for the Social Sciences (SPSS) software for windows (version 20.0) was used. For all analyses, significance threshold was set at $P < 0.05$.

Analysis of variance was used to assess changes in age across the five CAC score groups. Differences in sex and descent were tested using a Chi-square test. Analyses of differences in vascular risk profile (Table 6.1) were adjusted for age, sex and descent. Logistic regression and analysis of covariance was used were appropriate.

For categorical outcome parameters, ordinal and binary logistic regression were applied to test whether the OR changed significantly with increasing CAC. Linear

regression analysis was performed to assess differences in continuous outcome parameters. All analyses for outcome parameters were adjusted for age, sex and descent.

Results

Characteristics of the study population are presented in Table 6.1 for the total study cohort and five CAC score groups separately. In total, 328 subjects with a mean age of 66 years participated in the study. With increasing CAC, age, history of hypertension and diabetes increased, whereas the relative amount of women within the group decreased. There were no differences between CAC groups concerning other vascular risk factors (Table 6.1).

CAC and macrostructural brain damage

The associations of CAC with grey and white matter volumes are shown in Table 6.2. No significant associations were found.

Tables 6.2 and 6.3 show the association of CAC with periventricular and subcortical WML, volume of WML, presence of lacunar infarcts and CMB. Increasing CAC was associated with an approximately 1.3-fold higher probability to have more periventricular bands, periventricular WML in general and CMB (OR (95% CI) 1.34 (1.10-1.63), P = 0.004; OR (95% CI) 1.32 (1.08-1.62), P = 0.006; OR (95% CI) 1.36 (1.01-1.81), P = 0.04 respectively). Moreover, increasing CAC was associated with a more than twofold probability to have lacunar infarcts (OR (95% CI) 2.15 (1.10-4.20), P = 0.002). Subcortical WML and total volume of WML were not associated with CAC (Tables 6.2 and 6.3).

Table 6.1 Characteristics of the study population

		Coronary artery calcification load					
	Total	0	1 (1-10)	2 (11-100)	3 (101-400)	4 (>400)	P
	n=328	n=114	n=43	n=82	n=52	n=37	
Demographics							
Age (years)	65.6 (6.9)	62.3 (6.9)	67.5 (6.2)	65.5 (6.2)	68.5 (5.2)	70.1 (6.1)	< 0.001
Women	175 (53.4)	85 (74.6)	24 (55.8)	38 (46.3)	19 (36.5)	9 (24.3)	< 0.001
Offspring	173 (52.7)	63 (55.3)	28 (65.1)	32 (39.0)	31 (59.6)	19 (15.4)	0.50
Vascular risk profile							
Hypertension	76 (26.0)	17 (17.0)	6 (15.4)	20 (26.7)	14 (31.1)	19 (57.6)	< 0.001
MI	4 (1.3)	0 (0)	0 (0)	1 (1.3)	3 (6.5)	0 (0)	0.35
Diabetes	14 (4.7)	1 (1.0)	1 (2.6)	3 (3.9)	2 (4.4)	7 (20.0)	0.004
Stroke	9 (3.0)	3 (2.9)	0 (0)	1 (1.3)	3 (6.5)	2 (5.6)	0.59
Smoking	36 (11.1)	14 (12.5)	2 (4.8)	10 (12.2)	6 (11.5)	4 (10.8)	0.56
BMI	26.3 (3.7)	25.9 (3.4)	25.8 (2.9)	26.8 (3.6)	26.5 (4.6)	27.5 (3.6)	0.29
HDL-C	1.46 (0.43)	1.57 (0.45)	1.45 (0.46)	1.39 (0.37)	1.37 (0.44)	1.38 (0.41)	0.36
TG	1.74 (0.94)	1.57 (0.89)	1.71 (0.90)	2.00 (1.21)	1.77 (0.61)	1.65 (0.76)	0.32

Values represent numbers (percentage) for dichotomous variables or means (standard deviation) for continuous variables. All analyses of differences in vascular risk profile were adjusted for age, sex and descent.

BMI, body mass index (kg/m^2); HDL-C, high density-lipoprotein-cholesterol (mmol/L); MI, myocardial infarction; TG, triglycerides (mmol/L).

Table 6.2 Association of CAC with brain volumes and WML volume

	Standardized Beta	P
Brain tissue volume (cm^3)		
Gray matter	-0.045	0.37
White matter	0.006	0.91
Total WML volume (mm^3)	0.003	0.96

P-values are adjusted for age, sex and descent.

Table 6.3 Association of CAC with WML, lacunar infarcts and CMB

	OR	95% CI	P
White matter lesions			
Periventricular			
Frontal caps	1.20	0.995-1.46	0.06
Occipital caps	1.04	0.87-1.23	0.67
Bands	1.34	1.10-1.63	0.004
Total	1.32	1.08-1.62	0.01
Subcortical			
Frontal	1.15	0.96-1.39	0.14
Temporal	0.96	0.80-1.15	0.65
Parietal	1.12	0.93-1.34	0.23
Occipital	0.995	0.83-1.19	0.96
Total	1.09	0.92-1.29	0.31
Lacunar infarcts	2.15	1.10-4.20	0.002
Cerebral microbleeds	1.36	1.01-1.81	0.04

Values represent odds ratios (OR) (95% CI; 95% confidence interval). P-values are adjusted for age, sex and descent.

CAC and microstructural brain damage

Increasing CAC was associated with decreased microstructural grey matter integrity regarding all measured DTI and MTI parameters (all $P < 0.05$) except for grey matter AxD and mean MTR ($P = 0.09$ and $P = 0.06$ respectively) (Table 6.4). Increasing CAC was associated with decreased microstructural white matter integrity, expressed in increasing MD and AxD and decreasing normalized MTR peak height ($P = 0.05$, $P = 0.03$ and $P = 0.03$ respectively). The association of CAC with white matter FA and RD was borderline significant ($P = 0.09$ and $P = 0.05$ respectively) (Table 6.4).

Table 6.4 Association of CAC with mean grey and white matter DTI and MTI parameters

	Standardized Beta	P
DTI (*1000)		
FA		
Grey matter	-0.034	0.001
White matter	-0.105	0.09
MD		
Grey matter	0.105	0.04
White matter	0.098	0.05
AxD		
Grey matter	0.086	0.09
White matter	0.109	0.03
RD		
Grey matter	0.105	0.04
White matter	0.097	0.05
MTI		
Norm. MTR PH (/1000)		
Grey matter	-0.136	0.02
White matter	-0.129	0.03
Mean MTR (*1000)		
Grey matter	-0.111	0.06
White matter	-0.092	0.13
MTR PL (*1000)		
Grey matter	-0.145	0.02
White matter	-0.018	0.77

P-values are adjusted for age, sex and descent.

FA, fractional anisotropy; MD, mean diffusivity; AxD, axial diffusivity; RD, radial diffusivity; Norm. MTR PH, normalized magnetization transfer ratio peak height; Mean MTR, mean magnetization transfer ratio; MTR PL, magnetization transfer ratio peak location.

Figures 6.1 and 6.2 depict the spatial distribution of changing white matter DTI and MTI parameters with increasing CAC. There was a widespread increase of MD, AxD and RD showing an anterior-posterior gradient most pronounced in the corpus callosum. CAC associated decrease of FA and MTR was restricted to small regions in the centrum semiovale and callosal genu (FA) and the posterior limb of the left internal capsule (MTR) respectively. Furthermore, figure 6.2 shows the spatial distribution of decreasing grey matter MTR with increasing CAC. Changes were more or less symmetric and predominantly located in frontal/frontoparietal regions.

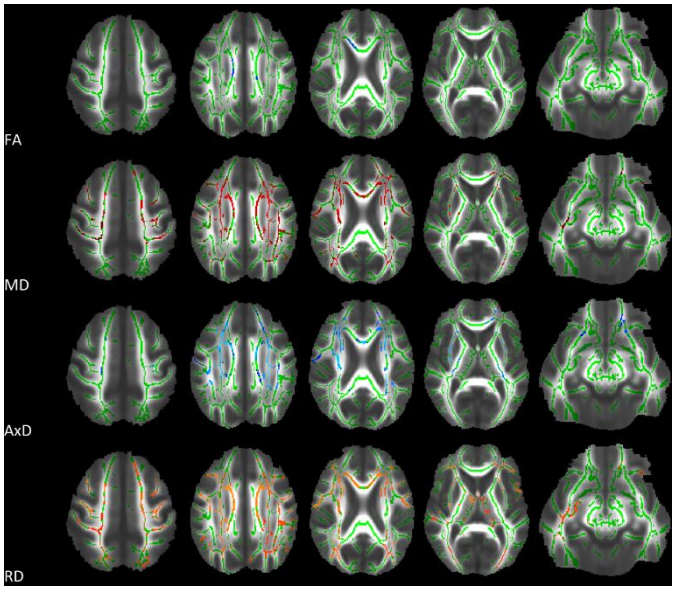

Figure 6.1 Spatial distribution of white matter DTI parameter changes with increasing CAC
Dark blue (FA, fractional anisotropy), red (MD, mean diffusivity), light blue (AxD, axial diffusivity) and orange (RD, radial diffusivity) indicates white matter regions showing decrease (FA) or increase (MD, AxD and RD) of white matter DTI parameters with increasing CAC (all $P < 0.05$). Results and mean white matter skeleton (green) are projected on the mean FA image of all study participants. Statistical analysis was adjusted for age, sex and descent.

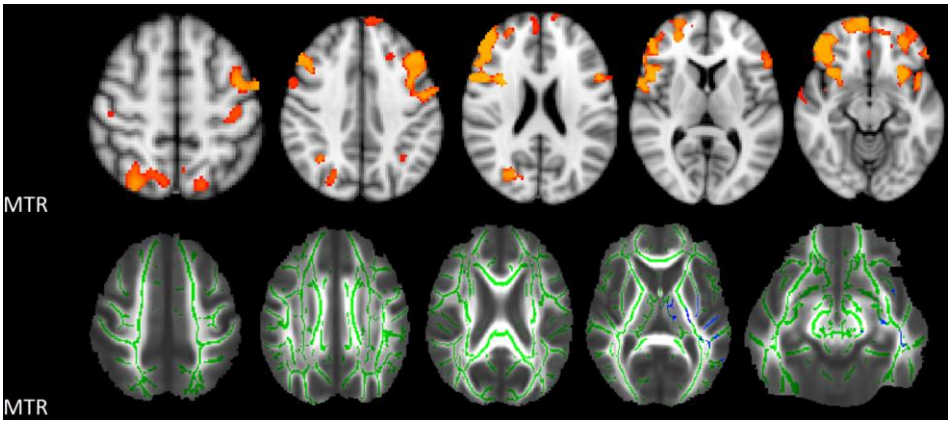

Figure 6.2 Spatial distribution of grey and white matter MTR changes with increasing CAC
Orange (grey matter) and dark blue (white matter) colour indicates decrease of MTR with increasing CAC using FSL-VBM (grey matter) and FSL TBSS (white matter) (both $P < 0.05$). Results are projected on the MNI152 space T1-weighted image provided by FSL (grey matter) and the mean FA image of all study participants (white matter). Green colour shows mean white matter skeleton. Statistical analysis was adjusted for age, sex and descent.

Discussion

The most important finding of our study is that CAC is associated with cerebral small vessel disease reflected in higher prevalences of WML, lacunar infarcts and CMB and decreased microstructural grey and white matter integrity. CAC associated WML are predominantly located periventricular. White matter microstructural damage is widespread with an anterior-posterior gradient most pronounced in the corpus callosum. Loss of grey matter microstructural integrity is predominantly located in frontal/frontoparietal regions.

Our findings suggest that CAC is not associated with grey and white matter atrophy. Vidal et al. described lower grey and white matter volumes with increasing CAC [159] whereas Bos et al. reported an association of CAC with lower grey but not white matter volumes [157]. Another study described an association of CAC with higher ventricular grade which diminished after adjustment for age [158]. Studies on the association between brain atrophy and markers of vascular disease have suggested that only subcortical atrophy (i.e. ventricular enlargement) but not cortical atrophy (i.e. sulcal widening) might have a microvascular aetiology [165]. Moreover, WML and lacunar infarcts were associated with brain atrophy independent of vascular risk factors, suggesting that neurodegenerative processes and vascular brain damage co-occur whereas the underlying pathophysiological mechanisms are not clear yet [166]. Our study population was slightly younger compared to the Rotterdam Scan Study [157] and considerably younger compared to the AGES-Reykjavik Study [159]. Possibly, brain volumetric changes in our study population were too subtle to be detected. Further studies are needed to unravel the possible vascular component of brain atrophy in elderly individuals.

CAC was associated with total periventricular WML load, more specifically periventricular bands and less pronounced frontal caps, but neither with subcortical WML nor total WML volume. Moreover, CAC was associated with presence of lacunar infarcts and CMB. By contrast, in the Rotterdam Scan Study, CAC was associated with total WML volume and presence of lacunar infarcts but not CMB [160]. In the AGES-Reykjavik Study and another study on CAC and cerebral small vessel disease, presence of cerebral infarcts and CMB was associated with CAC, which is in line with our results. In both mentioned studies, total volume of WML and advanced WML respectively were associated with CAC [159, 161]. Additionally, our results are in line with a study from Rosano et al., who reported higher white matter grade and more brain infarcts with increasing CAC in an elderly population [158]. All the mentioned studies did not differentiate between periventricular and subcortical WML. It is commonly accepted that periventricular and subcortical WML differ regarding the underlying histopathology. The former are thought to represent disruption of the ependymal periventricular lining, subependymal gliosis, increased periventricular water content and myelin loss [167, 168]. However, decline in total cerebral blood flow has been associated with increase in periventricular but not subcortical WML, suggesting a flow-component for the development of periventricular WML [169]. Dependent on the lesion severity, subcortical WML have been associated with widening of periarteriolar spaces (punctuate lesions) [167, 170] and perivascular loss of myelin, fibre loss, gliosis and arteriosclerosis (early confluent and confluent lesions) [167] consistent with advanced microangiopathy [171]. Furthermore, WML have been associated with inflammatory biomarkers of cerebrovascular disease [172]. Thus, the association of CAC with periventricular WML implies that CAC as overall marker of arteriosclerosis indicates low flow cerebrovascular damage. CAC is no marker of microangiopathic brain damage in the sense of subcortical WML. Total WML volume was relatively low compared to the studies, which

reported an association between CAC and WML volumes. Possibly, in our study, subcortical WML were too subtle at this mean age of the study population.

CAC is a marker of decreased white matter microstructural integrity, most pronounced with respect to an increase in AxD. This is conform the Rotterdam Scan Study [157]. Increasing CAC was accompanied by an increase in MD, AxD and RD, showing an anterior-to-posterior gradient, which is a frequently described pattern of age-related changes of white matter integrity [106, 128]. Vascular risk factors have been shown to be associated with loss of white matter integrity beyond the effects of age [173]. Our findings suggest that CAC is a marker of white matter microstructural damage in a spatial distribution paralleling the detrimental effects of the aging process. The CAC associated decrease of FA was restricted to a small area in the centrum semiovale and callosal genu. As a summary measure FA reflects to what extent AxD exceeds RD and thus the orientational coherence of the underlying tissue and is therefore less specific concerning underlying microstructural changes [103, 104]. Thus, increases in AxD and RD with increasing CAC do not necessarily have to be accompanied by a decrease in FA. CAC was associated with normalized white matter MTR peak height - a measure of uniformity of underlying voxels in terms of MTR values. Mean MTR was lower in all types of WML [174] and normal appearing brain tissue in individuals with known cerebrovascular risk factors [141]. CAC can be considered as marker of vascular white matter damage on the macromolecular level. Decrease of white matter MTR with increasing CAC was restricted to the posterior limb of the left internal capsule. MTR has been proposed to be relatively specific for white matter myelin status [132], but is additionally influenced by pathological conditions such as inflammation [150], oedema [151] and axon loss [153]. Likewise, RD has been suggested to be specific for myelin status in mice [134]. Studies in humans have shown that increases in RD might rather be driven by decreased axon packing

density through an increase in extracellular water, which can be induced by different underlying pathological processes [106]. Thus, it is not likely that the increase of RD with increasing CAC is driven by white matter demyelination.
CAC associated grey matter damage was mainly located in frontal and less pronounced frontoparietal regions. This is in line with the fact that e.g. age-related loss of grey matter volume is more pronounced in frontal compared to occipital brain regions [31]. Our findings suggest that CAC is a marker of early (vascular) grey matter damage again paralleling the detrimental effects of the aging process. One strength of our study is the large cohort of elderly individuals who underwent both coronary artery CT and brain MRI. Subjects were relatively young regarding the detection of subtle age-related vascular brain damage which belongs to the limitations.

In conclusion, this is the first study to investigate CAC associated brain pathology in a large study population of elderly individuals on the macro- and microstructural level including the spatial distribution of brain pathology. Beyond focal ischemic brain lesions, CAC was associated with widespread microstructural brain pathology spatially predominantly paralleling the detrimental effects of the aging process.

7

Cerebral microbleeds are predictive of mortality in the elderly

Stroke, 2011;42:638-44

I. Altmann-Schneider
S. Trompet
A.J.M. de Craen
A.C.G.M. van Es
J.W. Jukema
D.J. Stott
N. Sattar
R.G.J. Westendorp
M.A. van Buchem
J. van der Grond

Abstract

Background and purpose:

To investigate the prognostic value of cerebral microbleeds (CMB) regarding overall, cardiovascular-related, and stroke-related mortality and to investigate possible differences based on a cerebral amyloid angiopathy-type and nonlobar distribution of microbleeds.

Methods:

We included 435 subjects who were participants from the nested MRI substudy of the PROspective Study of Pravastatin in the Elderly at Risk (PROSPER). Cox proportional hazard models were applied to estimate the risk of overall, cardiovascular-related, and stroke-related death associated with microbleeds in general and microbleeds with a lobar distribution suggestive of the presence of cerebral amyloid angiopathy. The corresponding Kaplan-Meier survival curves were calculated.

Results:

Subjects with > 1 CMB had a 6-fold risk of stroke-related death compared to subjects without CMB (hazard ratio, 5.97; 95% CI, 1.60–22.26; P = 0.01). The diagnosis of nonlobar microbleeds was associated with > 2-fold risk of cardiovascular death compared to subjects without microbleeds (hazard ratio, 2.67; 95% CI, 1.23–5.81; P = 0.01). Subjects with probable cerebral amyloid angiopathy-type microbleeds had > 7-fold risk of stroke-related death compared to subjects without CMB (hazard ratio, 7.20; 95% CI, 1.44–36.10; P = 0.02).

Conclusions:

This is the first study investigating the association between microbleeds and risk of overall, cardiovascular- related, and stroke-related mortality in an elderly population. Our findings indicate that the diagnosis of microbleeds is potentially of clinical relevance. Larger studies are needed to expand our observations and to address potential clinical implications and cost-benefits of such a policy.

Introduction

Cerebral microbleeds (CMB) are focal hemosiderin deposits that result from minimal blood leakage from damaged small vessels1 and can be regarded as markers of pathological vascular changes [25]. Concerning histopathology, the two most common types of underlying small vessel damage are hypertensive vasculopathy and cerebral amyloid angiopathy (CAA) [23, 26, 27]. The location and distribution of CMB depend on the type of underlying vasculopathy; whereas hypertensive CMB preferentially occur in deep brain regions such as the basal ganglia, thalamus, or brain stem, CAA-type CMB are mainly located in the cerebral lobes but never in deep brain regions [24, 25, 28, 29]. CMB are commonly seen in patients with ischemic stroke [81], intracerebral haemorrhage [23], Alzheimer's disease [175], traumatic brain injury-associated diffuse axonal injury [176], and also in healthy elderly individuals [21]. The prevalence of CMB in the general population increases from ≈20% in subjects aged 60 to 69 years to ≈40% in subjects aged 80 years and older [28]. Presence of CMB was the strongest predictor of overall mortality among a range of MRI markers of vascular damage in a memory clinic population [22]. It remains to be elucidated whether CMB are predictive of mortality in the general population. Furthermore, it is not known to what extent CMB are specifically associated with cardiovascular mortality or noncardiovascular disease.

In the present study, we investigated the prognostic value of CMB regarding overall, cardiovascular-related, and stroke-related mortality in a population enriched for or at high risk for cardiovascular disease. Moreover, we investigated possible differences in prognostic value based on a CAA-type and nonlobar distribution of CMB.

Methods

Study participants

All subjects are participants from the nested MRI substudy of the PROspective Study of Pravastatin in the Elderly at Risk (PROSPER) [30]. Inclusion criteria for the PROSPER were men or women aged 70 to 82 years with a total cholesterol of 4.0 to 9.0 mmol/L and a history of either ischemic or haemorrhagic stroke, transient ischemic attack, myocardial infarction, arterial surgery, or amputation for vascular disease, or one of the following risk factors for vascular disease: current smoker, hypertension diagnosed, diabetes mellitus, or fasting blood glucose > 7 mmol/L. Of the included subjects, 43% had symptomatic vascular disease. These subjects experienced symptoms > 6 months before entering the study. Exclusion criteria have been described in detail elsewhere [177]. There were no specific inclusion criteria for the MRI substudy. All consenting subjects (646 of the 1100 eligible Dutch participants) were enrolled in the Netherlands from May 2, 1998. CMB were scored on MRI scans obtained at the end of the study. Ninety-two subjects did not undergo an MRI scan because of the following reasons: 44 subjects were ill or had contraindications for MRI, 40 subjects had died, six subjects had withdrawn informed consent, and two could not undergo a scan because of technical problems [178]. T2*-weighted scans for the detection of CMB were available for 435 subjects. Baseline characteristics of these 435 subjects and the remaining 665 Dutch PROSPER participants were similar, except for the proportion of smokers, which was significantly higher among the 665 Dutch participants (26.8% vs 20.5%; P = 0.02). Mortality of study participants was continuously followed-up after the official end of the study until December 31, 2009. The individual causes of death were obtained through the Central Bureau of Statistics of the Netherlands. All end points were adjudicated by the independent clinical events committee of PROSPER. The protocols meet

the criteria of the Declaration of Helsinki and were approved by the Medical Ethics Committees of each participating institution. Written informed consent was obtained from all participating patients.

MRI acquisition

All imaging was performed on an MR system operating at field strength of 1.5 T (Philips Medical Systems). Dual fast-spin echo (repetition time = 3000 ms; echo times = 27/120 ms; flip angle = 90°; slice thickness = 3 mm; 48 slices; no interslice gap; field of view = 220 x 220 mm; matrix = 256 x 204), fluid-attenuated inversion recovery (FLAIR) (repetition time = 8000 ms; echo time = 100 ms; inversion delay = 2000 ms; flip angle = 90°; slice thickness = 3 mm; 48 slices; no interslice gap; field of view = 220 x 176 mm; matrix = 256 x 153), and T2*-weighted images (multislice gradient echo sequence; repetition time = 2593 ms; echo time = 48 ms; flip angle = 60°; slice thickness = 6 mm; 22 slices; interslice gap = 6 mm; whole brain coverage; field of view = 220 x 198 mm; matrix = 256 x 176) were obtained from all subjects.

MRI analysis

Microbleeds

All MRI scans were read in consensus by two experienced raters (A.C.G.M.v.E. and M.A.v.B.), who were blinded to the clinical history. CMB were defined as focal areas of signal loss on T2-weighted images that increased in size on the T2*-weighted gradient-echo planar images ("blooming effect") [25]. In this way, CMB were differentiated from areas of signal loss based on vascular flow void. Areas of symmetrical hypointensity in the basal ganglia likely to represent calcification or nonhaemorrhagic iron deposits were disregarded. For each subject, number and location (corticosubcortical junction, deep white matter, basal ganglia, and infratentorial) of CMB were recorded. All study participants

were assigned to one of the following groups according to the number of CMB: no microbleeds, 1 microbleed, > 1 microbleed.

Subsequently, we applied the Boston criteria for CAA to all subjects. The Boston criteria are designed to estimate the likelihood of the presence of CAA during life by means of location and number of intracerebral haemorrhages. We categorized subjects as having no microbleeds, possible CAA (MRI demonstrating a single lobar, cortical, or corticosubcortical haemorrhage without any other cause of haemorrhage), probable CAA (MRI demonstrating multiple lobar, cortical, or corticosubcortical haemorrhages without any other cause of haemorrhage), or microbleeds not qualifying for CAA (nonlobar microbleeds) [24, 179, 180].

White matter lesions, atrophy, and cerebral infarction

Segmentation of white matter lesions (WML), intracranial volume, and brain parenchyma volume was performed automatically using Software for Neuro-Image Processing in Experimental Research [181], a program developed in-house for image processing. This segmentation was performed on the T2-weighted and FLAIR images. WML connected to the lateral ventricles were labelled as periventricular WML, and WML not connected to the lateral ventricles were labelled as deep WML [178]. The volumes of periventricular WML and deep WML were calculated automatically by Software for Neuro-Image Processing in Experimental Research. All measurements were performed blinded to subject identity, age, and sex. A measure reflecting whole brain atrophy and hippocampal atrophy was calculated using the following equations: atrophy (%) = [(intracranial volume-parenchymal volume)/intracranial volume] x 100% and hippocampal atrophy (%) = (hippocampal volume/intracranial volume) x 100%, respectively [182, 183]. Cortical infarcts were defined as cortical defects surrounded by a hyperintense zone on T2-weighted scans. Lacunar infarcts were defined as parenchymal defects, not extending into the cortex, surrounded by a hyperintense

zone (≥ 3 mm, < 15 mm in diameter) on a T2-weighted scan. Dilated perivascular spaces were distinguished from infarcts on the basis of their location, form, and the absence of a hyperintense zone around the parenchymal defect.

Statistical analysis

For statistical analysis, SPSS software for windows (version 17.0.1; SPSS) was used. Kaplan-Meier survival curves for overall, cardiovascular-related, and stroke-related mortality were calculated for no, 1, and > 1 microbleed, possible and probable CAA-type CMB, and nonlobar microbleeds. We applied Cox proportional hazard models to estimate the risk of overall, cardiovascular-related, and stroke-related death associated with these microbleed categories in two different ways: adjusting for age, sex, and use of statins (Model 1; n = 435 for overall mortality, n = 434 for cardiovascular-related and stroke-related mortality; the cause of death of one subject was missing) and additionally adjusting for cardiovascular risk factors (alcohol use, smoking, body mass index, high-density lipoprotein cholesterol, systolic and diastolic blood pressure, and history of hypertension/diabetes mellitus/ischemic or haemorrhagic stroke/transient ischemic attack; Model 2; n = 418 for overall mortality, n = 417 for cardiovascular-related and stroke-related mortality; the cause of death of one subject was missing).

Results

Baseline characteristics of the study population are shown in Table 7.1. In total, 435 participants with a mean age of 75.0 years and a female fraction of 43.6% were included in the present study. The mean follow-up duration for determining mortality was 7.0 (± 2.1) years. In this period, 153 subjects (34.9%) died, of whom 57 (37.3%) died of cardiovascular causes: 14 had an ischemic or

haemorrhagic stroke, 43 subjects died of cardiovascular causes not affecting the brain, and the cause of death of one subject was missing. The individual amount of CMB was not significantly different between subjects treated with statins and subjects treated with placebo (data not shown). History of hypertension was significantly associated with the diagnosis of CMB independent of the other mentioned cardiovascular risk factors (P = 0.005; data not shown).

First, we investigated the risk of overall, cardiovascular-related, and stroke-related death associated with the diagnosis of no, 1, or > 1 microbleed. Subjects with > 1 microbleed diagnosed had an increased risk of overall death compared to subjects without CMB after adjustment for age, sex, use of statins, and cardiovascular risk factors not reaching statistical significance (hazard ratio (HR), 1.41; 95% CI, 0.87–2.27; P = 0.16). The risk of cardiovascular death for these subjects was broadly similar (HR, 1.78; 95% CI, 0.86–3.70; P = 0.12; Table 7.2). Strikingly, subjects with > 1 microbleed diagnosed had ≈6-fold risk of stroke-related death compared to subjects without microbleeds after adjustment for age, sex, use of statins, and cardiovascular risk factors (HR, 5.97; 95% CI, 1.60–22.26; P = 0.01).

Table 7.1 Baseline characteristics of the study population

Demographics	
Total number of participants	435
Age (years)	75.0 (3.3)
Women	190 (43.7)
Use of statins	210 (48.3)
Cardiovascular risk factors	
Alcohol use (U/week)	6.66 (8.0)
Smoking	89 (20.5)
HDL-cholesterol (mmol/L)	1.31 (0.37)
BMI (kg/m2)	26.6 (3.6)
Systolic BP (mmHg)	156 (21)
Diastolic BP (mmHg)	84 (11)
History of hypertension	279 (64.1)
History of diabetes mellitus	66 (15.2)
History of stroke (ischemic or haemorrhagic) or transient ischemic attack	70 (16.1)
MRI characteristics	
Participants with microbleeds	104 (23.9)
Participants with CAA type microbleeds	72 (16.6)
Participants with non-lobar microbleeds	32 (7.4)
Brain atrophy (% of ICV)	27.2 (3.5)
Hippocampal volume (% of ICV)	0.5 (0.1)
Volume of WML (% of ICV)	0.5 (0.8)
Participants with lacunar infarcts	88 (20.2)
Participants with cortical infarcts	45 (10.3)

Values represent numbers (percentage) for dichotomous variables or means (standard deviation) for continuous variables unless otherwise stated.

CAA, cerebral amyloid angiopathy; BMI, body mass index; BP, blood pressure; HDL cholesterol, high-density lipoprotein cholesterol; ICV, intracranial volume; WML, white matter lesion.

Table 7.2 Risk of overall, cardiovascular-related mortality and stroke-related mortality associated with cerebral microbleeds

		Model 1			Model 2	
Microbleeds	d/n	HR (95% CI)	P	d/n	HR (95% CI)	P
Overall mortality		n = 435			n = 418	
0	115/331	1.00 (reference)		109/320	1.00 (reference)	
1	15/52	0.76 (0.45-1.31)	0.33	12/47	0.70 (0.38-1.28)	0.24
> 1	22/52	1.23 (0.78-1.95)	0.38	22/51	1.41 (0.87-2.27)	0.16
Cardiovascular mortality		n = 434			n = 417	
0	40/330	1.00 (reference)		39/319	1.00 (reference)	
1	7/52	1.05 (0.47-2.34)	0.91	4/47	0.60 (0.21-1.71)	0.34
> 1	10/52	1.61 (0.80-3.24)	0.18	10/51	1.78 (0.86-3.70)	0.12
Stroke-related mortality		n = 434			n = 417	
0	9/330	1.00 (reference)		8/319	1.00 (reference)	
1	0/52	no cases		0/47	no cases	
> 1	5/52	3.41 (1.13-10.31)	0.03	5/51	5.97 (1.60-22.26)	0.01

d indicates deceased; HR, hazard ratio; n, total number of subjects.

Values are HR adjusted for age, sex, and use of statins (Model 1) and additionally for cardiovascular risk factors (Model 2), respectively, with 95% CI.

Figure 7.1 shows the corresponding Kaplan-Meier survival curves for overall (Figure 7.1A), cardiovascular (Figure 7.1B), and stroke-related mortality (Figure. 7.1C).

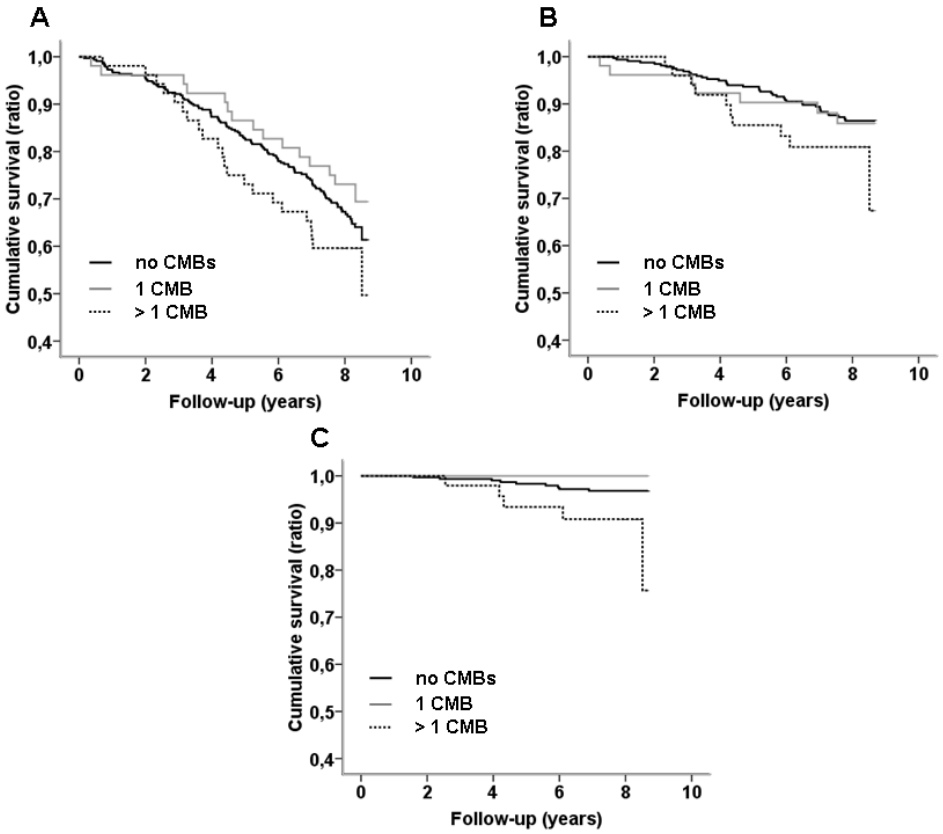

Figure 7.1 Kaplan-Meier survival curves for cerebral microbleeds in general: (A) overall mortality, (B) cardiovascular mortality, and (C) stroke-related mortality. Lines represent cumulative survival for three microbleed categories: no microbleeds, 1 microbleed, and > 1 microbleed.

Subjects with nonlobar microbleeds diagnosed had > 2-fold risk of cardiovascular death compared to subjects without CMB after adjustment for age, sex, use of statins, and cardiovascular risk factors (HR, 2.67; 95% CI, 1.23–5.81; P = 0.01; Table 7.3). This association remained unchanged after additional adjustment for other cerebral changes on MRI (cerebral and hippocampal atrophy, WML, cortical and lacunar infarctions; HR, 3.03; 95% CI, 1.34–6.85; P = 0.01).

Table 7.3 Risk of overall and cardiovascular mortality associated with cerebral microbleeds scores using the Boston criteria

		Model 1			Model 2	
Boston criteria	d/n	HR (95% CI)	P	d/n	HR (95% CI)	P
Overall mortality		n = 435			n = 418	
No microbleeds	115/331	1.00 (reference)		109/320	1.00 (reference)	
Probable CAA	14/32	1.27 (0.73-2.22)	0.40	14/31	1.49 (0.83-2.66)	0.18
Possible CAA	9/40	0.59 (0.30-1.16)	0.13	7/36	0.51 (0.24-1.12)	0.09
Non-lobar microbleeds	14/32	1.25 (0.71-2.18)	0.44	13/31	1.32 (0.73-2.40)	0.36
Cardiovascular mortality		n = 434			n = 434	
No microbleeds	40/330	1.00 (reference)		39/319	1.00 (reference)	
Probable CAA	5/32	1.31 (0.51-3.33)	0.58	5/31	1.67 (0.63-4.46)	0.32
Possible CAA	2/40	0.39 (0.09-1.60)	0.19	0/36	no cases	
Non-lobar microbleeds	10/32	2.62 (1.30-5.29)	0.01	9/31	2.67 (1.23-5.81)	0.01
Stroke-related mortality		n = 434			n = 417	
No microbleeds	9/330	1.00 (reference)		8/319	1.00 (reference)	
Probable CAA	3/32	3.27 (0.86-12.37)	0.08	3/31	7.20 (1.44-36.10)	0.02
Possible CAA	0/40	no cases		0/36	no cases	
Non-lobar microbleeds	2/32	2.18 (0.46-10.23)	0.32	2/31	2.85 (0.49-16.46)	0.24

CAA indicates cerebral amyloid angiopathy; d, deceased; HR, hazard ratio; n, total number of subjects. Values are HR adjusted for age, sex, and use of statins (Model 1) and additionally for cardiovascular risk factors (Model 2), respectively, with 95% CI.

The corresponding Kaplan-Meier survival curves are shown in Figure 7.2A. Approximately 65% of these subjects had CMB located in the basal ganglia diagnosed, 52% had cerebellar CMB diagnosed, 32% had lobar CMB diagnosed, 13% had CMB located in the brain stem diagnosed, and 45% had CMB in at least two of the mentioned locations diagnosed. The HR for cardiovascular mortality were, respectively, 3.06, (95% CI, 1.12–8.34; P = 0.03; deceased/total number of subjects = 6/19, basal ganglia), 4.18 (95% CI, 1.57–11.11; P = 0.004; deceased/total number of subjects = 6/15, cerebellum), 2.51 (95% CI, 0.68–9.23; P = 0.17; deceased/total number of subjects = 3/10, lobar), and 1.62 (95% CI, 0.19–14.12; P = 0.66; deceased/total number of subjects = 1/4 brain stem).

Subjects with probable CAA-type microbleeds diagnosed were exposed to > 7-fold risk of stroke-related death compared to subjects without CMB after adjustment for age, sex, use of statins, and cardiovascular risk factors (HR, 7.20; 95% CI, 1.44–36.10; P = 0.02). The corresponding Kaplan-Meier survival curves are shown in Figure 7.2B. Neither probable CAA-type CMB nor possible CAA-type CMB were associated with an increased risk of overall or cardiovascular death. Combining probable and possible CAA patients in one group did not change these results.

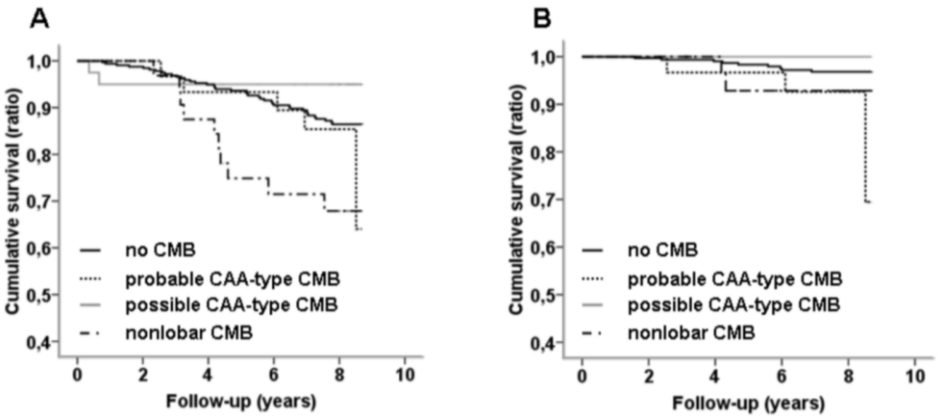

Figure 7.2 Kaplan-Meier survival curves for cerebral microbleeds scored using the Boston criteria: (A) cardiovascular mortality and (B) stroke-related mortality. Lines represent cumulative survival for the different categories of the Boston criteria.

Discussion

The most important findings of this population-based study in elderly individuals are that nonlobar microbleeds are significantly and independently associated with cardiovascular mortality and that probable CAA-type microbleeds are significantly associated with stroke-related mortality.

Nonlobar CMB seem to represent a sensitive marker of increased cardiovascular risk beyond traditional cardiovascular risk factors. Presence of nonlobar CMB was significantly associated with an increased risk of cardiovascular-related but not stroke-related death, independent of cardiovascular risk factors and other cerebral changes on MRI, such as cortical and hippocampal atrophy, WML, and cortical and lacunar infarctions, which have been partly shown to be associated with mortality as well [20, 22, 35, 79].

CMB have been shown to be associated with primary and recurrent intracerebral haemorrhage [184-191], and especially nonlobar microbleeds are strongly associated with hypertension and elevated systolic blood pressure, the traditional risk factors for haemorrhagic and ischemic stroke [28, 192, 193]. Against this background our results are striking, indicating that nonlobar CMB can be regarded as an additional marker of an unfavourable cardiovascular risk profile beyond traditional cardiovascular risk factors, such as hypertension or smoking, and other imaging markers of hypertension, such as left ventricular hypertrophy, which has been established as a predictor of excess cardiovascular mortality [194]. Further studies will be needed to compare the predictive strength of nonlobar CMB against already-established imaging markers of cardiovascular mortality such as left ventricular hypertrophy. However, the value of this finding is limited by the small proportion of subjects with nonlobar CMB diagnosed who died from cardiovascular disease or stroke during follow-up.

CAA-type CMB seem to be markers of an increased risk of stroke-related death, independent of cardiovascular risk factors. However, the number of subjects who died from stroke was small. Furthermore, we could not differentiate between haemorrhagic and ischemic stroke as primary outcome and therefore are not able to further comment about possible associations between CAA-type microbleeds and haemorrhagic or ischemic stroke. Further studies are needed to assess the validity and possible underlying mechanisms of the association between probable CAA-type microbleeds and stroke-related mortality.

The association of CMB with mortality depends on the number of CMB diagnosed in subjects. We could show that subjects with 1 microbleed in general or possible CAA-type microbleeds diagnosed had no increased risk of mortality, whereas subjects with > 1 microbleed in general or probable CAA-type microbleeds diagnosed were exposed to an increased risk of death. Within the group of subjects with nonlobar microbleeds, presence of ≥ 1 CMB was

associated with an increased risk of mortality. Until now, there was only one study investigating the association between CMB and overall mortality in a memory clinic population [22]. In this study, the diagnosis of ≥ 3 microbleeds was associated with an increased risk of overall death. However, because the conspicuity and therefore the accuracy of detection of CMB are strongly affected by the used MRI technique, available MRI field strength, and image post-processing [25], it remains difficult to compare these studies.

A strength of our study is the population-based setting in elderly individuals with or at high risk for vascular disease developing. Although our results might not be generalizable to the general elderly population, we were able to assess the predictive value of CMB in a population in which CMB are most likely to be clinically relevant. Furthermore, the large sample size and high prevalence of CMB in this specific population allowed us to assess the association between CMB and different outcome parameters, such as overall, cardiovascular-related, and stroke-related death, and to analyse these associations for different classifications of CMB and CMB in separate anatomic regions. However, there are also several limitations of this study. First, the adjudication of the primary outcome from the national registry instead of formal follow-up limited the possibility to reliably assess the association between CMB and different outcome parameters. One example is the missing differentiation between haemorrhagic and ischemic strokes. Second, the number of events during follow-up was relatively small, so the association between 1 microbleed in general or possible CAA and stroke-related mortality could not be assessed. Because we did not include other established neuroimaging markers of, for instance, cardiovascular mortality, such as left ventricular hypertrophy, in our study design we were not able to compare the predictive strength of CMB against these markers. Further studies will be needed to address this issue. Furthermore, our results are limited

to a small group of elderly individuals enriched for or at high risk for cardiovascular disease and therefore were neither generalizable to the whole study cohort nor to the general elderly population.

In conclusion, this is the first study to our knowledge investigating the association between CMB and risk of overall, cardiovascular-related, and stroke-related mortality in an elderly population enriched for or at high risk for cardiovascular disease. Our findings indicate that the diagnosis of CMB is potentially of clinical relevance. Elderly people with CMB and additional cardiovascular risk factors could benefit from special cardiovascular monitoring to prevent death from cardiovascular complications. Larger studies are needed to expand our observations and to address potential clinical implications and cost-benefits of such a policy.

Summary and conclusions

The aim of this thesis was to investigate the radiological phenotype of the human brain in familial longevity with regard to brain structure. For this purpose, dedicated MR imaging techniques were applied to study the phenotype of the human brain on the macrostructural as well as microstructural level. To increase our insight in the aging process in general, potential modifying factors of age-related structural brain changes such as coronary artery calcification and risk of mortality associated with cerebral microbleeds as an imaging correlate of cerebral small vessel disease were assessed.

Chapter 2 aimed to identify whether the MRI phenotype of the brain in human longevity is marked by protection from age-related brain atrophy. Common age-related loss of whole brain, cortical grey matter and white matter volume was found in the whole study population but no differences were observed between offspring and control subjects. However, left amygdalar volume was larger in offspring as compared to control subjects, whereas no association of left amygdalar volume was found with chronological age in both offspring and control subjects. Our findings suggest that at a mean age of 66 years human familial longevity is not marked by preserved whole brain, grey and white matter volumes. Furthermore, human familial longevity is characterized by a larger left amygdalar volume, most probably as a result of early development caused by a genetic familial trait. As amygdalar volumes are known to be lower in several neurodegenerative and neuropsychiatric diseases, we hypothesized that human familial longevity might be marked by a lower susceptibility to age-related brain damage.

Hallmarks of cerebral small vessel disease, i.e. white matter lesions, lacunar infarcts and cerebral microbleeds were assessed (semi-)quantitatively in **chapter 3**. Human familial longevity was associated with a lower susceptibility to

periventricular as well as subcortical white matter lesions and lacunar infarcts but not cerebral microbleeds. Interestingly, these associations were independent of the cardiovascular risk profile of the study population. These findings may imply that human familial longevity is marked by a genetically determined lower susceptibility to vascular brain damage in the course of aging which is not mediated by a genetically determined lower susceptibility to cardiovascular damage.

Chapter 4 and **5** deal with the radiological phenotype of the brain in human longevity on the microstructural level. Using diffusion tensor imaging (DTI) white matter microstructural integrity was found to be preserved. By means of tract based spatial statistics (TBSS), a voxel-wise analysis approach of the spatial distribution of changes in white matter microstructure, human longevity was found to be characterized by preserved white matter integrity mainly in the genu and body of the corpus callosum. Moreover, we found a widespread age-related loss of white matter integrity with an anterior-posterior gradient, which has frequently been described in literature and lends support to a "last-in-first-out-theory," assuming that the predominantly frontally located late-myelinating regions, which consist of thinner myelinated axons, are more prone to age-related myelin breakdown. Bringing the results for chronological and biological aging together, we can conclude that human longevity is associated with preserved white matter microstructural integrity in regions which are especially prone to age-related damage. Taking the annual rate of change of white matter diffusion parameters into account, we could calculate a biological age benefit of 4.5 years with regard to white matter integrity for offspring with the propensity to become long-lived as compared to control subjects. These findings raised the question whether preserved white matter microstructure in human longevity could be explained by a lower susceptibility to age-related loss of myelin. For this purpose

magnetization transfer imaging (MTI) was performed. White matter MTI parameters were not different between offspring and control subjects, suggesting that preserved white matter integrity in human familial longevity is caused by a lower susceptibility to pathology other than demyelination.

Coronary artery calcification was assessed as a potential modifying factor of age-related vascular brain damage on the macro- and microstructural level in **chapter 6**. Periventricular white matter lesions, lacunar infarcts and cerebral microbleeds but not brain atrophy were associated with coronary artery calcification. Moreover, loss of grey and white matter microstructural integrity was found with increasing coronary artery calcification predominantly in frontal/frontoparietal regions. The association of coronary artery calcification with focal ischemic lesions as well as widespread microstructural brain damage points to a generalized process equally affecting the heart and the brain. However, as described in chapter three, the genetically determined lower susceptibility to vascular brain damage is independent of a genetically determined lower susceptibility to cardiovascular damage

In **chapter 7** we found that hypertension-related nonlobar microbleeds were associated with an increased risk of cardiovascular mortality independent of cardiovascular risk factors. By contrast, cerebral amyloidy angiopathy (CAA) - related lobar microbleeds were associated with an increased risk of stroke-related death. Additionally, number of microbleeds (more specifically presence of more than one microbleed) was associated with a considerably increased risk of stroke-related mortality. Considering these findings, cerebral microbleeds are of potential clinical relevance and elderly individuals with cerebral microbleeds and cardiovascular risk factors could benefit from special cardiovascular monitoring/intervention to prevent death from cardiovascular complications.

The main purpose of this thesis was to analyse the phenotype of the brain in human familial longevity from a neuroimaging point of view. Several neuroimaging hallmarks of aging were less pronounced in subjects who are genetically enriched to become long-lived.

Strikingly, human familial longevity was marked by a lower susceptibility to neuroimaging correlates of cerebral small vessel disease independent of traditional cardiovascular risk factors although these were also less distinct in the longevity phenotype. With the vast number of pathophysiological pathways of cerebral small vessel disease in mind (e.g. vascular risk factor-related, sporadic and hereditary CAA, genetic, inflammatory etc.) [162], we hypothesized that the lower susceptibility to white matter lesions in human familial longevity might not be driven by a lower susceptibility to cardiovascular damage but rather be determined by other not yet clearly identified mechanisms. Besides cardiovascular risk factors and genes, inflammatory markers have been shown to be associated with white matter lesions and it is known that lower systemic inflammation is associated with longevity in the elderly. Thus, lower systemic inflammation could be a possible explanation for the lower susceptibility to vascular brain damage in the sense of white matter lesions.

Interestingly, white matter microstructural integrity was preserved in those regions which consist of late-myelinating thinner axons and are thought to be most prone to age-related deterioration according to the "last-in-first-out-theory". However, longitudinal studies are needed to investigate whether other white matter regions are also preserved from age-related deterioration either because this part of the longevity phenotype becomes only obvious at a later stage in life or because effects are already present in other regions at this mean age but are too subtle to be picked up by MR imaging techniques.

Using magnetization transfer imaging together with diffusion tensor imaging we could show that the preservation of white matter microstructural integrity cannot

be explained by a lower susceptibility to age-related demyelination but rather by a relatively lower decrease in axonal packing density through an increasing amount of extracellular water, which can be induced by different underlying pathological processes. Further studies are needed to disentangle the underlying histopathological substrate and its pathophysiological pathway.
Larger amgdalar volume was associated with biological but not chronological aging and therefore most likely due to a genetic familial trait. As amygdalar volumes are known to be lower in several neurodegenerative and neuropsychiatric diseases, we hypothesized that human familial longevity might be marked by a lower susceptibility to age-related disorders. To disentangle the exact functional impact of this finding in human familial longevity however is a matter of further (functional) studies.

Beyond focal ischemic lesions, coronary artery calcification, as an overall marker of atherosclerosis, was associated with widespread microstructural brain damage mainly paralleling the detrimental effects of the aging process on the heart and the brain. Thus, coronary artery calcification is not only a biomarker of cardiovascular disease but also of cerebrovascular damage.

In elderly individuals with cardiovascular disease or an increased risk thereof, hypertension related nonlobar microbleeds were associated with an increased risk of cardiovascular death whereas cerebral amyloid angiopathy (CAA)-related lobar microbleeds were associated with an increased risk of stroke-related death. We conclude that elderly individuals with cerebral microbleeds and cardiovascular risk factors could benefit from special cardiovascular monitoring/intervention to prevent death from cardiovascular complications.

In conclusion, the structural phenotype of the brain in human familial longevity is considerably different from that of environmentally and age-matched control subjects. Both features which are most likely caused by early development and a lower susceptibility to known age-related structural brain changes on the macro- as well as microstructural level are hallmarks of the brain phenotype in longevity. However, one might also argue that the greater brain damage in the control group as compared to the offspring of long-lived families could contribute to an accelerated process of aging in "normally" aging people. The contributing mechanisms have yet to be identified but may involve homeostatic control and body function. Keeping in mind that there is a gradual transition from healthy or successful brain aging to what is generally accepted as "normal" brain aging and pathological brain changes as disease correlates, our study results implicate that the brains of offspring of nonagenarian siblings are less susceptible to neurodegenerative brain changes such as (vascular) dementia, Alzheimer's disease and cerebrovascular disease. Our findings should be considered as starting points for future studies on the functional implications of the presented results and studies on the underlying pathways of brain structure preservation in human longevity to be able to translate the gained knowledge to health interventions for the general population to make elderly people in general live healthier for longer and to gain more insight in known pathological brain changes during aging such as Alzheimer's disease and cerebrovascular disease.

Samenvatting en conclusies

Het doel van dit proefschrift was het in kaart brengen van de radiologische phenotype van het brein op structureel niveau in een studiepopulatie, die geselecteerd is op familiaire langlevendheid. Het onderzoek werd uitgevoerd in het kader van de Leiden Langleven Studie. In het kort werd deze studie opgezet om familiaire factoren voor langlevendheid te onderzoeken. De studiepopulatie, die in het kader van dit proefschrift werd onderzocht, bestaat uit kinderen van langlevende Nederlanders, die genetisch een verhoogde kans hebben zelf langlevend te worden en hun echtgenoten, die wat betreft hun leeftijd en omgevingsfactoren een ideale controle groep vormen. De gemiddelde leeftijd van alle studiedeelnemers was 66 jaar. Om de phenotype van het brein op zowel macro- als microstructureel niveau te kunnen bestuderen werden specifieke MRI (magnetization transfer imaging)-technieken gebruikt. Om het inzicht in het verouderingsproces in het algemeen te vergroten, werden bovendien potentieel modificerende factoren van structurele veranderingen van het brein tijdens veroudering bestudeert. Voorbeelden hiervoor zijn verkalking van de coronairen en het risiko op sterfte dat verbonden is aan de diagnose van cerebrale microbloedingen, die wederom een beeldvormende afspiegeling van ziekte van de kleine bloedvaten in de hersenen zijn.

In **hoofdstuk 2** werd onderzocht of de MRI phenotype van het brein van mensen, die geselecteerd zijn op familiaire langlevendheid, gekenmerkt wordt door relatief minder volumeverlies. Wij vonden in de gehele studiepopulatie normaal leeftijds-gerelateerd verlies van het volume van het hele brein, de grijze en de witte stof. Echter konden er geen verschillen worden aangetoond tussen kinderen uit langlevende families en hun echtgenoten. Het volume van de linker amygdala van de kinderen uit langlevende families was groter vergeleken met de controle groep, maar was niet geassocieerd met leeftijd in de hele studiepopulatie. Uit deze bevindingen werd geconcludeerd dat familiaire langlevendheid op een

gemiddelde leeftijd van 66 jaar niet gekenmerkt wordt door minder volumeverlies van het hele brein, de grijze en witte stof. Familiaire langlevendheid wordt wel gekarakteriseerd door een groter volume van de linker amygdala, hetgeen meest waarschijnlijk ontstaat door familiaire aanleg in de vroege ontwikkelingsfase. Het is bekend dat een kleiner volume van de amygdalae geassocieerd is met verschillende neurodegeneratieve en neuropsychiatrische ziektes. Op basis hiervan werd de hypothese opgesteld dat lagere vatbaarheid voor ouderdoms-gerelateerde brein schade in de zin van een relatief groter volume van de linker amygdala mogelijk een uiting is van familiaire langelevendheid.

Verschillende beeldvormende kenmerken van ziekte van de kleine bloedvaten in het brein, zoals witte stof laesies, lacunaire infarcten en cerebrale microbloedingen, werden (semi-)quantitatief in **hoofdstuk 3** onderzocht. Familiaire langlevendheid was geassocieerd met een lagere vatbaarheid voor periventriculaire en subcorticale witte stof laesies en lacunaire infarcten maar niet cerebrale microbloedingen. Interessant genoeg waren deze associaties onafhankelijk van het cardiovasculaire risikoprofiel van de studiepopulatie. Op basis van deze bevindingen werd de hypothese opgesteld dat de phenotype van familiaire langlevendheid gekenmerkt wordt door een genetisch bepaalde lagere vatbaarheid voor vasculaire brein schade tijdens het verouderingsproces. Meest waarschijnlijk is dit niet op een genetisch bepaalde lagere vatbaarheid voor cardiovasculaire schade gebaseerd.

In **hoofdstuk 4** en **5** werd de radiologische phenotype van het brein in familiaire langlevendheid op microstructureel niveau onderzocht. Met behulp van diffusion tensor imaging (DTI) werd aangetoond dat de microstructurele integriteit van de witte stof in mensen, die geselecteerd zijn voor familiaire langlevendheid, hoger is vergeleken met de controle groep. Middels een voxel-based analyse-techniek

(tract based spatial statistics; TBSS) werd aangetoond dat de integriteit van de witte stof met name hoger is in de genu en corpus van het corpus callosum. Bovendien werd in de hele studiepopulatie een uitgebreid leeftijds-gerelateerd verlies van witte stof integriteit gevonden met een gradient van anterieure naar posterieure witte stof regio's. Dit is al vaak in de literatuur beschreven en steunt de zogenoemde "last-in-first-out"-theory, die veronderstelt dat met name de frontaal gelocaliseerde witte stof gebieden, die uit dunnere axonen bestaan en pas laat in de ontwikkeling myeliniseren, vatbaarder zijn voor myeline schade in het kader van veroudering. Met het hoog op boven beschreven resultaten hebben wij geconcludeerd dat familiaire langlevendheid gekenmerkt wordt door betere integriteit van de witte stof met name in regio's, die bijzonder vatbaar zijn voor schade tijdens het verouderingsproces. Rekening houdend met de jaarlijkse verandering van witte stof diffusie parameters in de hele studiepopulatie, werd een biologisch leeftijdsvoordeel van 4,5 jaar berekend wat betreft de integriteit van de witte stof voor kinderen uit langlevende families vergeleken met hun echtgenoten. Op basis van deze bevindingen stelt zich de vraag of de beschreven betere integriteit van de witte stof in mensen, die geselecteerd zijn op familiaire langlevendheid, veroorzaakt wordt door een lagere vatbaarheid voor verlies van myeline tijdens het verouderingsproces. Dit werd middels magnetization transfer imaging (MTI) nader onderzocht. MTI parameters van de witte stof waren niet verschillend tussen kinderen uit langlevende families en de controle groep. Dit suggereert dat de betere integriteit van de witte stof van kinderen uit langlevende families waarschijnlijk niet door een lagere vatbaarheid voor demyelinisatie maar andere pathologische processen in het brein tijdens de veroudering wordt veroorzaakt.

Verkalking van de coronairen werd als een potentieel modificerende factor van leeftijds-gerelateerde vasculaire brein schade op macro- en microstructureel

niveau in **hoofstuk 6** onderzocht. Periventriculaire witte stof laesies, lacunaire infarcten en cerebrale microbloedingen maar niet brein atrofie waren geassocieerd met verkalking van de coronairen. Bovendien naam de integriteit van de grijze en witte stof voornamelijk in frontale en frontoparietale brein regio's met toenemende ernst van verkalking van de coronairen af. De associatie tussen verkalking van de coronairen en zowel focale ischemische laesies in het brein als uitgebreide schade op microstructureel niveau wijst op een gegeneraliseerd process, die in gelijke mate het hart en het brein aantast. Echter is, zoals in hoofdstuk 3 beschreven, de genetisch bepaalde lagere vatbaarheid voor vasculaire brein schade onafhankelijk van een genetisch bepaalde lagere vatbaarheid voor cardiovasculaire schade.

In **hoofdstuk 7** wordt beschreven dat niet-lobaire cerebrale microbloedingen, die gerelateerd zijn aan hypertensie met een verhoogd risico op cardiovasculaire mortaliteit geassocieerd zijn onafhankelijk van cardiovasculaire risiko factoren. Daarentegen zijn lobaire microbloedingen, die met name voorkomen in het kader van cerebrale amyloid angiopathie (CAA) geassocieerd met een verhoogd risiko op sterfte door stroke. Bovendien was het aantal microbloedingen - om precies te zijn de diagnose van meer dan één microbloeding - geassocieerd met een opmerkelijk verhoogd risiko op sterfte door stroke. Gezien deze bevindingen zijn cerebrale microbloedingen potentieel klinisch relevant en oudere mensen met cerebrale microbloedingen én cardiovasculaire risiko factoren zouden baat kunnen hebben bij speciale cardiovasculaire monitoring/interventies om sterfte door cardiovasculaire complicaties te voorkomen.

Het doel van dit proefschrift was het in kaart brengen van de phenotype van het brein in familiaire langlevendheid vanuit het perspectief van neuroradiologische beeldvorming. Meerdere beeldvormende kenmerken van veroudering waren

minder uitgesproken in mensen, die genetisch op familiaire langlevendheid geselecteerd zijn.

Het was een opmerkelijke bevinding dat familiaire langlevendheid gekenmerkt was door een lagere vatbaarheid voor beeldvormende afspiegelingen van ziekte van de kleine bloedvaten in het brein onafhankelijk van traditionele cardiovasculaire risiko factoren, alhoewel deze in de op familiaire langlevendheid geselecteerde groep eveneens minder uitgesproken waren. Met het oog op de grote hoeveelheid pathophysiologische pathways van de ziekte van de kleine bloedvaten in de hersenen (zoals bijvoorbeeld gerelateerd aan vasculaire risiko factoren, sporadisch en erfelijk CAA, genetisch, inflammatoir ezv.), hebben wij de hypothese opgesteld dat de lagere vatbaarheid voor witte stof laesies van mensen, die geselecteerd zijn op familiaire langlevendheid, mogelijk niet veroorzaakt wordt door een lagere vatbaarheid voor cardiovasculaire schade maar eerder bepaald wordt door andere nog niet goed gedefinieerde mechanismen. Naast cardiovasculaire risiko factoren en genen, is een associatie aagetoond tussen inflammatoire markers en langlevendheid bij oudere mensen. Derhalve zou een lager niveau van systemische inflammatie een mogelijke verklaring kunnen zijn voor de lagere vatbaarheid voor vasculaire brein schade in de zin van witte stof laesies bij mensen die geselecteerd zijn op familiaire langlevendheid.

Interessant genoeg was de integriteit van de witte stof in gebieden hoger, die dunnere axonen bevatten en pas laat in de ontwikkeling myeliniseren en waarvan gedacht wordt dat ze het meest vatbaar zijn voor leeftijds-gerelateerde beschadiging volgens de “last-in-first-out”-theory. Er zijn echter longitudinale studies nodig om te onderzoeken of andere witte stof gebieden eveneens minder vatbaar zijn voor leeftijds-gerelateerde beschadiging of omdat dit gedeelte van de phenotype van langlevendheid pas in een later stadium duidelijk detecteerbaar wordt of omdat effecten in andere regio’s op deze gemiddelde leeftijd al aanwezig

maar te subtiel zijn om door beeldvormende (MRI) technieken al te kunnen worden opgespoord.
Middels MTI en DTI hebben wij aangetoond dat de betere integriteit van de witte stof niet verklaard kon worden door een lagere vatbaarheid voor leeftijds-gerelateerde demyelinisatie, maar eerder door een relatief geringere afname van de "axonal packing density" door een toenemende hoeveelheid extracellulair water, dat door verschillenden onderliggende pathologische processen kan worden veroorzaakt. Toekomstige studies moeten zich richten op het ontravelen van het onderliggende histopathologische substraat en de pathophysiologische pathway.
Een groter volume van de linker amygdala was geassocieerd met biologische maar niet chronologische veroudering en daarom meest waarschijnlijk gebaseerd op familiaire aanleg. Het is bekend dat het volume van de amygdalae lager is bij meerdere neurodegeneratieve en neuropsychiatrische ziektes. Lagere vatbaarheid voor leeftijds-gerelateerde ziektes zou daarom een mogelijk kenmerk van de phenotype van langlevendheid kunnen zijn. Om het exacte functionele betekenis van onze bevinding te ontravelen zijn toekomstige (functionele) studies nodig.

Verkalking van de coronairen als algemeen marker voor arterioslcerose was naast focale ischemische laesies ook geassocieerd met uigebreide brein schade op microstructureel niveau en loopt hierbij voor het overgrote deel gelijk aan de schadelijke effecten van het verouderingsprocess zelf op het hart en het brein. Derhalve kan verkalking van de coronairen niet alleen als biomarker voor cardiovasculaire ziekte maar ook voor cerbrovasculaire ziekte worden gezien.
In een studiepopulatie bestaande uit mensen op oudere leeftijd met cardiovasculaire ziekte of een hoog risiko hierop waren hypertensie-gerelateerde niet-lobaire microbloedingen geassocieerd met een verhoogd risiko op cardiovasculaire sterfte, waartegen CAA-gerelateerde lobaire microbloedingen

met een verhoogd risiko op sterfte door stroke geassocieerd waren. Uit deze bevindingen concluderden wij dat oudere individuen met cerebrale mirobloedingen én cardiovasculaire risiko factoren profijt zouden kunnen trekken van speciaal cardiovasculair monitoring/interventies om sterfte door cardiovasculaire complicaties te voorkomen.

Samenvattend kan worden vastgesteld dat de structurele phenotype van het brein in familiaire langlevendheid opmerkelijk anders is dan in de controle groep, die wat betreft leeftijd en omgevingsfactoren vergelijkbaar is. Zowel eigenschappen, die meest waarschijnlijk in de vroege ontwikkelingsfase door familiaire aanleg veroorzaakt worden als een lagere vatbaarheid voor bekende ouderdoms-gerelateerde veranderingen van het brein op macro- en microstructureel niveau zijn kenmerken van het brein phenotype in familiaire langlevendheid. Anderzijds zou men kunnen argumenteren dat de grotere brein schade in de controle grope vergeleken met kinderen uit langlevende families een teken zou kunnen zijn van een versneld verouderingsprocess in “normaal” verouderende mensen. De hieraan bijdragende mechanismen moeten nog geidentificieerd worden maar zouden controle over de homeostase en lichamelijke functies kunnen omvatten. Onze bevindingen zouden als uitgangspunt voor toekomstige studies moeten worden gezien, die met name gericht zijn op de functionele implicaties en onderliggende mechanismen van de in dit proefschrift gepresenteerde resultaten. Hierdoor zou het mogelijk kunnen worden de verworven kennis naar interventies in de gezondheidszorg voor de algemene bevolking te vertalen om het mogelijk te maken dat mensen op oudere leeftijd langer gezond kunnen leven.

Zusammenfassung und Schlussfolgerungen

Ziel der vorliegenden Dissertation war die Charakterisierung des radiologischen Phänotyps des Gehirns von Probanden mit familiärer Disposition zur Langlebigkeit. Zur Beschreibung dieses Phänotyps auf sowohl makrostrukturellem als auch mikrostrukturellem Niveau wurden verschiedene Bildgebungstechniken, basierend auf der Kernspintomographie (Magnetresonanztomographie; MRT), angewendet. Um einen tieferen Einblick in den Alterungsprozess des menschlichen Gehirns im Allgemeinen zu erhalten, wurde der Einfluss verschiedener, potentiell modifizierender Faktoren auf den Alterungsprozess untersucht, wie z. B. die Verkalkung der Koronaren und die mit zerebralen Mikroblutungen - als Bildgebungskorrelat der zerebralen Mikroangiopathie - verbundene Sterblichkeit.

In **Kapitel 2** wird beschrieben, ob der mit Hilfe der MRT analysierte Phänotyp des Gehirns von Probanden mit familiärer Disposition zur Langlebigkeit durch ein relativ geringeres Ausmaß an Atrophie der Hirnsubstanz gekennzeichnet ist. Interessanterweise wurde die bekanntlich im Rahmen des normalen Alterungsprozesses auftretende Abnahme des Gesamtvolumens des Gehirns und des Volumens der kortikalen grauen und weißen Substanz in der gesamten Studienpopulation beobachtet. Ein Unterschied zwischen Probanden mit familiärer Disposition zur Langlebigkeit und Probanden der Kontrollgruppe war jedoch nicht nachweisbar. Das Volumen der linken Amygdala von Probanden mit familiärer Disposition zur Langlebigkeit war größer als dasjenige von Probanden der Kontrollgruppe, jedoch bemerkenswerterweise in beiden Gruppen nicht mit dem chronologischen Alter der Probanden assoziiert. Basierend auf diesen Ergebnissen wurde geschlussfolgert, dass im durchschnittlichen Alter von 66 Jahren die familiäre Disposition zur Langlebigkeit (noch) keinen Einfluss hat auf die Volumina der gesamten Hirnsubstanz, der kortikalen grauen und weißen Substanz. Familiäre Langlebigkeit ist jedoch gekennzeichnet durch ein größeres

Volumen der linken Amygdala. Dies entsteht in Anbetracht unserer Ergebnisse wahrscheinlich schon in der frühen Entwicklungsphase als Folge familiärer genetische Prädisposition. Da bekanntlich einige neurodegenerative und neuropsychiatrische Erkrankungen durch ein kleineres Volumen der Amygdalae charakterisiert werden, lassen unsere Ergebnisse vermuten, dass familiäre Langlebigkeit zu einem gewissen Grade vor altersbedingter Hirnschädigung schützt.

Kapitel 3 vergleicht das Ausmaß der zerebralen Mikroangiopathie zwischen Probanden mit familiärer Disposition zur Langlebigkeit und Probanden der Kontrollgruppe. Dies geschieht durch semiquantitative Erfassung von u.a. Marklagerläsionen, lakunären Infarkten und zerebralen Mikroblutungen. Familiäre Langlebigkeit war mit einer geringeren Anfälligkeit für sowohl periventrikuläre als auch subkortikale Marklagerläsionen und lakunäre Infarkte verbunden. Probanden mit familiärer Disposition zur Langlebigkeit und Probanden der Kontrollgruppe hatten eine vergleichbare Anfälligkeit für zerebrale Mikroblutungen. Interessanterweise waren die beschriebenen Ergebnisse unabhängig vom kardiovaskulären Risikoprofil der Studienpopulation. Dies könnte bedeuten, dass familiäre Langlebigkeit durch eine genetisch bedingt niedrigere Anfälligkeit für altersbedingte vaskuläre Hirnschäden gekennzeichnet ist, die nicht durch eine genetisch bedingt niedrigere Anfälligkeit für die Entwicklung kardiovaskulärer Risikofaktoren erklärbar ist.

Kapitel 4 und **5** beschreiben den radiologischen Phänotyp des Gehirns von Probanden mit familiärer Disposition zur Langlebigkeit auf mikrostrukturellem Niveau. Mit Hilfe von diffusionsgewichteten Aufnahmen (DTI, diffusion-weighted imaging) konnte gezeigt werden, dass die mikrostrukturelle Integrität der weißen Substanz von Probanden mit familiärer Disposition zur Langlebigkeit höher ist als diejenige von Probanden der Kontrollgruppe. Die Verwendung von

tract-based spatial statistics (TBSS), einer Analysemethode, die auf Voxelniveau die Darstellung der räumlichen Verteilung mikrostruktureller Schäden der weißen Substanz ermöglicht, ergab, dass bei Probanden mit familiärer Disposition zur Langlebigkeit die mikrostrukturelle Unversehrtheit der weißen Substanz vornehmlich im Corpus und Genu des Corpus callosum verglichen mit Probanden der Kontrollgruppe höher ist. Darüber hinaus wurde in der gesamten Studienpopulation ein ausgedehnter altersbedingter, von anterior nach posterior abnehmender Verlust der mikrostrukturellen Integrität der weißen Substanz nachgewiesen. Dieses altersbedingte Phänomen wird in der Literatur häufig beschrieben und unterstützt die sogenannte „Last-in-first-out"-Theorie, wonach angenommen wird, dass die hauptsächlich frontal liegenden spät-myelinisierenden Regionen, die aus dünneren Axonen aufgebaut sind, anfälliger sind für altersbedingte Beschädigung des Myelins. In Anbetracht unserer Ergebnisse für den biologischen und chronologischen Alterungsprozess kann geschlussfolgert werden, dass familiäre Langlebigkeit mit einer geringeren Anfälligkeit für mikrostrukturelle Schäden der weißen Substanz assoziiert ist, und zwar vor allem in Gebieten, die sehr anfällig sind für altersbedingte mikrostrukturelle Schäden. Unter Berücksichtigung der jährlichen Änderungsrate der Diffusionsparameter betrug der biologische Altersvorteil von Probanden mit familiärer Disposition zur Langlebigkeit im Vergleich zu Probanden der Kontrollgruppe hinsichtlich der mikrostrukturellen Integrität der weißen Substanz ungefähr 4,5 Jahre. Diese Ergebnisse warfen die Frage auf, ob die relative mikrostrukturelle Unversehrtheit der weißen Substanz bei Probanden mit familiärer Disposition zur Langlebigkeit möglicherweise durch eine niedrigere Anfälligkeit für altersbedingten Verlust von Myelin erklärt werden könnte. Dies wurde mit Hilfe der Magnetisierungs-Transfer-Bildgebung (MTI; magnetization transfer imaging) untersucht, wobei keine Unterschiede zwischen Probanden mit familiärer Disposition zur Langlebigkeit und Probanden der Kontrollgruppe nachweisbar waren. Es ist somit

wahrscheinlich, dass die beschriebene relative mikrostrukturelle Unversehrtheit der weißen Substanz bei familiärer Disposition zur Langlebigkeit nicht durch eine niedrigere Anfälligkeit für altersbedingte Demyelinisierung verursacht wird.

In **Kapitel 6** wird die Verkalkung der Koronaren als potentiell modifizierender Faktor altersbedingter vaskulärer Hirnschädigung sowohl auf makro- als auch mikrostrukturellem Niveau untersucht. Im Gegensatz zur Hirnatrophie waren periventrikuläre Marklagerläsionen, lakunäre Infarkte und Mikroblutungen mit Verkalkung der Koronaren assoziiert. Außerdem nahm mit zunehmender Verkalkung der Koronaren die mikrostrukturelle Integrität der weißen Substanz vor allem frontal und frontoparietal ab. Die beschriebene Verbindung zwischen Koronarverkalkung und sowohl fokalen ischämischen Hirnläsionen als auch ausgedehnter Schädigung auf mikrostrukturellem Niveau deutet auf einen generalisierten Prozess hin, der sich gleichermaßen auf Herz und Gehirn auswirkt. Die genetisch geringere Anfälligkeit für vaskuläre Hirnschädigung ist jedoch, wie in Kapitel 3 beschrieben, unabhängig von einer genetisch geringeren Anfälligkeit für kardiovaskuläre Risikofaktoren.

Kapitel 7 beschreibt die Ergebnisse bezüglich der Anwesenheit zerebraler Mikroblutungen und des damit verbundenen Sterblichkeitsrisikos. Nicht-lobäre Mikroblutungen waren mit einem erhöhten kardiovaskulären Mortalitätsrisiko verbunden, unabhängig von kardiovaskulären Risikofaktoren. Im Gegensatz dazu waren die durch zerebrale Amyloidangiopathie (cerebral amyloid angiopathy; CAA) bedingten lobären Mikroblutungen mit einem erhöhten Sterblichkeitsrisiko durch Schlaganfall assoziiert. Unsere Ergebnisse deuten darauf hin, dass zerebrale Mikroblutungen potentiell klinisch relevant sind und dass ältere Menschen mit zerebralen Mikroblutungen und zusätzlichen kardiovaskulären Risikofaktoren von speziellem kardiovaskulären Monitoring

profitieren könnten hinsichtlich einer Senkung der Sterblichkeit durch kardiovaskuläre Ursachen.

Das Hauptthema dieser Dissertation war die Beschreibung des Phänotyps des menschlichen Gehirns von Probanden mit familiärer Disposition zur Langlebigkeit aus der Bildgebungsperspektive. Mehrere Bildgebungskennzeichen der Hirnalterung waren bei Probanden mit familiärer Disposition zur Langlebigkeit weniger ausgeprägt als bei Probanden der Kontrollgruppe.
Bemerkenswerterweise war familiäre Langlebigkeit gekennzeichnet durch eine geringere Anfälligkeit für Bildgebungskorrelate der zerebralen Mikroangiopathie unabhängig von traditionellen kardiovaskulären Risikofaktoren, obwohl diese im Langlebigkeits-Phänotyp weniger ausgeprägt waren. Vor dem Hintergrund der großen Zahl pathophysiologischer Erklärungsmechanismen (wie z. B. bedingt durch vaskuläre Risikofaktoren, sporadisch, erblich (CAA), genetisch oder entzündlich), wurde die Hypothese aufgestellt, dass die geringere Anfälligkeit für Marklagerläsionen von Probanden mit familiärer Disposition zur Langlebigkeit wahrscheinlich nicht durch eine geringere Anfälligkeit für kardiovaskuläre Risikofaktoren sondern eher durch noch nicht näher definierte Mechanismen bedingt wird. Außer kardiovaskulären Risikofaktoren und Genen sind auch Entzündungsmarker mit dem Auftreten von Marklagerläsionen assoziiert. Außerdem ist bekannt, dass ein niedrigeres systemisches Entzündungsniveau mit Langlebigkeit assoziiert ist. Darum könnte ein niedrigeres systemisches Entzündungsniveau eine mögliche Erklärung sein für die geringere Anfälligkeit für vaskuläre Hirnschädigung in Form von Marklagerläsionen.
Interessanterweise war die mikrostrukturelle Integrität der weißen Substanz in denjenigen Regionen höher, die aus spät-myelinisierenden Axonen bestehen und von denen man annimmt, dass sie am anfälligsten sind für altersbedingte Schädigung im Sinne der „Last-in-first-out“-Theorie. Es sind jedoch longitudinale

Studien notwendig, um zu untersuchen, ob auch andere Regionen der weißen Subs-tanz gegenüber dem Alterungsprozess geschützt sind, entweder weil dieser Teil des Phänotyps der Langlebigkeit sich erst später manifestiert oder weil die Unterschiede zu anderen Hirnregionen in diesem Alter noch zu subtil sind, um mit den beschriebenen Bildgebungsmethoden entdeckt werden zu können.

Unter Verwendung von MTI zusammen mit DTI wurde beschrieben, dass die relative mikrostrukturelle Unversehrtheit bestimmter Regionen der weißen Substanz nicht durch eine geringere Anfälligkeit für altersbedingte Demyelinisierung erklärt werden kann, sondern eher durch eine relativ geringere Abnahme der Dichte der Axone durch Zunahme der extrazellulären Flüssigkeit, die wiederum durch unterschiedliche pathologische Prozesse hervorgerufen werden kann. Das zugrundeliegende histopathologische Substrat und die zugehörigen pathophysiologischen Mechanismen bleiben zukünftigen Studien vorbehalten.
Familiäre Langlebigkeit war gekennzeichnet durch ein größeres Volumen der linken Amygdala. Das Fehlen einer Assoziation mit dem chronologischen Alter der Probanden legt nahe, dass dieses Merkmal schon in der frühen Entwicklungsphase als Folge familiärer genetischer Prädisposition entsteht. Da das Volumen der Amygdalae bekanntlich bei mehreren neurodegenerativen und neuropsychiatrischen Krankheiten vermindert ist, wurde die Hypothese aufgestellt, dass familiäre Langlebigkeit möglicherweise durch eine geringere Anfälligkeit für diese Krankheiten gekennzeichnet ist. Zukünftige (funktionelle) Studien müssen jedoch die genaue funktionelle Bedeutung dieser Ergebnisse klären.

Die Verkalkung der Koronaren war als allgemeiner Marker für Arteriosklerose neben fokalen ischämischen Läsionen auch mit ausgedehnten Hirnschädigungen auf mikrostrukturellem Niveau assoziiert und läuft hiermit parallel zu den Schädigungen des Gehirns durch den Alterungsprozess selbst. Die Verkalkung der

Koronaren ist daher nicht nur ein Biomarker für kardiovaskuläre Erkrankungen, sondern auch für zerebrovaskuläre Schäden.

Bei älteren Menschen mit Prädisposition zu oder manifester kardiovaskulärer Erkrankung waren nicht-lobäre Mikroblutungen mit einer erhöhten kardiovaskulären Sterblichkeit verbunden, während CAA-bedingte Mikroblutungen mit einer erhöhten Sterblichkeit durch Schlaganfall assoziiert waren. Ältere Menschen mit sowohl zerebralen Mikroblutungen als auch kardiovaskulären Risikofaktoren könnten daher zur Senkung der kardiovaskulären Sterblichkeit von zusätzlichem kardiovaskulären Monitoring profitieren.

Zusammenfassend kann festgestellt werden, dass sich der strukturelle Phänotyp des Gehirns von Probanden mit familiärer Disposition zur Langlebigkeit beachtlich von demjenigen der, Umweltfaktoren und Alter betreffend vergleichbaren, Kontrollgruppe unterscheidet. Sowohl Merkmale, die sehr wahrscheinlich als Folge familiärer genetischer Prädisposition entstehen als auch eine geringere Anfälligkeit für bekannte altersbedingte strukturelle Hirnschäden auf sowohl makro- als auch mikrostrukturellem Niveau kennzeichnen den Phänotyp des Gehirns von Probanden mit familiärer Disposition zur Langlebigkeit. Man könnte jedoch auch argumentieren, dass die größere Hirnschädigung in der Kontrollgruppe zu einem schnelleren Alterungsprozess „normal“ alternder Menschen führt. Die zugrundeliegenden Mechanismen müssen noch identifiziert werden, könnten aber u.a. Homöostase und Körperfunktion beinhalten. Angesichts der Tatsache, dass der Übergang von gesundem/erfolgreichem Altern (healthy/successful aging) zu „normalem“ Altern und pathologischen Veränderungen des Gehirns als Zeichen von Krankheit fließend ist, suggerieren die Ergebnisse dieser Studie, dass die Gehirne von Probanden mit familiärer Disposition zur Langlebigkeit weniger anfällig sind für neurodegenerative Veränderungen wie (vaskuläre) Demenz, Morbus

Alzheimer und zerebrovaskuläre Erkrankungen. Die im Rahmen dieser Dissertation beschriebenen Ergebnisse sollten als Ausgangspunkt für zukünftige Studien dienen, die sowohl die funktionellen Folgen als auch zugrundeliegenden Mechanismen untersuchen. Erst dann können die hier gewonnenen Erkenntnisse auf eine Weise in die klinische Praxis umgesetzt werden, die es der allgemeinen Bevölkerung ermöglicht, länger gesünder zu leben, und können bekannte pathologische Veränderungen während des Alterungsprozesses wie z.B. Morbus Alzheimer und zerebrovaskuläre Erkrankungen besser verstanden werden.

Reference list

1. Scheltens P, Barkhof F, Leys D, et al. A semiquantative rating scale for the assessment of signal hyperintensities on magnetic resonance imaging. *J Neurol Sci.* 1993;114:7-12.
2. Oeppen J, Vaupel JW. Demography. Broken limits to life expectancy. *Science.* 2002;296:1029-31.
3. Rowe JW, Kahn RL. Human aging: usual and successful. *Science.* 1987;237:143-9.
4. Westendorp RG. What is healthy aging in the 21st century? *Am J Clin Nutr.* 2006;83:404S-9S.
5. Zwaan BJ. The evolutionary genetics of ageing and longevity. *Heredity (Edinb).* 1999;82 (Pt 6):589-97.
6. Schoenmaker M, de Craen AJ, de Meijer PH, et al. Evidence of genetic enrichment for exceptional survival using a family approach: the Leiden Longevity Study. *Eur J Hum Genet.* 2006;14:79-84.
7. Rozing MP, Houwing-Duistermaat JJ, Slagboom PE, et al. Familial longevity is associated with decreased thyroid function. *J Clin Endocrinol Metab.* 2010;95:4979-84.
8. Vaarhorst AA, Beekman M, Suchiman EH, et al. Lipid metabolism in long-lived families: the Leiden Longevity Study. *Age (Dordr).* 2011;33:219-27.
9. Wijsman CA, Rozing MP, Streefland TC, et al. Familial longevity is marked by enhanced insulin sensitivity. *Aging Cell.* 2011;10:114-21.
10. Vernooij MW, Smits M. Structural neuroimaging in aging and Alzheimer's disease. *Neuroimaging Clin N Am.* 2012;22:33-viii.
11. Raz N, Rodrigue KM. Differential aging of the brain: patterns, cognitive correlates and modifiers. *Neurosci Biobehav Rev.* 2006;30:730-48.
12. Bezerra DC, Sharrett AR, Matsushita K, et al. Risk factors for lacune subtypes in the Atherosclerosis Risk in Communities (ARIC) Study. *Neurology.* 2012;78:102-8.

13. Roob G, Schmidt R, Kapeller P, et al. MRI evidence of past cerebral microbleeds in a healthy elderly population. *Neurology.* 1999;52:991-4.
14. Wardlaw JM, Allerhand M, Doubal FN, et al. Vascular risk factors, large-artery atheroma, and brain white matter hyperintensities. *Neurology.* 2014;82:1331-8.
15. Stanford W, Thompson BH, Weiss RM. Coronary artery calcification: clinical significance and current methods of detection. *AJR Am J Roentgenol.* 1993;161:1139-46.
16. Thompson BH, Stanford W. Imaging of coronary calcium: a case for electron beam computed tomography. *J Thorac Imaging.* 2001;16:8-15.
17. Agatston AS, Janowitz WR, Hildner FJ, et al. Quantification of coronary artery calcium using ultrafast computed tomography. *J Am Coll Cardiol.* 1990;15:827-32.
18. Arad Y, Spadaro LA, Goodman K, et al. Predictive value of electron beam computed tomography of the coronary arteries. 19-month follow-up of 1173 asymptomatic subjects. *Circulation.* 1996;93:1951-3.
19. Detrano R, Hsiai T, Wang S, et al. Prognostic value of coronary calcification and angiographic stenoses in patients undergoing coronary angiography. *J Am Coll Cardiol.* 1996;27:285-90.
20. Ikram MA, Vernooij MW, Vrooman HA, et al. Brain tissue volumes and small vessel disease in relation to the risk of mortality. *Neurobiol Aging.* 2009;30:450-6.
21. Tsushima Y, Tanizaki Y, Aoki J, et al. MR detection of microhemorrhages in neurologically healthy adults. *Neuroradiology.* 2002;44:31-6.
22. Henneman WJ, Sluimer JD, Cordonnier C, et al. MRI biomarkers of vascular damage and atrophy predicting mortality in a memory clinic population. *Stroke.* 2009;40:492-8.

23. Fazekas F, Kleinert R, Roob G, et al. Histopathologic analysis of foci of signal loss on gradient-echo T2*-weighted MR images in patients with spontaneous intracerebral hemorrhage: evidence of microangiopathy-related microbleeds. *AJNR Am J Neuroradiol.* 1999;20:637-42.
24. Greenberg SM. Cerebral amyloid angiopathy: prospects for clinical diagnosis and treatment. *Neurology.* 1998;51:690-4.
25. Greenberg SM, Vernooij MW, Cordonnier C, et al. Cerebral microbleeds: a guide to detection and interpretation. *Lancet Neurol.* 2009;8:165-74.
26. Knudsen KA, Rosand J, Karluk D, et al. Clinical diagnosis of cerebral amyloid angiopathy: validation of the Boston criteria. *Neurology.* 2001;56:537-9.
27. Tanaka A, Ueno Y, Nakayama Y, et al. Small chronic hemorrhages and ischemic lesions in association with spontaneous intracerebral hematomas. *Stroke.* 1999;30:1637-42.
28. Vernooij MW, van der Lugt A, Ikram MA, et al. Prevalence and risk factors of cerebral microbleeds: the Rotterdam Scan Study. *Neurology.* 2008;70:1208-14.
29. Woo D, Sauerbeck LR, Kissela BM, et al. Genetic and environmental risk factors for intracerebral hemorrhage: preliminary results of a population-based study. *Stroke.* 2002;33:1190-5.
30. ten Dam VH, Box FM, de Craen AJ, et al. Lack of effect of pravastatin on cerebral blood flow or parenchymal volume loss in elderly at risk for vascular disease. *Stroke.* 2005;36:1633-6.
31. Raz N, Gunning FM, Head D, et al. Selective aging of the human cerebral cortex observed in vivo: differential vulnerability of the prefrontal gray matter. *Cereb Cortex.* 1997;7:268-82.

32. Resnick SM, Pham DL, Kraut MA, et al. Longitudinal magnetic resonance imaging studies of older adults: a shrinking brain. *J Neurosci.* 2003;23:3295-301.
33. Neary D, Snowden JS, Mann DM. The clinical pathological correlates of lobar atrophy. *Dementia.* 1993;4:154-9.
34. Sluimer JD, Vrenken H, Blankenstein MA, et al. Whole-brain atrophy rate in Alzheimer disease: identifying fast progressors. *Neurology.* 2008;70:1836-41.
35. Kuller LH, Arnold AM, Longstreth WT, Jr., et al. White matter grade and ventricular volume on brain MRI as markers of longevity in the cardiovascular health study. *Neurobiol Aging.* 2007;28:1307-15.
36. Mueller EA, Moore MM, Kerr DC, et al. Brain volume preserved in healthy elderly through the eleventh decade. *Neurology.* 1998;51:1555-62.
37. Peper JS, Brouwer RM, Boomsma DI, et al. Genetic influences on human brain structure: a review of brain imaging studies in twins. *Hum Brain Mapp.* 2007;28:464-73.
38. Herskind AM, McGue M, Holm NV, et al. The heritability of human longevity: a population-based study of 2872 Danish twin pairs born 1870-1900. *Hum Genet.* 1996;97:319-23.
39. Ljungquist B, Berg S, Lanke J, et al. The effect of genetic factors for longevity: a comparison of identical and fraternal twins in the Swedish Twin Registry. *J Gerontol A Biol Sci Med Sci.* 1998;53:M441-M446.
40. Mai JK, Paxinos G, Voss T. *Atlas of the human brain.* 2008.
41. Hulshoff Pol HE, Schnack HG, Posthuma D, et al. Genetic contributions to human brain morphology and intelligence. *J Neurosci.* 2006;26:10235-42.
42. Poulin SP, Dautoff R, Morris JC, et al. Amygdala atrophy is prominent in early Alzheimer's disease and relates to symptom severity. *Psychiatry Res.* 2011;194:7-13.

43. Burke J, McQuoid DR, Payne ME, et al. Amygdala volume in late-life depression: relationship with age of onset. *Am J Geriatr Psychiatry.* 2011;19:771-6.
44. Dere E, Pause BM, Pietrowsky R. Emotion and episodic memory in neuropsychiatric disorders. *Behav Brain Res.* 2010;215:162-71.
45. Bitter SM, Mills NP, Adler CM, et al. Progression of amygdala volumetric abnormalities in adolescents after their first manic episode. *J Am Acad Child Adolesc Psychiatry.* 2011;50:1017-26.
46. Hahn A, Stein P, Windischberger C, et al. Reduced resting-state functional connectivity between amygdala and orbitofrontal cortex in social anxiety disorder. *Neuroimage.* 2011;56:881-9.
47. Harding AJ, Stimson E, Henderson JM, et al. Clinical correlates of selective pathology in the amygdala of patients with Parkinson's disease. *Brain.* 2002;125:2431-45.
48. Prestia A, Boccardi M, Galluzzi S, et al. Hippocampal and amygdalar volume changes in elderly patients with Alzheimer's disease and schizophrenia. *Psychiatry Res.* 2011;192:77-83.
49. Coffey CE, Wilkinson WE, Parashos IA, et al. Quantitative cerebral anatomy of the aging human brain: a cross-sectional study using magnetic resonance imaging. *Neurology.* 1992;42:527-36.
50. Laakso MP, Partanen K, Lehtovirta M, et al. MRI of amygdala fails to diagnose early Alzheimer's disease. *Neuroreport.* 1995;6:2414-8.
51. Malykhin NV, Bouchard TP, Camicioli R, et al. Aging hippocampus and amygdala. *Neuroreport.* 2008;19:543-7.
52. Mu Q, Xie J, Wen Z, et al. A quantitative MR study of the hippocampal formation, the amygdala, and the temporal horn of the lateral ventricle in healthy subjects 40 to 90 years of age. *AJNR Am J Neuroradiol.* 1999;20:207-11.

53. Cherubini A, Peran P, Caltagirone C, et al. Aging of subcortical nuclei: microstructural, mineralization and atrophy modifications measured in vivo using MRI. *Neuroimage.* 2009;48:29-36.
54. Good CD, Johnsrude IS, Ashburner J, et al. A voxel-based morphometric study of ageing in 465 normal adult human brains. *Neuroimage.* 2001;14:21-36.
55. Jernigan TL, Archibald SL, Fennema-Notestine C, et al. Effects of age on tissues and regions of the cerebrum and cerebellum. *Neurobiol Aging.* 2001;22:581-94.
56. Lemaitre H, Crivello F, Grassiot B, et al. Age- and sex-related effects on the neuroanatomy of healthy elderly. *Neuroimage.* 2005;26:900-11.
57. Walhovd KB, Westlye LT, Amlien I, et al. Consistent neuroanatomical age-related volume differences across multiple samples. *Neurobiol Aging.* 2011;32:916-32.
58. Ho AJ, Raji CA, Becker JT, et al. The effects of physical activity, education, and body mass index on the aging brain. *Hum Brain Mapp.* 2011;32:1371-82.
59. Ikram MA, Vrooman HA, Vernooij MW, et al. Brain tissue volumes in the general elderly population. The Rotterdam Scan Study. *Neurobiol Aging.* 2008;29:882-90.
60. Blackmon K, Barr WB, Carlson C, et al. Structural evidence for involvement of a left amygdala-orbitofrontal network in subclinical anxiety. *Psychiatry Res.* 2011;194:296-303.
61. Cremers H, van Tol MJ, Roelofs K, et al. Extraversion is linked to volume of the orbitofrontal cortex and amygdala. *PLoS One.* 2011;6:e28421.
62. Spoletini I, Piras F, Fagioli S, et al. Suicidal attempts and increased right amygdala volume in schizophrenia. *Schizophr Res.* 2011;125:30-40.

63. van Tol MJ, Demenescu LR, van der Wee NJ, et al. Functional magnetic resonance imaging correlates of emotional word encoding and recognition in depression and anxiety disorders. *Biol Psychiatry.* 2012;71:593-602.
64. Smith SM, Jenkinson M, Woolrich MW, et al. Advances in functional and structural MR image analysis and implementation as FSL. *Neuroimage.* 2004;23 Suppl 1:S208-S219.
65. Woolrich MW, Jbabdi S, Patenaude B, et al. Bayesian analysis of neuroimaging data in FSL. *Neuroimage.* 2009;45:S173-S186.
66. Smith SM, De SN, Jenkinson M, et al. Normalized accurate measurement of longitudinal brain change. *J Comput Assist Tomogr.* 2001;25:466-75.
67. Smith SM, Zhang Y, Jenkinson M, et al. Accurate, robust, and automated longitudinal and cross-sectional brain change analysis. *Neuroimage.* 2002;17:479-89.
68. Smith SM. Fast robust automated brain extraction. *Hum Brain Mapp.* 2002;17:143-55.
69. Jenkinson M, Smith S. A global optimisation method for robust affine registration of brain images. *Med Image Anal.* 2001;5:143-56.
70. Jenkinson M, Bannister P, Brady M, et al. Improved optimization for the robust and accurate linear registration and motion correction of brain images. *Neuroimage.* 2002;17:825-41.
71. Zhang Y, Brady M, Smith S. Segmentation of brain MR images through a hidden Markov random field model and the expectation-maximization algorithm. *IEEE Trans Med Imaging.* 2001;20:45-57.
72. Ashburner J, Friston KJ. Voxel-based morphometry--the methods. *Neuroimage.* 2000;11:805-21.
73. Andersson JLR, Jenkinson M, Smith S. Non-linear optimisation. FMRIB technical report TR07JA1. www.fmrib.ox.ac.uk/analysis/techrep.

74. Andersson JLR, Jenkinson M, Smith S. Non-linear registration, aka Spatial normalisation. FMRIB technical report TR07JA2. www.fmrib.ox.ac.uk/analysis/techrep.
75. Patenaude B, Smith S, Kennedy D, et al. A Bayesian Model of Shape and Appearance for Subcortical Brain Segmentation. *Neuroimage.* 2011.
76. Pantoni L, Garcia JH. The significance of cerebral white matter abnormalities 100 years after Binswanger's report. A review. *Stroke.* 1995;26:1293-301.
77. Awad IA, Spetzler RF, Hodak JA, et al. Incidental subcortical lesions identified on magnetic resonance imaging in the elderly. I. Correlation with age and cerebrovascular risk factors. *Stroke.* 1986;17:1084-9.
78. Bryan RN, Wells SW, Miller TJ, et al. Infarctlike lesions in the brain: prevalence and anatomic characteristics at MR imaging of the elderly--data from the Cardiovascular Health Study. *Radiology.* 1997;202:47-54.
79. Bokura H, Kobayashi S, Yamaguchi S, et al. Silent brain infarction and subcortical white matter lesions increase the risk of stroke and mortality: a prospective cohort study. *J Stroke Cerebrovasc Dis.* 2006;15:57-63.
80. Vermeer SE, Hollander M, van Dijk EJ, et al. Silent brain infarcts and white matter lesions increase stroke risk in the general population: the Rotterdam Scan Study. *Stroke.* 2003;34:1126-9.
81. Werring DJ, Coward LJ, Losseff NA, et al. Cerebral microbleeds are common in ischemic stroke but rare in TIA. *Neurology.* 2005;65:1914-8.
82. Cottier JP, Edjlali M, Gaillard MA, et al. Pathology of small cerebral arteries demonstrated by MRI: a marker of aging? *Geriatr Psychol Neuropsychiatr Vieil.* 2011;9:465-75.
83. Altmann-Schneider I, Trompet S, de Craen AJ, et al. Cerebral microbleeds are predictive of mortality in the elderly. *Stroke.* 2011;42:638-44.

84. Atwood LD, Wolf PA, Heard-Costa NL, et al. Genetic variation in white matter hyperintensity volume in the Framingham Study. *Stroke.* 2004;35:1609-13.
85. Carmelli D, DeCarli C, Swan GE, et al. Evidence for genetic variance in white matter hyperintensity volume in normal elderly male twins. *Stroke.* 1998;29:1177-81.
86. Westendorp RG, van HD, Rozing MP, et al. Nonagenarian siblings and their offspring display lower risk of mortality and morbidity than sporadic nonagenarians: The Leiden Longevity Study. *J Am Geriatr Soc.* 2009;57:1634-7.
87. Bokura H, Kobayashi S, Yamaguchi S. Distinguishing silent lacunar infarction from enlarged Virchow-Robin spaces: a magnetic resonance imaging and pathological study. *J Neurol.* 1998;245:116-22.
88. Kuo HK, Lipsitz LA. Cerebral white matter changes and geriatric syndromes: is there a link? *J Gerontol A Biol Sci Med Sci.* 2004;59:818-26.
89. Mattson MP, Duan W, Chan SL, et al. Neuroprotective and neurorestorative signal transduction mechanisms in brain aging: modification by genes, diet and behavior. *Neurobiol Aging.* 2002;23:695-705.
90. Schmidt H, Zeginigg M, Wiltgen M, et al. Genetic variants of the NOTCH3 gene in the elderly and magnetic resonance imaging correlates of age-related cerebral small vessel disease. *Brain.* 2011;134:3384-97.
91. Martiskainen M, Pohjasvaara T, Mikkelsson J, et al. Fibrinogen gene promoter -455 A allele as a risk factor for lacunar stroke. *Stroke.* 2003;34:886-91.
92. Schuur M, van Swieten JC, Schol-Gelok S, et al. Genetic risk factors for cerebral small-vessel disease in hypertensive patients from a genetically isolated population. *J Neurol Neurosurg Psychiatry.* 2011;82:41-4.

93. Serizawa M, Nabika T, Ochiai Y, et al. Association between PRKCH gene polymorphisms and subcortical silent brain infarction. *Atherosclerosis.* 2008;199:340-5.

94. Lee SC, Park SJ, Ki HK, et al. Prevalence and risk factors of silent cerebral infarction in apparently normal adults. *Hypertension.* 2000;36:73-7.

95. Price TR, Manolio TA, Kronmal RA, et al. Silent brain infarction on magnetic resonance imaging and neurological abnormalities in community-dwelling older adults. The Cardiovascular Health Study. CHS Collaborative Research Group. *Stroke.* 1997;28:1158-64.

96. Vermeer SE, Koudstaal PJ, Oudkerk M, et al. Prevalence and risk factors of silent brain infarcts in the population-based Rotterdam Scan Study. *Stroke.* 2002;33:21-5.

97. Vermeer SE, den HT, Koudstaal PJ, et al. Incidence and risk factors of silent brain infarcts in the population-based Rotterdam Scan Study. *Stroke.* 2003;34:392-6.

98. Poels MM, Vernooij MW, Ikram MA, et al. Prevalence and risk factors of cerebral microbleeds: an update of the Rotterdam scan study. *Stroke.* 2010;41:S103-S106.

99. Maxwell SS, Jackson CA, Paternoster L, et al. Genetic associations with brain microbleeds: Systematic review and meta-analyses. *Neurology.* 2011;77:158-67.

100. Pfefferbaum A, Sullivan EV, Hedehus M, et al. Age-related decline in brain white matter anisotropy measured with spatially corrected echo-planar diffusion tensor imaging. *Magn Reson Med.* 2000;44:259-68.

101. Sullivan EV, Adalsteinsson E, Hedehus M, et al. Equivalent disruption of regional white matter microstructure in ageing healthy men and women. *Neuroreport.* 2001;12:99-104.

102. Alexander AL, Lee JE, Lazar M, et al. Diffusion tensor imaging of the brain. *Neurotherapeutics.* 2007;4:316-29.
103. Bartzokis G, Lu PH, Heydari P, et al. Multimodal magnetic resonance imaging assessment of white matter aging trajectories over the lifespan of healthy individuals. *Biol Psychiatry.* 2012;72:1026-34.
104. Basser PJ, Pierpaoli C. Microstructural and physiological features of tissues elucidated by quantitative-diffusion-tensor MRI. *J Magn Reson B.* 1996;111:209-19.
105. Abe O, Aoki S, Hayashi N, et al. Normal aging in the central nervous system: quantitative MR diffusion-tensor analysis. *Neurobiol Aging.* 2002;23:433-41.
106. Bennett IJ, Madden DJ, Vaidya CJ, et al. Age-related differences in multiple measures of white matter integrity: A diffusion tensor imaging study of healthy aging. *Hum Brain Mapp.* 2010;31:378-90.
107. Burzynska AZ, Preuschhof C, Backman L, et al. Age-related differences in white matter microstructure: region-specific patterns of diffusivity. *Neuroimage.* 2010;49:2104-12.
108. Pfefferbaum A, Adalsteinsson E, Sullivan EV. Frontal circuitry degradation marks healthy adult aging: Evidence from diffusion tensor imaging. *Neuroimage.* 2005;26:891-9.
109. Salat DH, Tuch DS, Greve DN, et al. Age-related alterations in white matter microstructure measured by diffusion tensor imaging. *Neurobiol Aging.* 2005;26:1215-27.
110. Bartzokis G, Beckson M, Lu PH, et al. Age-related changes in frontal and temporal lobe volumes in men: a magnetic resonance imaging study. *Arch Gen Psychiatry.* 2001;58:461-5.

111. Bartzokis G, Cummings JL, Sultzer D, et al. White matter structural integrity in healthy aging adults and patients with Alzheimer disease: a magnetic resonance imaging study. *Arch Neurol.* 2003;60:393-8.
112. Marner L, Nyengaard JR, Tang Y, et al. Marked loss of myelinated nerve fibers in the human brain with age. *J Comp Neurol.* 2003;462:144-52.
113. Pfefferbaum A, Sullivan EV, Carmelli D. Genetic regulation of regional microstructure of the corpus callosum in late life. *Neuroreport.* 2001;12:1677-81.
114. Chiang MC, McMahon KL, de Zubicaray GI, et al. Genetics of white matter development: a DTI study of 705 twins and their siblings aged 12 to 29. *Neuroimage.* 2011;54:2308-17.
115. Altmann-Schneider I, van der Grond J, Slagboom PE, et al. Lower Susceptibility to Cerebral Small Vessel Disease in Human Familial Longevity: The Leiden Longevity Study. *Stroke.* 2012.
116. Behrens TE, Woolrich MW, Jenkinson M, et al. Characterization and propagation of uncertainty in diffusion-weighted MR imaging. *Magn Reson Med.* 2003;50:1077-88.
117. Behrens TE, Johansen-Berg H, Woolrich MW, et al. Non-invasive mapping of connections between human thalamus and cortex using diffusion imaging. *Nat Neurosci.* 2003;6:750-7.
118. Behrens TE, Berg HJ, Jbabdi S, et al. Probabilistic diffusion tractography with multiple fibre orientations: What can we gain? *Neuroimage.* 2007;34:144-55.
119. Smith SM, Jenkinson M, Johansen-Berg H, et al. Tract-based spatial statistics: voxelwise analysis of multi-subject diffusion data. *Neuroimage.* 2006;31:1487-505.
120. Chiang MC, Barysheva M, Shattuck DW, et al. Genetics of brain fiber architecture and intellectual performance. *J Neurosci.* 2009;29:2212-24.

121. Davis SW, Dennis NA, Buchler NG, et al. Assessing the effects of age on long white matter tracts using diffusion tensor tractography. *Neuroimage.* 2009;46:530-41.
122. Bartzokis G, Sultzer D, Lu PH, et al. Heterogeneous age-related breakdown of white matter structural integrity: implications for cortical "disconnection" in aging and Alzheimer's disease. *Neurobiol Aging.* 2004;25:843-51.
123. Griebe M, Forster A, Wessa M, et al. Loss of callosal fibre integrity in healthy elderly with age-related white matter changes. *J Neurol.* 2011;258:1451-9.
124. Leritz EC, Shepel J, Williams VJ, et al. Associations between T(1) white matter lesion volume and regional white matter microstructure in aging. *Hum Brain Mapp.* 2013.
125. Jones DK, Cercignani M. Twenty-five pitfalls in the analysis of diffusion MRI data. *NMR Biomed.* 2010;23:803-20.
126. Hjelmborg JvB, Iachine I, Skytthe A, et al. Genetic influence on human lifespan and longevity. *Hum Genet.* 2006;119:312-21.
127. Skytthe A, Pedersen NL, Kaprio J, et al. Longevity studies in GenomEUtwin. *Twin Res.* 2003;6:448-54.
128. Altmann-Schneider I, de Craen AJ, Veer IM, et al. Preserved white matter integrity is a marker of familial longevity. *Ann Neurol.* 2013.
129. de Goeij MC, Halbesma N, Dekker FW, et al. Renal function in familial longevity: the Leiden Longevity Study. *Exp Gerontol.* 2014;51:65-70.
130. Bos SD, Beekman M, Maier AB, et al. Metabolic health in families enriched for longevity is associated with low prevalence of hand osteoarthritis and influences OA biomarker profiles. *Ann Rheum Dis.* 2013;72:1669-74.

131. Grossman RI, Gomori JM, Ramer KN, et al. Magnetization transfer: theory and clinical applications in neuroradiology. *Radiographics.* 1994;14:279-90.
132. Wozniak JR, Lim KO. Advances in white matter imaging: a review of in vivo magnetic resonance methodologies and their applicability to the study of development and aging. *Neurosci Biobehav Rev.* 2006;30:762-74.
133. Holland PR, Bastin ME, Jansen MA, et al. MRI is a sensitive marker of subtle white matter pathology in hypoperfused mice. *Neurobiol Aging.* 2011;32:2325-6.
134. Song SK, Sun SW, Ramsbottom MJ, et al. Dysmyelination revealed through MRI as increased radial (but unchanged axial) diffusion of water. *Neuroimage.* 2002;17:1429-36.
135. Draganski B, Ashburner J, Hutton C, et al. Regional specificity of MRI contrast parameter changes in normal ageing revealed by voxel-based quantification (VBQ). *Neuroimage.* 2011;55:1423-34.
136. Ge Y, Grossman RI, Babb JS, et al. Age-related total gray matter and white matter changes in normal adult brain. Part I: volumetric MR imaging analysis. *AJNR Am J Neuroradiol.* 2002;23:1327-33.
137. Armstrong CL, Traipe E, Hunter JV, et al. Age-related, regional, hemispheric, and medial-lateral differences in myelin integrity in vivo in the normal adult brain. *AJNR Am J Neuroradiol.* 2004;25:977-84.
138. Benedetti B, Charil A, Rovaris M, et al. Influence of aging on brain gray and white matter changes assessed by conventional, MT, and DT MRI. *Neurology.* 2006;66:535-9.
139. Schiavone F, Charlton RA, Barrick TR, et al. Imaging age-related cognitive decline: A comparison of diffusion tensor and magnetization transfer MRI. *J Magn Reson Imaging.* 2009;29:23-30.

140. Ropele S, Enzinger C, Sollinger M, et al. The impact of sex and vascular risk factors on brain tissue changes with aging: magnetization transfer imaging results of the Austrian stroke prevention study. *AJNR Am J Neuroradiol.* 2010;31:1297-301.
141. Homayoon N, Ropele S, Hofer E, et al. Microstructural tissue damage in normal appearing brain tissue accumulates with Framingham Stroke Risk Profile Score: magnetization transfer imaging results of the Austrian Stroke Prevention Study. *Clin Neurol Neurosurg.* 2013;115:1317-21.
142. Callaghan MF, Freund P, Draganski B, et al. Widespread age-related differences in the human brain microstructure revealed by quantitative magnetic resonance imaging. *Neurobiol Aging.* 2014;35:1862-72.
143. Mascalchi M, Toschi N, Ginestroni A, et al. Gender, age-related, and regional differences of the magnetization transfer ratio of the cortical and subcortical brain gray matter. *J Magn Reson Imaging.* 2014;40:360-6.
144. Seiler S, Ropele S, Schmidt R. Magnetization Transfer Imaging for in vivo Detection of Microstructural Tissue Changes in Aging and Dementia: A Short Literature Review. *J Alzheimers Dis.* 2014.
145. van den Bogaard SJ, Dumas EM, Milles J, et al. Magnetization transfer imaging in premanifest and manifest Huntington disease. *AJNR Am J Neuroradiol.* 2012;33:884-9.
146. van Buchem MA, McGowan JC, Kolson DL, et al. Quantitative volumetric magnetization transfer analysis in multiple sclerosis: estimation of macroscopic and microscopic disease burden. *Magn Reson Med.* 1996;36:632-6.
147. Bodini B, Cercignani M, Toosy A, et al. A novel approach with "skeletonised MTR" measures tract-specific microstructural changes in early primary-progressive MS. *Hum Brain Mapp.* 2013.

148. Beaulieu C. The basis of anisotropic water diffusion in the nervous system - a technical review. *NMR Biomed.* 2002;15:435-55.
149. Ou X, Sun SW, Liang HF, et al. Quantitative magnetization transfer measured pool-size ratio reflects optic nerve myelin content in ex vivo mice. *Magn Reson Med.* 2009;61:364-71.
150. Gareau PJ, Rutt BK, Karlik SJ, et al. Magnetization transfer and multicomponent T2 relaxation measurements with histopathologic correlation in an experimental model of MS. *J Magn Reson Imaging.* 2000;11:586-95.
151. Vavasour IM, Laule C, Li DK, et al. Is the magnetization transfer ratio a marker for myelin in multiple sclerosis? *J Magn Reson Imaging.* 2011;33:713-8.
152. Cook LL, Foster PJ, Mitchell JR, et al. In vivo 4.0-T magnetic resonance investigation of spinal cord inflammation, demyelination, and axonal damage in chronic-progressive experimental allergic encephalomyelitis. *J Magn Reson Imaging.* 2004;20:563-71.
153. van Waesberghe JH, Kamphorst W, De Groot CJ, et al. Axonal loss in multiple sclerosis lesions: magnetic resonance imaging insights into substrates of disability. *Ann Neurol.* 1999;46:747-54.
154. Sullivan EV, Rohlfing T, Pfefferbaum A. Longitudinal study of callosal microstructure in the normal adult aging brain using quantitative DTI fiber tracking. *Dev Neuropsychol.* 2010;35:233-56.
155. Silver NC, Barker GJ, MacManus DG, et al. Magnetisation transfer ratio of normal brain white matter: a normative database spanning four decades of life. *J Neurol Neurosurg Psychiatry.* 1997;62:223-8.
156. Stanisz GJ, Kecojevic A, Bronskill MJ, et al. Characterizing white matter with magnetization transfer and T(2). *Magn Reson Med.* 1999;42:1128-36.

157. Bos D, Vernooij MW, Elias-Smale SE, et al. Atherosclerotic calcification relates to cognitive function and to brain changes on magnetic resonance imaging. *Alzheimers Dement.* 2012;8:S104-S111.
158. Rosano C, Naydeck B, Kuller LH, et al. Coronary artery calcium: associations with brain magnetic resonance imaging abnormalities and cognitive status. *J Am Geriatr Soc.* 2005;53:609-15.
159. Vidal JS, Sigurdsson S, Jonsdottir MK, et al. Coronary artery calcium, brain function and structure: the AGES-Reykjavik Study. *Stroke.* 2010;41:891-7.
160. Bos D, Ikram MA, Elias-Smale SE, et al. Calcification in major vessel beds relates to vascular brain disease. *Arterioscler Thromb Vasc Biol.* 2011;31:2331-7.
161. Kim BJ, Lee SH, Kim CK, et al. Advanced coronary artery calcification and cerebral small vessel diseases in the healthy elderly. *Circ J.* 2011;75:451-6.
162. Pantoni L. Cerebral small vessel disease: from pathogenesis and clinical characteristics to therapeutic challenges. *Lancet Neurol.* 2010;9:689-701.
163. Maclullich AM, Ferguson KJ, Reid LM, et al. Higher systolic blood pressure is associated with increased water diffusivity in normal-appearing white matter. *Stroke.* 2009;40:3869-71.
164. Sala M, de RA, van den Berg A, et al. Microstructural brain tissue damage in metabolic syndrome. *Diabetes Care.* 2014;37:493-500.
165. Kawasaki R, Cheung N, Mosley T, et al. Retinal microvascular signs and 10-year risk of cerebral atrophy: the Atherosclerosis Risk in Communities (ARIC) study. *Stroke.* 2010;41:1826-8.
166. Godin O, Maillard P, Crivello F, et al. Association of white-matter lesions with brain atrophy markers: the three-city Dijon MRI study. *Cerebrovasc Dis.* 2009;28:177-84.

167. Fazekas F, Kleinert R, Offenbacher H, et al. Pathologic correlates of incidental MRI white matter signal hyperintensities. *Neurology.* 1993;43:1683-9.

168. Sze G, De Armond SJ, Brant-Zawadzki M, et al. Foci of MRI signal (pseudo lesions) anterior to the frontal horns: histologic correlations of a normal finding. *AJR Am J Roentgenol.* 1986;147:331-7.

169. ten Dam VH, van den Heuvel DM, de Craen AJ, et al. Decline in total cerebral blood flow is linked with increase in periventricular but not deep white matter hyperintensities. *Radiology.* 2007;243:198-203.

170. Fazekas F, Kleinert R, Offenbacher H, et al. The morphologic correlate of incidental punctate white matter hyperintensities on MR images. *AJNR Am J Neuroradiol.* 1991;12:915-21.

171. Fazekas F, Schmidt R, Scheltens P. Pathophysiologic mechanisms in the development of age-related white matter changes of the brain. *Dement Geriatr Cogn Disord.* 1998;9 Suppl 1:2-5.

172. Wright CB, Moon Y, Paik MC, et al. Inflammatory biomarkers of vascular risk as correlates of leukoariosis. *Stroke.* 2009;40:3466-71.

173. Kennedy KM, Raz N. Pattern of normal age-related regional differences in white matter microstructure is modified by vascular risk. *Brain Res.* 2009;1297:41-56.

174. Spilt A, Goekoop R, Westendorp RG, et al. Not all age-related white matter hyperintensities are the same: a magnetization transfer imaging study. *AJNR Am J Neuroradiol.* 2006;27:1964-8.

175. Pettersen JA, Sathiyamoorthy G, Gao FQ, et al. Microbleed topography, leukoaraiosis, and cognition in probable Alzheimer disease from the Sunnybrook dementia study. *Arch Neurol.* 2008;65:790-5.

176. Scheid R, Preul C, Gruber O, et al. Diffuse axonal injury associated with chronic traumatic brain injury: evidence from T2*-weighted gradient-echo imaging at 3 T. *AJNR Am J Neuroradiol.* 2003;24:1049-56.
177. Shepherd J, Blauw GJ, Murphy MB, et al. The design of a prospective study of Pravastatin in the Elderly at Risk (PROSPER). PROSPER Study Group. PROspective Study of Pravastatin in the Elderly at Risk. *Am J Cardiol.* 1999;84:1192-7.
178. van den Heuvel DM, Admiraal-Behloul F, ten Dam VH, et al. Different progression rates for deep white matter hyperintensities in elderly men and women. *Neurology.* 2004;63:1699-701.
179. Greenberg SM, Briggs ME, Hyman BT, et al. Apolipoprotein E epsilon 4 is associated with the presence and earlier onset of hemorrhage in cerebral amyloid angiopathy. *Stroke.* 1996;27:1333-7.
180. van Rooden S, van der Grond J, van den Boom R, et al. Descriptive analysis of the Boston criteria applied to a Dutch-type cerebral amyloid angiopathy population. *Stroke.* 2009;40:3022-7.
181. Admiraal-Behloul F, van den Heuvel DM, Olofsen H, et al. Fully automatic segmentation of white matter hyperintensities in MR images of the elderly. *Neuroimage.* 2005;28:607-17.
182. van der Flier WM, van den Heuvel DM, Weverling-Rijnsburger AW, et al. Magnetization transfer imaging in normal aging, mild cognitive impairment, and Alzheimer's disease. *Ann Neurol.* 2002;52:62-7.
183. van Es AC, van der Grond J, de Craen AJ, et al. Caudate nucleus hypointensity in the elderly is associated with markers of neurodegeneration on MRI. *Neurobiol Aging.* 2008;29:1839-46.
184. Offenbacher H, Fazekas F, Schmidt R, et al. MR of cerebral abnormalities concomitant with primary intracerebral hematomas. *AJNR Am J Neuroradiol.* 1996;17:573-8.

185. Kato H, Izumiyama M, Izumiyama K, et al. Silent cerebral microbleeds on T2*-weighted MRI: correlation with stroke subtype, stroke recurrence, and leukoaraiosis. *Stroke.* 2002;33:1536-40.
186. Naka H, Nomura E, Wakabayashi S, et al. Frequency of asymptomatic microbleeds on T2*-weighted MR images of patients with recurrent stroke: association with combination of stroke subtypes and leukoaraiosis. *AJNR Am J Neuroradiol.* 2004;25:714-9.
187. Greenberg SM, Eng JA, Ning M, et al. Hemorrhage burden predicts recurrent intracerebral hemorrhage after lobar hemorrhage. *Stroke.* 2004;35:1415-20.
188. Roob G, Lechner A, Schmidt R, et al. Frequency and location of microbleeds in patients with primary intracerebral hemorrhage. *Stroke.* 2000;31:2665-9.
189. Jeong SW, Jung KH, Chu K, et al. Clinical and radiologic differences between primary intracerebral hemorrhage with and without microbleeds on gradient-echo magnetic resonance images. *Arch Neurol.* 2004;61:905-9.
190. Imaizumi T, Horita Y, Hashimoto Y, et al. Dotlike hemosiderin spots on T2*-weighted magnetic resonance imaging as a predictor of stroke recurrence: a prospective study. *J Neurosurg.* 2004;101:915-20.
191. Jeon SB, Kang DW, Cho AH, et al. Initial microbleeds at MR imaging can predict recurrent intracerebral hemorrhage. *J Neurol.* 2007;254:508-12.
192. van Es AC, van der Grond J, de Craen AJ, et al. Risk factors for cerebral microbleeds in the elderly. *Cerebrovasc Dis.* 2008;26:397-403.
193. Lee SH, Park JM, Kwon SJ, et al. Left ventricular hypertrophy is associated with cerebral microbleeds in hypertensive patients. *Neurology.* 2004;63:16-21.

194. Chuang ML, Manning WJ. Left ventricular hypertrophy and excess cardiovascular mortality is late gadolinium enhancement the imaging link? *J Am Coll Cardiol.* 2009;53:292-4.

List of publications

van Hezewijk M, Creutzberg CL, Putter H, Chin A, **Schneider I**, Hoogeveen M, Willemze R, Marijnen CA. Efficacy of a hypofractionated schedule in electron beam radiotherapy for epithelial skin cancer: Analysis of 434 cases. *Radiother Oncol.* 2010;95:245-9.

Altmann-Schneider I, Trompet S, de Craen AJ, van Es AC, Jukema JW, Stott DJ, Sattar N, Westendorp RG, van Buchem MA, van der Grond J. Cerebral microbleeds are predictive of mortality in the elderly. *Stroke*. 2011;42:638-44.

Altmann-Schneider I, de Craen AJ, Slagboom PE, Westendorp RG, van Buchem MA, Maier AB, van der Grond J. Brain tissue volumes in familial longevity: the Leiden Longevity Study. *Aging Cell*. 2012;11:933-9.

Altmann-Schneider I, van der Grond J, Slagboom PE, Westendorp RG, Maier AB, van Buchem MA, de Craen AJ. Lower susceptibility to cerebral small vessel disease in human familial longevity: the Leiden Longevity Study. *Stroke*. 2013;44:9-14.

Hafkemeijer A, **Altmann-Schneider I**, Oleksik AM, van de Wiel L, Middelkoop HA, van Buchem MA, van der Grond J, Rombouts SA. Increased functional connectivity and brain atrophy in elderly with subjective memory complaints. *Brain Connect*. 2013;3:353-62.

Altmann-Schneider I, de Craen AJ, Veer IM, van den Berg-Huysmans AA, Slagboom PE, Westendorp RG, van Buchem MA, van der Grond J; Leiden Longevity Study Group. Preserved white matter integrity is a marker of familial longevity. *Ann Neurol*. 2013;74:883-92.

Altmann-Schneider I, van der Grond J, van den Berg-Huysmans AA, de Craen A, Slagboom E, Westendorp R, van Buchem M. De Leiden Lang Leven Studie: weerspiegelt het brein een lang leven? *Neuropraxis.* 2013;17:167-72.

Kroft LJ, van der Bijl N, van der Grond J, **Altmann-Schneider I**, Slagboom PE, Westendorp RG, de Roos A, de Craen AJ. Low computed tomography coronary artery calcium scores in familial longevity: the Leiden Longevity Study. *Age (Dordr)*. 2014;36:9668.

Sala M, de Roos A, van den Berg A, **Altmann-Schneider I**, Slagboom PE, Westendorp RG, van Buchem MA, de Craen AJ, van der Grond J. Microstructural brain tissue damage in metabolic syndrome. *Diabetes Care*. 2014;37:493-500.

Hafkemeijer A, **Altmann-Schneider I**, de Craen AJ, Slagboom PE, van der Grond J, Rombouts SA. Associations between age and gray matter volume in anatomical brain networks in middle-aged to older adults. *Aging Cell*. 2014;13:1068-74.

Widya RL, Kroft LJM, **Altmann-Schneider I**, van den Berg-Huysmans A, van der Bijl N, de Roos A, Lamb HJ, van Buchem MA, Slagboom PE, van Heemst D, van der Grond J. Visceral adipose tissue is associated with microstructural brain tissue damage. *Obesity*. 2015; In press.

Altmann-Schneider I, de Craen AJ, van den Berg-Huysmans AA, Slagboom P, Westendorp RG, van Buchem MA, van der Grond J. An in vivo study on brain microstructure in biological and chronological ageing. *PLoS One.* 2015;10.

Curriculum vitae

Irmhild Altmann-Schneider werd geboren op 19 augustus 1982 te Stuttgart, Duitsland. Na het behalen van haar Diploma gymnasium („Abitur“) op het Theodor-Heuss-Gymnasium te Esslingen, Duitsland, begon zij in 2002 met de studie Geneeskunde aan de Eberhard-Karls-Universiteit te Tübingen, Duitsland.

Tijdens haar studie liep zij stage in verschillende ziekenhuizen, o.a. op de afdelingen Gastroenterologie te Skien, Norwegen, en Medische Oncologie in het Universitair Medisch Centrum Mannheim, Duitsland. Gedurende de doctoraalfase van haar studie geneeskunde deed zij promotieonderzoek naar “Tumor-geassocieerde peptiden uit de niercelcarcinoom antigenen apolipoprotein L1, G250 en GUCY1A3” op de afdeling Immunologie in het Universitair Medisch Centrum Tübingen onder leiding van Prof. Stefan Stevanovic en ontving hiervoor in 2008 de titel “Dr. med.”. Voor haar onderzoek ontving zij een beurs van het Doctoral Programme “Cellular mechanisms of immune-associated processes” gefinancieerd door de “German Research Council (Deutsche Forschungsgemeinschaft)”. In het kader van het Erasmus international exchange programme liep zij twee semi-arts stages in het Leids Universitair Medisch Centrum te Leiden op de afdelingen Medische Oncologie en Radiotherapie. Na het behalen van haar artsexamen in juni 2009 begon zij in juli 2009 aan haar promotieonderzoek op de afdelingen Radiologie en Ouderengeneeskunde in het Leids Universitair Medisch Centrum onder begeleiding van Dr. Jeroen van der Grond, Dr. Ton de Craen, Prof. Mark van Buchem en Prof. Rudi Westendorp. Haar promotieonderzoek was onderdeel van het Netherlands Consortium for Healthy Ageing (NCHA). Tijdens haar promotieonderzoek volgde zij als gasthoorder gedeeltelijk het masterprogramma “Vitality and Aging” aan de Leyden Academy on Vitality and Ageing (LAVA,

Leiden) onder leiding van Prof. Rudi Westendorp. Op 16 december 2012 is zij begonnen aan haar opleiding tot radioloog in het Leids Universitair Medisch Centrum (opleider Prof. Hans Bloem).